Daniel Knez, BSc

Preparation and Electron Microscopy of Graphene

MASTER THESIS

For obtaining the academic degree
Diplom-Ingenieur

Master Programme of
Technical Physics

Graz University of Technology

Supervisor:

Ao.Univ.-Prof. Dipl.-Ing. Dr.techn. Ferdinand Hofer

Co-Supervisor:

Dipl.-Ing. Dr.techn. Evelin Fisslthaler

Institute of Electron Microscopy and Nanoanalysis

Graz, January 2013

Deutsche Fassung:
Beschluss der Curricula-Kommission für Bachelor-, Master- und Diplomstudien vom 10.11.2008
Genehmigung des Senates am 1.12.2008

EIDESSTATTLICHE ERKLÄRUNG

Ich erkläre an Eides statt, dass ich die vorliegende Arbeit selbstständig verfasst, andere als die angegebenen Quellen/Hilfsmittel nicht benutzt, und die den benutzten Quellen wörtlich und inhaltlich entnommene Stellen als solche kenntlich gemacht habe.

Graz, am ……. ……..
(Unterschrift)

Englische Fassung:

STATUTORY DECLARATION

I declare that I have authored this thesis independently, that I have not used other than the declared sources / resources, and that I have explicitly marked all material which has been quoted either literally or by content from the used sources.

……. ……..
date (signature)

Abstract

Graphene, a single atom layer of graphite, is the first representative of a completely new class of materials, which are considered to be a future key technology due to their unusual physical properties. It is very promising for a wide field of applications. For instance the usage for building sensors with single-molecule sensitivity, flexible transparent electrodes in displays and solar cells, fast semiconductors, investigations of quantum mechanical phenomena at room temperature or solely water permeable membranes, just to mention a few, are imaginable. For the characterisation of graphene and other two-dimensional crystals electron microscopy, in particular transmission electron microscopy (TEM) turned out to be the most efficient technique. Within the scope of this thesis the structure and characteristics of such crystals are briefly presented whereas the emphasis is placed on graphene. In the experimental section two examples for commercially available graphene enhanced TEM grids were benchmarked. Furthermore different sample preparation methods for mechanically exfoiled graphene were tested and improved in order to archive free-standing single layer graphene membranes for the investigation via (S)TEM in terms of their structure, properties and especially their thickness. For the Pre-TEM characterisation several methods, namely optical microscopy, atomic force microscopy (AFM), Raman spectroscopy and scanning electron microscopy (SEM) were used. The intent of this study is to give a overview of the used methods, mention some results of current studies and estimate the future of graphene (and other two-dimensional materials) research at FELMI-ZFE.

Kurzfassung

Graphen ist der Name einer Form von kristallinem Kohlenstoff mit hexagonaler Graphitstruktur, welcher eine Dicke von maximal zehn Atomlagen aufweist. Es ist der erste Vertreter einer vollkommen neuen Materialklasse, die der zweidimensionalen Kristalle, welche sich durch ihre außergewöhnlichen physikalischen Eigenschaften auszeichnet und mittlerweile als zukünftige Schlüsseltechnologie angesehen wird. Eine Vielzahl an möglichen Anwendungen, wie hochempfindliche Sensoren, flexible Elektroden für Displays und Solarzellen, schnellere Halbleiter, als Testumgebung für quantenmechanische Experimente bei Raumtemperatur oder Membranen die für alle Gase, inklusive Helium undurchlässig sind, nicht jedoch für Wasserdampf, wurden mittlerweile präsentiert. Zur Erforschung hat sich die Elektronenmikroskopie und im Besonderen die Transmissionselektronenmikroskopie als geeignet erwiesen. Im Rahmen dieser Arbeit sollen die außergewöhnlichen Eigenschaften von Graphen und ihre Anwendungsbedeutung vorgestellt werden. Einige der wichtigsten Herstellungsverfahren werden präsentiert. Der Fokus liegt hierbei auf der mechanischen Exfolierung, welche auch in dieser Arbeit, in unterschiedlichen Varianten verwendet wurde um Graphen selbst herzustellen. Weiters wurden kommerziell verfügbare TEM-Netzchen mit aufgebrachtem Graphen evaluiert. Eine Vielzahl an, am FELMI-ZFE verfügbaren Charakterisierungsmethoden wurden angewandt. Optische Mikroskopie, Rasterkraftmikroskopie, Raman-Spektroskopie und Rasterelektronenmikroskopie wurden verwendet um dünne Flächen bereits im Vorfeld der TEM-Untersuchungen zu identifizieren. Die Intention dieser Arbeit ist es, einen kompakten Überblick über das weite Feld der Graphenforschung zu geben und Möglichkeiten für ihre Zukunft am FELMI-ZFE abzuschätzen.

Acknowledgement

This thesis would not be possible without the support of a lot of people. At this point I want to give my acknowledgements to them.
First of all I want to thank my co-supervisor Evelin for her professional and moral support. She always was the first point of contact for all kind of problems concerning my work and introduced me into the way of scientific work.
A particular debt of gratitude is also owed to my supervisor Prof. Ferdinand Hofer, the head of FELMI-ZFE for giving me the chance to work on this very interesting field of research at this sophisticated institute and for providing me the professional and financial framework.
I also want to thank Boril Chernev for the Raman measurements, Franz Schmidt for his support especially concerning the EELS plasmon characterisations and Mihaela Albu for her help with the Titan investigations. Special thanks is also owed to Harald Plank and Tim Aschl who helped me to perform and evaluate the AFM measurements.
Further acknowledgements have to be given to the whole FELMI-ZFE laboratory team, in particular Martina Dienstleder, Manuel Paller and Julia Töglhofer for supporting me with my work in the laboratory.
Most importantly I want to thank my family and especially my sister and my parents for their backup, their love and their financial support, not only for this work, but for my whole academic study. They always supported me unconditionally and gave me the chance to study freely without any thoughts about my financial situation. Finally I want to thank all of my friends for their company and their mental support.

Contents

1 Introduction

Graphene is the name given to a specific modification of carbon. It is a two dimensional material with a honeycomb structure were the carbon atoms are sp^2 -hybridized. These sheets are the basic building block of other carbon modifications - they can be stacked to form graphite, rolled up to form carbon nanotubes or wrapped to form fullerenes (see chapter 2). Due to its extraordinary properties graphene rapidly became a very widespread field of research since its first confirmed isolation in 2004 by Andre Geim, Konstantin Novoselov and their co-workers at Manchester University [1]. Before 2004 two-dimensional crystals were thought to be thermodynamically unstable [2][3]. Geim and Novoselov got the Nobelprize for Physics in 2010 "for groundbreaking experiments regarding the two-dimensional material graphene" [4]. The explosion of interest is shown in figure 1.1 with the help of the number of published graphene related publications listed in Science Direct (`www.sciencedirect.com`). The value for 2012, painted red in this figure, is the number of articles published until the 4^{th} of october.

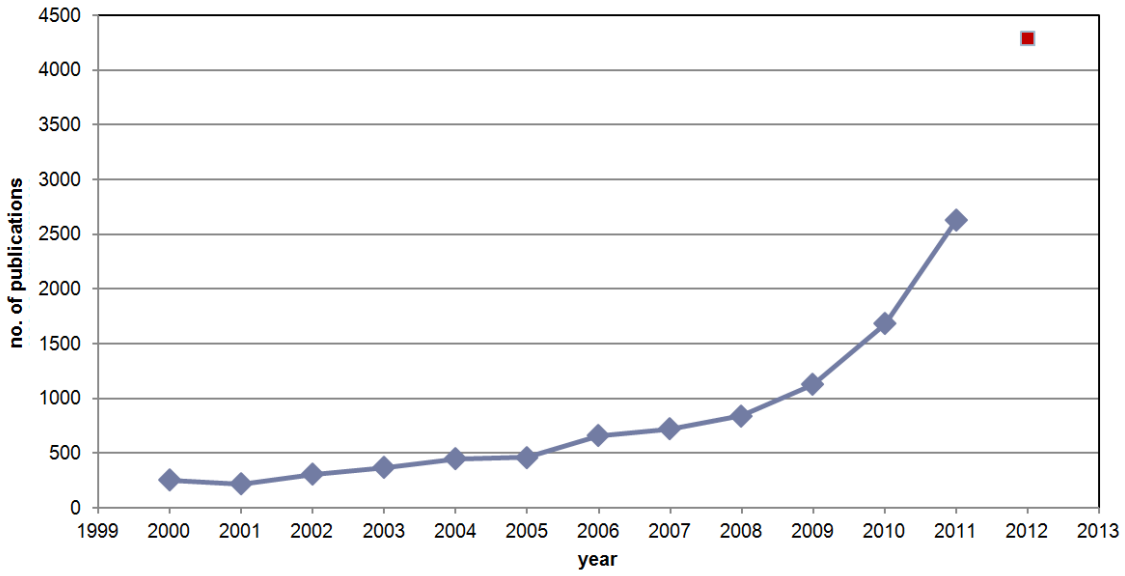

Figure 1.1: Number of published graphene related articles over years (source of data: `www.sciencedirect.com`)

2 Structure and Properties

2.1 Carbon and its allotropes

Carbon is a non-metallic element of the 14^{th} group (main group IV) on the perodic table. In the crust of the earth it is the 15^{th} most abundant and in universe the fourth most abundant element by mass. It is a fundamental component of all known live forms. The human body consists of 18.5 w% carbon [5]. It is tetravalent, thus there are four electrons available for covalent bondings. Carbon can be found in different molecular configurations in nature, referred to as the allotropes of carbon. Diamond, graphite and amorphous carbon are the most important ones, each with completely different physical properties. Figure 2.1 gives some examples for the diversity of carbon.

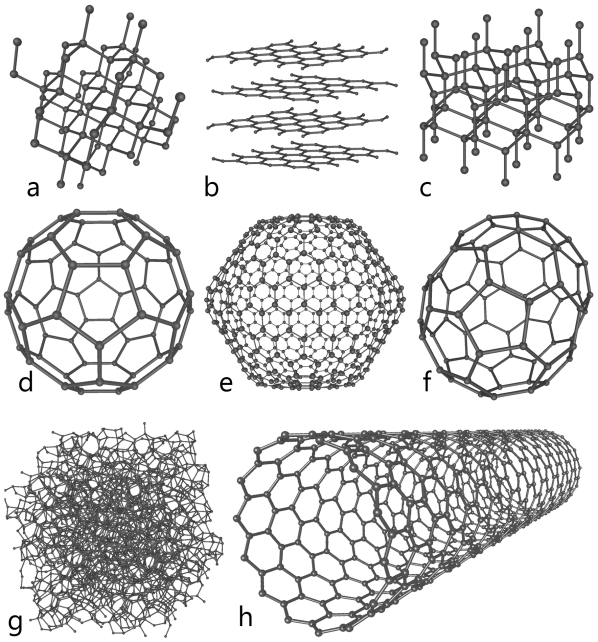

Figure 2.1: Structure of some important carbon allotropes; a: diamond, b: graphite, c: lonsdaleite, d: buckminsterfullerene (C_{60}), e: C_{540}, f: C_{70}, g: amorphous carbon, h: single-walled carbon nanotube (CNT) (from wikipedia.org)

2.1.1 Diamond and Graphite

Diamond and graphite are the most familiar allotropes of carbon, with graphite being its most stable form (in terms of thermodynamics). Both materials exhibit quite antithetic physical properties. Diamond is a non-conducting, very hard and optically transparent material, while graphite is conducting, quite soft and highly opaque. In diamond the carbon atoms are sp^3-hybridised and each atom is covalently bonded to four other carbons, with a distance of 154 pm, forming a tetrahedron.

Graphite on the other hand is sp^2-hybridised. Hence one s orbital and two p orbitals form a trigonal planar structure. The covalently bonded (σ-bond) carbon atoms are arranged in hexagonal rings with a side length of 142 pm. The sheets are stacked over each other with a separation of 335 pm, weakly bound by van der Waals forces. Figure 2.2 schematically shows the structure of graphite with bonding relations. Due to the big energy discrepancy between the intra-planar covalent (4.3 eV) and the van der Waals inter-planar bondings (0.07 eV) the physical properties of graphite are very anisotropic (values from [6]). This is the reason why it is possible to separate the planes from each other.

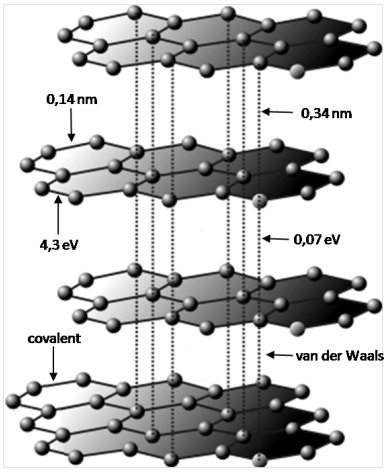

Figure 2.2: Graphite lattice structure with bonding relations

2.1.2 Graphene

'Graphene' is the name given for one to ten planar sheets of graphite. Everyone who uses a pencil has already produced graphene without knowing. While one writes, the graphite in the lead is cleaved into thin flakes which stick on the paper. With high probability among these flakes even monolayer graphene could be found. Despite the fact graphene synthesis seems to be that facile, there are several reasons why graphene research effectively did not take place before 2004. Due to the Peierls-Landau instability law, 2D materials were believed to be unstable (see section 2.2.1). On the other hand it is challenging to find graphene flakes among the thick graphite pieces with conventional microscopic methods providing the necessary resolution (eg. AFM or STM), due to their low throughput. Moreover monolayers are in great minority among the thicker flakes and are nearly completely transparent in an optical microscope. The optical identification method, introduced by Novoselov and Geim [1] (see 4.1), made that possible for the first time.
At the first glance it is surprising that thin graphite sheets with just a few to one layers in thickness have completely different properties compared to bulk graphite. It can be distinguished between 3 types of graphene regarding the electronic properties dependent on the thickness: Single layer (SLG), double- or bilayer and few layer graphene (FLG). On the former we will

focus within the scope of the present thesis. SLG can be seen as the basic element of several carbon allotropes. For instance fullerenes, carbon nanotubes or graphite can be formed out of graphene sheets, as figure 2.3 illustrates.

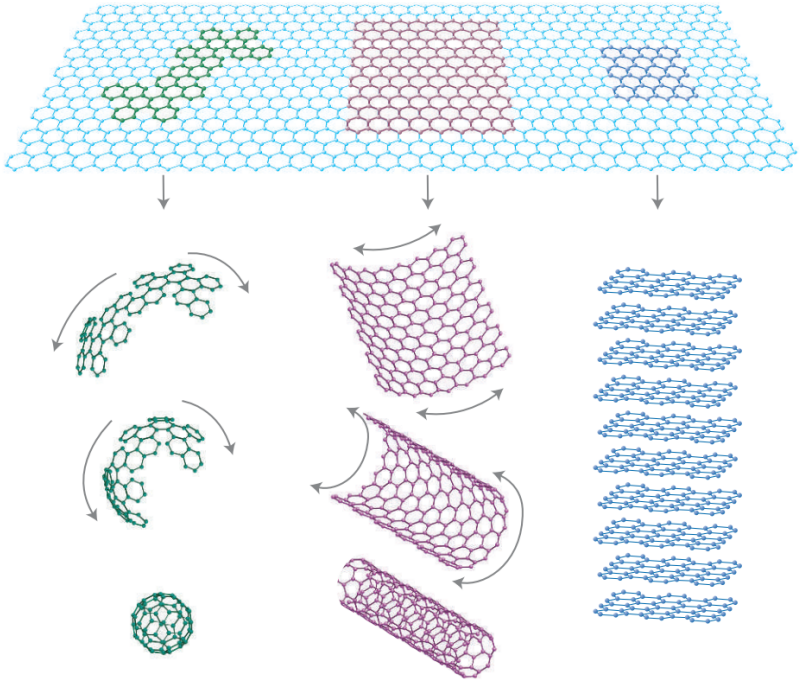

Figure 2.3: Graphene as the basic element of C_{60} fullerene molecules, carbon nanotubes and graphite [7]

2.1.3 Graphene nanoribbons

As one narrows the width of graphene sheets towards quasi one dimensional ribbons, they again exhibit a change of electronic properties, dependent on the width and their edge structure. In principle there are two directions how graphene nanoribbons (GNR) can be oriented. In literature they are referred to as armchair and zig-zag oriented nanoribbons, as shown in figure 2.4. Ribbons in zig-zag orientation feature metallic properties, while armchair oriented GNR can be metallic or semi-conducting, dependent on their width. The energy band gap of a ribbon with armchair orientation is inversely proportional to its width [8].

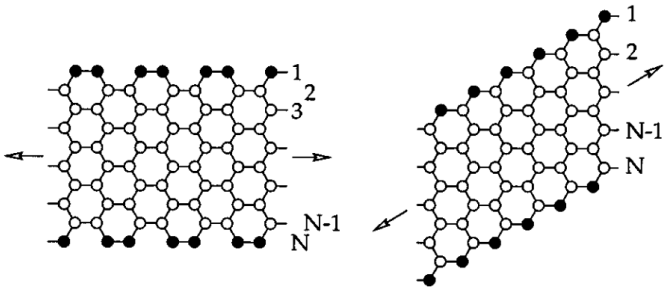

Figure 2.4: The two possible orientations of graphene nanoribbons; left: armchair orientation, right: zig-zag orientation (adapted from [9])

Nanoribbons are very promising for the construction of graphene transistors, as they offer the possibility to influence the band gap precisely. Pure graphene sheets with a zero-gap are not applicable for building a transistor because it would be impossible to realize an 'Off'-state.

2.1.4 Amorphous carbon

Amorphous carbon does not exhibit any crystal structure, despite some short range order, as shown in figure 2.1 on picture g. It has usually a lot of dangling π-bonds and is thus very reactive and often hydrogenated. Hence the interatomic distances and bond angles variate. It can be characterised by its sp^2-sp^3 ratio. Common materials with a high amorphous carbon content are for instance coal and soot. Indeed these are highly polycrystalline materials in a amorphous carbon matrix. In the scope of this study amorphous carbon mainly appears in terms of unwanted contamination.

2.2 Properties of Graphene

The outstanding physical properties of graphene will be described in this section.

2.2.1 Structure

Graphene single layers have a honeycomb lattice structure with 2 carbon atoms per unit cell. It consists of 2 sublattices (named A and B in figure 2.5, adapted from [10]), where every carbon atom is surrounded by 3 atoms of the complementary sublattice (δ are the nearest neighbour vectors). The basis lattice vectors $\mathbf{a}_1$ and $\mathbf{a}_2$ are given by equ. 2.1. The distance between the nearest neighbours is about a=1.42 Å, but varies at room temperature between 1.3 Å and 1.54 Å [11]. The existence of two sublattices is the reason for a phenomena called chirality. In general we speak about chirality of the property of an object when it is not identical to its mirror image. That means that every sublattice is responsible for one dispersion branch which are (nearly) completely independent. The contributions from each sublattice can be handled theoretically by defining a pseudospin quantum number.

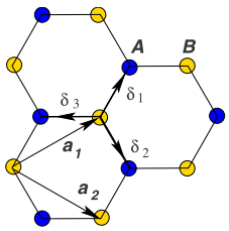

Figure 2.5: 2 sublattices (A,B) with lattice vectors [10]

$$\mathbf{a}_1 = \frac{a}{2}(3,\sqrt{3}) \quad \& \quad \mathbf{a}_2 = \frac{a}{2}(3,-\sqrt{3}) \tag{2.1}$$

Until 2004 it was believed that 2D-materials are thermodynamically unstable, as proposed theoretically by Peierls and Landau with their Peierls-Landau instability law [3], [2] and also by Mermin [12]. They argued that the contribution of thermal fluctuations is divergent for a low dimensional crystal, which leads to a atom displacement comparable to the interatomic distance for any temperature above 0 K. This was also supported by experimental observations, like a decreasing melting point with decreasing thickness of thin films [13]. It is believed that graphene is stable because it exhibits a rippled structure caused by thermal fluctuations [7][11]. Meyer et al. analysed the structure and dimensions of these ripples by TEM investigations (broadening of diffraction spots due to ripples) [14] and determined an amplitude of 0.5 nm and a lateral size of 5 nm. This was also confirmed by Bangert et al. [15]. Similar ripples can also be found in other 2D systems like MoS_2 [16].

2.2.2 Optical properties

Monolayer graphene has an absorption of 2.3 % [17], which is unusually high considering its thickness. Nevertheless it is still quite low and thus graphene may be a promising choice for transparent electrodes. ITO (indium tin oxide), the todays most widely used material for that, has a transparency of around 90 % and a specific resistivity of $110 \times 10^{-6}\,\Omega\,\mathrm{cm}$ [18]. It is very unflexible and the supply of indium is quite limited. Additionally its transparency decreases

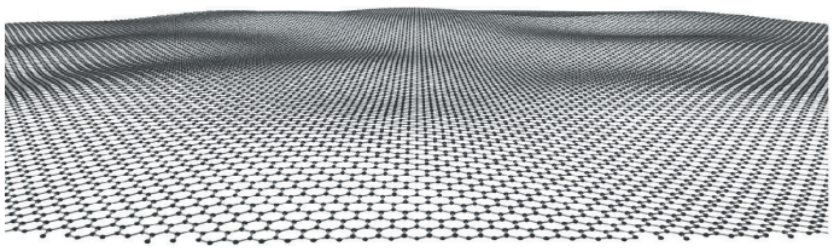

Figure 2.6: Simulated rippled graphene structure with an amplitude of 0.5 nm and a lateral size of 5 nm, in compliance with experimental data (from the supporting information of [14])

very fast for wavelengths below 500 nm.
The light transmittance of graphene can be described with equ. 2.2 in terms of the fine structure constant as described in [10] & [17].

$$T = (1+0.5\pi\alpha)^{-2} \approx 1-\pi\alpha \approx 0.977A = 1-T \tag{2.2}$$

$$A = 1-T \tag{2.3}$$

T... Transmittance
A... Absorbance
α... Fine structure constant ($\alpha = \frac{e^2}{\hbar c}$)
$\hbar$... Plancks constant
c... Speed of light
e... Electron charge

It is remarkable that the transmittance is (nearly) independent on the wavelength of the light and is thus almost constant from ultraviolet to infrared. Due to this suspended graphene colourless. Since the single sheets are almost not interacting when stacked, the transmittance of FLG is roughly proportional to the number of layers [10].

2.2.3 Electronic Properties

2.2.3.1 Dispersion relation

The band structure of graphene was first described by Wallace in 1946 [19]. Due to the two dimensional honeycomb lattice structure graphene exhibits a linear dispersion relation at low energies, described by equ. 2.5, without a band gap. Usually it is referred to as zero-gap semiconducter or zero-overlap semimetal. That means that the conduction- and valence bond meet at 6 corners of the Brillouin zone border, the Dirac points. There are two different sets, usually

labeled K and K', each with three points. The two inequivalent corners, called Dirac points of the Brillouin zone are given by equ. 2.4 [20].
As one p orbital is not affected by the σ- bonds it provides an extra electron which leads to the formation of a π bond with the π electrons of the neighbour atoms. Hence, the valence electrons are delocalised over long distances. All π-bonded electrons form the π-band, which is responsible for most of the outstanding electronic properties of graphene. Figure 2.7 shows the dispersion relation for the first Brillouin zone on the right.

$$\mathbf{K} = (\frac{2\pi}{3a}, \frac{2\pi}{3\sqrt{3}a}) \quad \& \quad \mathbf{K'} = (\frac{2\pi}{3a}, -\frac{2\pi}{3\sqrt{3}a}) \tag{2.4}$$

Few-layer graphene: Already bilayer graphene, in classical Bernal (AB) stacking shows a different band structure compared to SLG, since it is parabolic around the Fermi energy with a very small overlap of 0.16 meV. With rising layer count the metallic character becomes more and more dominant. For more than 10 layers the difference in band overlap compared to graphite (41 meV) is less than 10 % [21]. The electronic properties of bilayer or few-layer graphene are also dependent on the stacking order and orientation.

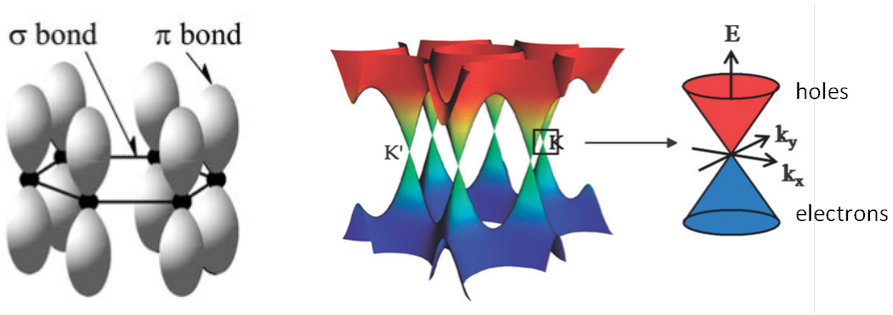

Figure 2.7: Left: schematic of the in-plane σ-bonds and the perpendicular π-bonds (from [22]); right: bandstructure of graphene, the blow up shows the conical low energy region with the zero-gap at one of the Dirac points (adapted from [23])

$$E(k) \approx \hbar v_F \sqrt{k_x^2 + k_y^2} \tag{2.5}$$

E(k)...	Energy
v_F...	Fermi velocity
k_x, k_y...	Wave vector components

2.2.3.2 Dirac fermions

One of the most important consequences of the extraordinary linear dispersion relation near the K points is that low energy electrons (or even holes) behave like relativistic massless particles, so called Dirac fermions, while moving through the periodic potentials of the hexagonal lattice structure. Charge carriers can change continuously between electrons and holes and travel over thousands of inter-atomic distances without being scattered. Thus it is possible to observe quantum electrodynamics phenomena, like the quantum Hall effect in graphene even at room temperature. The effective travel speed is given by the Fermi velocity v_F ($v_F \approx 10^6$ m/s respectively $1/300^{th}$ the speed of light). Therefore they can be described with the Dirac equation for relativistic fermions, rather than with the Schrödinger equation.

2.2.3.3 Electron mobility

At room temperature graphene has the highest electron mobility of all known materials. Experimentally reported values are in excess of $15\,000\,\mathrm{cm}^2/\mathrm{Vs}$ for mechanically exfoiled graphene on SiO_2 [1], limited by defect scattering and probably by impurities between the graphene flake and the SiO_2 surface [24]. Additionally, scattering by optical phonons of the substrate is larger at room temperature than the intrinsic phonon scattering. This limits the electron mobility of graphene on SiO_2 [25]. At room temperature the mobility is theoretically limited by acoustic phonon scattering to $200\,000\,\mathrm{cm}^2/\mathrm{Vs}$. For free-standing graphene and low temperatures ($\sim$5 K) even values in excess of $200\,000\,\mathrm{cm}^2/\mathrm{Vs}$ were reported [24]. This corresponds to a specific electrical resistivity of $10^{-6}\,\Omega\,\mathrm{cm}$.

2.2.3.4 Klein paradox

The characteristic property of relativistic fermions is that they can move through any potential barrier of any height or width and without any reflecting component. This reflection less tunneling, which is far away from being intuitive, is called the Klein paradox. The reason for this is that electrons can immediately transform to holes as they strike an electrostatic barrier and back again when they reach the other side. This is also a consequence of the linear dispersion relation without band gap.
The electronic properties of graphene are still a matter of research and some questions still remain to be answered. For further reading on this issue especially the publications by Novoselov, Geim and their co-workers [1], [26] and [27] are recommended. The reviews by Geim [7] [28], Geim and MacDonald [29] and Das Sarma et al. [20], which is complimentary to the review of Castro Neto et al. [30], give a good introduction for this gigantic field of research.

2.2.4 Mechanical Properties

Remarkable graphene facts can also be found in terms of its mechanical properties. It is one of the strongest materials known. A in-plane Youngs modulus of around 1 TPa was measured by Lee et al. [31] by nanoindentation via AFM on free-standing, mechanically cleaved graphene membranes. The breaking strength measured in their study was 42 N/m. That means that it is 100 times stronger than the strongest steel [4]. Beside its stiffness graphene is also very light, weighing only 0.77 mg/m^2. A hammock made out of single layer graphene with an area of 1 m^2 would hold a cat ($\sim$4 kg) while weighing as much as one of the cats whiskers. (This illustration of the strength of graphene was taken from the Nobel prize announcement [4].) However, in practice the macroscopic mechanical properties are limited due to the presence of defects and grain boundaries.
Nevertheless, already epoxy nanocomposite materials with graphene were synthesised, exhibiting better mechanical properties compared to CNT composites [32].

2.2.5 Thermal properties

Since the carbon atoms have a quite low mass and the in-plane covalent bonds in graphene are very strong, the in-plane sound velocity is also very high ($\approx$20 km/s [33]). This directly leads to a very high thermal conductivity κ, which is thus phonon dominated in graphene. Balandin et al. [34] determined values up to κ=(5300$\pm$480) W/m K at room temperature. Copper, for instance, has a thermal conductivity of 400 W/m K, while diamond has exhibited the highest known thermal conductivity of a natural material (with 2300 W/m K) until these investigations on graphene were performed. (This is even much lower than in graphene.) The mean free path of graphene phonons was found to be $\approx$ 775 nm [35].

2.2.6 Other 2D-Materials

Several other two-dimensional materials were reported since 2004. Already in 2005 Novoselov et al. [27] produced monolayers of other materials, namely boron nitride (BN), molybdenum disulfide (MoS_2), niobiumdiselenide ($NbSe_2$) and $Bi_2Sr_2CaCu_2O_x$, by mechanical exfoliation. The two most famous of them will be briefly presented in this section: boron nitride and molybdenum disulfide.

2.2.6.1 Boron nitride (BN)

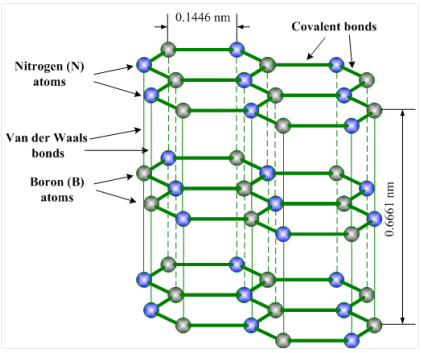

Figure 2.8: Hexagonal BN structure with bonding relations

Boron nitride was the second isolated 2D material synthesised. BN has a hexagonal structure and a wide band gap of 5.9 eV and is thus dielectric [36]. Novoselov et al. [27] rubbed bulk hexagonal boron nitride (h-BN) against another solid material in order to prepare monolayer BN. The structure of h-BN is very similar to graphite. Figure 2.8 shows the lattice with its parameters [37]. Coleman et al. [38] used isopropanol (IPA) as solvent for liquid exfoliation by sonication and centrifugation. Also CVD based approaches for the BN synthesis on copper with ammonia borane (NH_3-BH_3) as source were reported [36] and [39]. Since it has a similar lattice constant compared to graphene, with a lattice mismatch of less than 2 % (2.445 Å in graphene and 2.5 Å in BN), it can be used to tune the band gap by stacking [40]. Figure 2.10 shows on the left side a HRTEM picture of a BN monolayer. The dotted line marks an intensity profile path and the corresponding profile is drawn beneath.

2.2.6.2 Molybdenum disulfide (MoS_2)

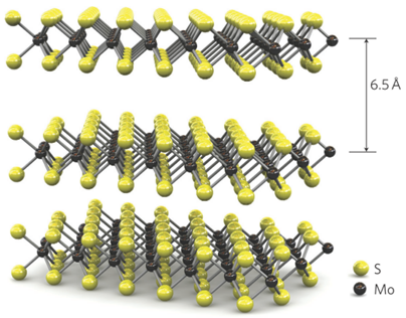

Figure 2.9: MoS_2 structure

Molybdenum disulfide can be produced by mechanical exfoliation with a scotch tape [16] or by rubbing against another solid [27]. It can also be exfoliated in a liquid environment using N-methyl-pyrrolidone (NMP) [38]. Both, Novoselov et al. and Coleman et al. also exfoliated several other 2D materials with their methods. Ramakrishna Matte et al. on the other hand used litium for intercalation and water for exfoliation [41]. MoS_2 is a semiconductor with a direct band-gap of 1.8 eV. Transistors based on single layers were already produced [42]. MoS_2 also exhibits a rippled structure like graphene, with a ripple height between 6 Å to 10 Å. This was demonstrated by Brivio et al. in [16] by HRTEM investigations. Figure 2.9 illustrates the structure of MoS_2 (from [42]). The right picture in figure 2.10 on the other hand shows an HRTEM picture of MoS_2 at atomic resolution in the top line with an intensity profile of the path marked with a dotted line beneath.

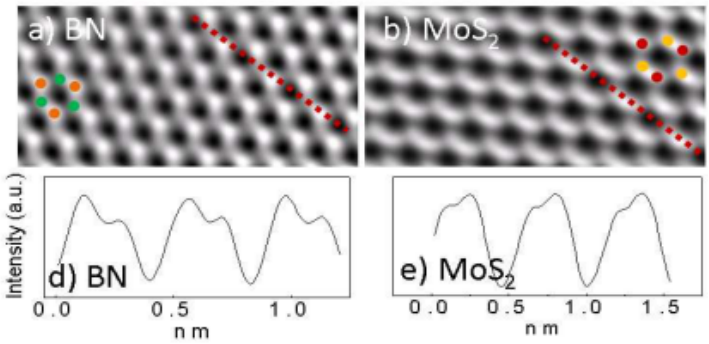

Figure 2.10: HRTEM images of BN (left) and MoS_2 monolayers (with an defocus of -10 tu -30 nm) each with an intensity profile beneath. The path of the profile is drawn with a dotted line in the HRTEM picture (adapted from the supporting information of [38])

For further reading on the large class of two-dimensional materials and their synthesis the review article [43] is recommended. Furthermore single layers of different 2D materials can be combined in order to synthesise a new class of artificial 3D structures with tailored properties [44]. Silicene, another mentionable 2D crystal has, in contrast to the already mentioned materials, no natural origin. It will be described shortly in the following section.

2.2.6.3 Silicene

Silicene is the name given to a hexagonal, two-dimensional modification of silicon. Si is located just below carbon in the periodic table of elements in group IV. Si atoms thus have a similar electronic configuration as those of C. However, in Si the sp^3 hybridization is much more stable than the sp^2 hybridization, in contrast to carbon where the two hybridizations are closer in energy. Hence a Si structure analogue to graphite is not known in nature. As a consequence silicene can not be prepared by exfoliation methods from bulk silicon. It was predicted theoretically by Takeda and Shiraishi in 1994, [45], that the electronic properties of silicene are very similar to those of graphene, including the linear dispersion relation with a zero-gap. They also predicted the existence of germacene, the germanium analogue to graphene. Vogt et al. successfully synthesized silicene on a silver(111) substrate [46] in 2012. Also other groups claim to be the first who provided evidence for silicene on Ag with similar approaches [47, 48].

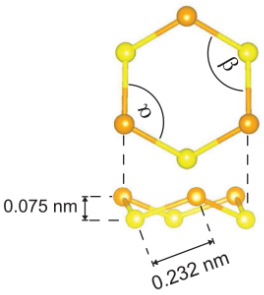

Figure 2.11: Buckled silicene ring

The distance between the Si atoms in a hexagonal silicene structure is 0.232 nm grown on a Ag(111) surface (0.235 nm is the value for bulk silicon) [46]. Since silicon atoms always tend to form sp_3-bonds, silicene exhibits a buckled hexagonal structure (also referred to as β-silicene). Figure 2.11, adapted from [46]), illustrates the buckled structure of the Si hexagons with the bonding length and angles (with $\alpha \approx 110°$ and $\beta \approx 112°$-$120°$). The two colours

correspond to the two sublattices. Dirac fermions were observed [49] and the Fermi velocity was determined to be $1.3 \times 10^{-6}\,\mathrm{m\,s^{-1}}$ [46], comparable with graphene. Until now silicene has only been grown on silver surfaces and no succeeded production of stand-alone silicene sheets has been reported. Figure 2.12 illustrates the hexagonal structure (right), with two different colours (red and yellow) for each sublattice lying on two different planes due to the buckled structure (a_1, a_2 are the lattice vectors, the atoms of a unit cell are labled with A and B). On the left side of the figure, STM images of the substrate surface (a) and the silicene structure grown on the surface (b) is shown. In (c) a simulated picture of the surface is depicted, illustrating the origin of the structures in the latter STM image.

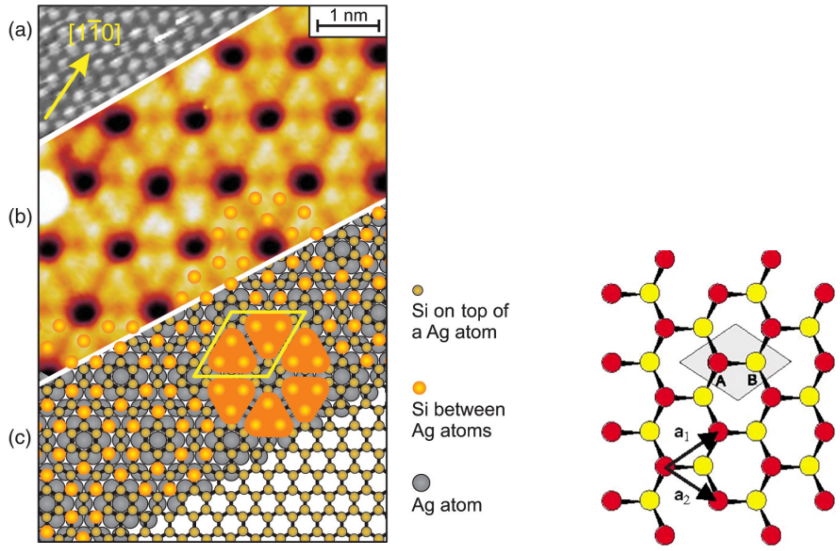

Figure 2.12: left: (a) clean AG(111) surface in STM, (b) STM picture of a silicene sheet, (c) simulated image of silicene on a Ag(111), the surface Si atoms are drawn as larger orange balls(adapted from [46]), at the right corner the resulting silicene sheet without Ag is illustrated; right: silicene lattice with lattice vectors a_1 and a_2, A and B are the atoms of a unit cell, the colours red and yellow mark the two sublattices (adapted from [50])

Silicene may be interesting for the semiconductor industry, since a lot of established methods for the production of silicon based semiconductors could be used. For further reading on this novel material, the mentioned publications are recommended (especially [48] and [46]). Kara et al. published the first review article on silicene in 2012 [50].

2.2.7 Doping

The electronic properties of graphene can be tuned by doping with other materials. Since it is a 2D material, all of its atoms are exposed to the environment. Thus, graphene in its pristine form is very sensitive to surface adsorbed species. This makes it ideal for sensing applications (detection of even individual NO_2 molecules was reported [51] for instance), but in terms of its use as semiconducting material this behaviour is rather unwanted. The substrate,

chemical residues and ambient air can be forms of this undesired doping. In order to control properties like the Fermi level, the band gap or the dispersion relation, in principle two doping mechanisms can be used, electrical and chemical doping. Electrical doping uses the electric field effect in graphene by applying a gate voltage (as reported for instance by [1]). It can be used to change the Fermi level, but the band gap cannot be influenced. Chemical doping on the other hand makes use of foreign species, which are interacting with the carbon atoms. Of course both methods can be combined [52]. Figure 2.13 illustrates how doping influences the band structure of graphene in terms of the band gap and the Fermi level (E_f).

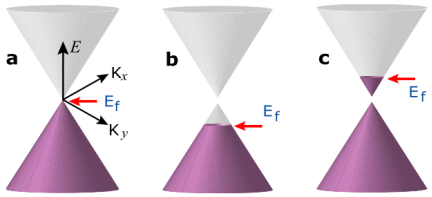

Figure 2.13: Illustration of the graphene band structure near the Dirac points dependent on type of doping; a) pristine graphene; b) p-type doping c) n-type doping (from [53])

2.2.7.1 Chemical doping

Chemical doping can be classified by its action principle into surface transfer doping and substitutional doping.

Substitutional doping Single carbon atoms in the lattice are replaced by atoms with different number of valence electrons. Nitrogen (n-type) and boron (p-type) are preferable because of their similar atomic sizes compared to carbon. Substitutional doping with N or B does not change the linearity of the dispersion relation close to the Dirac points but it opens a band gap and affects the Fermi level (see figure 2.13) [54].
Several publications are available concerning substitutional doping. For instance, N-doped graphene has been produced and characterized by Zhao et al. [55]. They used CVD processes with ammonia as nitrogen source for graphene synthesis and several characterisation techniques including STM, X-ray photoemission and Raman spectroscopy. Meyer et al. investigated similar samples by TEM [56]. Panchakarla et al. [54] also did investigations via Raman spectroscopy, AFM and TEM (including EELS) on B- and N-doped graphene synthesised by an arc-discharge based method.

Surface transfer doping This is archived by adsorbates on the graphene surface, which are exchanging electrons with the carbon atoms of the graphene lattice without changing its hexagonal structure. It is thus also often referred to as adsorbate-induced doping. The delocalized π-electrons, which are crucial for the electronic properties of graphene, are mainly

affected by adsorbed atoms or molecules.
Graphene can be functionalised by various materials like atoms, molecules, transition-metal nano-particles, metal oxides, conjugated compounds or polymer chains to obtain a multiplicity of properties.

Hydrogenation Another important approach for the functionalisation of graphene via doping is hydrogenation. Hydrogen [57] attached on the surface can be used for instance for the purpose of opening a band gap. Fully hydrogenated graphene has a completely different structure based on sp^3 hybridised carbon atoms and is also referred to as Ât'Graphane'. However, on a substrate the graphene structure is preserved as the hydrogenation is only one-sided.
Using different dopants and other functionalisation techniques like edge tailoring in principle even electronic circuits like illustrated in figure 2.14 are imaginable. Electronic components, like resistors, diodes, capacitors, molecular switches and transistors can be thus realised, while the non-conducting parts can be implemented by selective hydrogenation (grey areas). For further reading on graphene functionalisation the review by Yan et al. [58] is recommended.

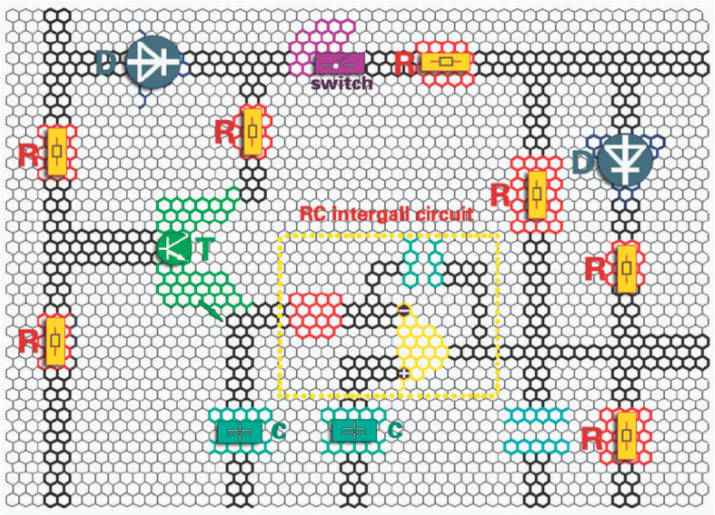

Figure 2.14: Schematic of a completely graphene-based integrated electronic circuit (from [58])

3 Synthesis

3.1 Mechanical exfoliation

3.1.1 Scotch tape method

The original method used by Novoselov and Geim [1] was simplified and adapted to our requirements. This method and similar approaches are also referred to as 'micromechanical cleavage', 'microcleaving' or 'drawing method' in literature. In this section our modified method will be described.
Mechanical exfoliation is still the best method for the small scale production within the scope of graphene investigations in a laboratory. High quality monolayer flakes with sizes of several 10 µm and electron mobilities of up to 15 000 cm^2/Vs can be produced relatively easy. Even graphene flakes with a size of up to 1 mm in length were reported [10]. Two different graphite sources where used for our experiments, HOPG (Highly Oriented Pyrolytic Graphite) and natural graphite flakes.
The latters were provided by a graphite mine in St.Stefan ob Leoben in Styria, kindly supplied by Grafitbergbau-Kaisersberg GesmbH. Natural graphite in general exhibits a quite imperfect structure due to a lot of defects and impurities.
Artificial pyrolytic graphite on the other hand is a graphite material with a high degree of crystallographic orientation. It is obtained by heat treatment of pyrolytic carbon or by chemical vapor deposition at high temperatures (above 2500 K). Annealing at approximately 3300 K of the pyrolytic graphite under compressive stress results in HOPG, which is thus a form of high-purity and highly-ordered pyrolytic graphite.
Surprisingly natural graphite provides better results with our preparation method. Though the quantity of the produced flakes is higher with HOPG, they have a much more shattered structure with only small thin areas. HOPG was used in the original work [1] and seems to work better with their method (see section 'original scotch tape method' at the end of this chapter). However, many other authors in literature and even Novoselov and Geim later used simplified methods similar to ours.

3.1.1.1 Cleaning

At first a silicon wafer that is as clean as possible is needed. In order to achieve this we used the following standard cleaning procedure:
The wafer is flushed with deionized (DI) water, followed by ethanol and isopropanol. A cutton bud is then wetted with isopropanol and passed over the surface carefully, which is subsequently again flushed with isopropanol. The piece of wafer is then directly transferred into a isopropanol bath in an ultrasonic cleaner and sonicated for 15 minutes. Finally it is flushed with Isopropanol p.a. and dried with clean pressurised air.
Plasma cleaning of the substrate in an oxygen plasma, like implied in [1], destroyed the optical properties of the substrate in our experiments. Even a few seconds yielded a visibly cratered structure over wide areas.
We also tried to clean the substrate with a so called 'piranha - solution', which is a mixture of hydrochloric acid (HCl) (in some sources with sulfuric acid (H_2SO_4) instead of HCl), hydrogen peroxide (H_2O_2) and deionized water as used in [1] and mentioned in [59] and [60]. We tried a mixing ratio of $HCl : H_2O_2 : H_2O = 1 : 2 : 8$ and treated our substrate for 45 minutes at room temperature. Unfortunately we did not archive a significant improvement of our results due to the piranha etching, so we kept to the standard cleaning procedure.

3.1.1.2 Spin casting

In order to improve the flake sizes, (due to stronger adhesive forces between graphene and polymer materials compared to SiO_2, as mentioned in [61]) it seems to be favourable to coat the substrate with a very thin (around 10 nm) polymer coating. Furthermore, the easier dissoluble coating facilitates the transfer procedure to a TEM grid. PMMA seems to be the material of choice for this purpose due to its optical properties that are similar to those of SiO_2. But any other commonly used spin castable polymer material with an appropriate refraction index should be usable. We used polystyrene in our experiments, see section 5.3 on page 52 for details.

3.1.1.3 Thinning

For the thinning of graphite we used adhesive tape of the type 3M Scotch Magic 810 (see figure 3.1). Other commonly used tapes (eg. 3M Scotch Magic 811 or Tesa Standard Tape), were also tried, but Scotch Magic 810 showed the best results, especially in terms of unwanted adhesive residues on the substrate.
In order to thin the graphite flakes we put some of them on a piece of scotch tape (around 15 cm in length). We folded it next to the flakes so as to surround them completely with the sticky side of the tape. Afterwards we peeled the tape apart very slowly. We repeated this 5 to 10 times until we saw more and more transparent (=thin) graphite areas on the tape.

Figure 3.1: The used adhesive tape type (left), raw natural graphite flakes (middle) and thinned graphite sheets on the tape (right)

3.1.1.4 Transfer

After the thinning step we transferred the flakes from the adhesive tape to our cleaned Si/SiO_2 - substrate. Therefore we stuck the tape with the flakes on the SiO_2 - surface. To insure that as much flakes as possible stick on the wafer we have to pass plastic tweezers (or any other soft material) carefully and repetitively over the sample. This step should last around 5 to 10 minutes. Finally we peel the tape off very slowly (for around 30 seconds). Due to van der Waals forces between the flakes and the wafer surface the upper layers of the flakes stick to it and are occasionally peeled off the rest of the flake sticking to the tape. Koenig et al. [62] determined the adhesion energy of monolayer graphene on a SiO_2 - surface being 0,45 J/m^2. In comparison the interlayer binding energy of graphite is 0,19 J/m^2 [63]. Apparently the graphite layers stick more likely on the substrate than to each other.

3.1.1.5 Identification

Now there are a lot of graphite flakes on the wafer. In order to find the thinnest flakes we used the optical identification method described in 4.1 in page 29.

3.1.1.6 Original scotch tape method

In contrast to our modified method, Novoselov and Geim used another approach for preparing graphene with a scotch tape. They explained their method in the supporting information of [1]. As starting material they used HOPG. They put a piece in an oxygen plasma in order to prepare mesas on top of the platelets. The mesas were around 5 µm high and had lateral dimensions between 20 µm and 2 mm. The structured HOPG surface was then pressed on a 1 µm layer of wet photoresist spun over glass. After drying, the mesas stuck on the photoresist and they removed the rest of the HOPG. Then they started the thinning with an scotch tape. The photoresist was then removed in aceton and the thin flakes float in the solvent. Finally they dipped a Si wafer with a 300 nm SiO_2 into the solution and some flakes became captured

on the surface.
This method seemed to be a little bit complicated and precarious, so we did not give consideration to it. It should be also mentioned that even Novoselov and Geim modified and simplified this method in their later work [29].

3.1.1.7 Other micromechanical cleavage methods

Rubbing method: Another approach in the context of micromechanical cleavage is the separation of monolayers from the bulk crystal by rubbing it against another solid material similar to drawing with chalk on a blackboard. This method was used by Novoselov et al. in [27]. Besides graphene they also prepared other two dimensional materials (BN, MoS_2, $NbSe_2$ and $Bi_2Sr_2CaCu_2O_x$) in this study. Nemes-Incze et al. also used this method in their publication [64].

Pestling: In [65] Chuvilin et al. used an agate mortar in order to grind graphite under a layer of ethanol. After ultrasonication and deposition on a holey carbon TEM grid they found thin graphite flakes down to one layer in thickness.

3.2 Thermal decomposition

3.2.1 SiC

In this approach silicon carbide is annealed at high temperatures between 1000 and 1500 °C in ultra-high vacuum. On the surface of the SiC substrate epitaxial graphene is produced due to the sublimation of Si from the surface. The remaining carbon then forms graphitic structures on the material. The thickness and the quality of the obtained graphene, depends amongst other factors on the surface of the substrate (whether it is carbon- or silicon dominated). Although most of the methods reported use the Si surface, also C face synthesis of graphene on 6H-SiC is possible [22]. SiC is a rather insulating material with a band gap of around 3 eV (for 6H-SiC) and can thus be used as substrate material. Hence, no transfer may be necessary.
Berger et al. [66] used the Si face (SiC(0001)) of a 6H-SiC single crystal to produce graphitic structures (1-3 layers) and archived mobilities of 1100 cm^2/Vs. Initially they improved the surface quality by H_2 etching, and after removing the oxide layer by annealing at 1000 °C they heated the sample to 1250-1450 °C. The obtained thickness of the structures depends mainly on the temperature. Meanwhile it is possible to produce large area (wafer-scale) graphene layers with mobilities of up to 2000 cm^2/Vs ([67]). Along with the CVD method, the SiC decomposition technique is quite promising for graphene mass production, especially regarding semiconductor fabrication (see two interesting reviews for further reading: [10] and [68]).

3.2.2 Solid carbon sources

Sun et al. [69] demonstrated that also solid carbon sources atop a metal catalyst can be used for graphene production, similar to a CVD process. A PMMA thin film of around 100 nm thickness was spun on a copper film. Thus prepared samples were annealed for 10 minutes at temperatures between 800 and 1000 °C. Under low pressure conditions and in a reductive atmosphere (Ar and H_2) a single uniform graphene layer has been produced. The process is illustrated in figure 3.2.

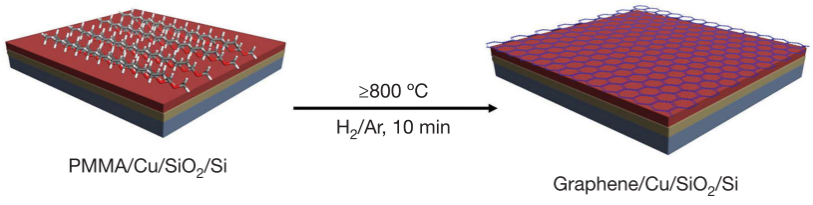

Figure 3.2: Illustration of the graphene production via a solid carbon source (adapted from [69])

3.3 Chemical vapor deposition (CVD)

Chemical vapor deposition (CVD) is a chemical process widely used in industry for depositing thin layers of solid materials with high purity on surfaces. This technique can also be used to grow thin graphite coatings down to one layer in thickness. Hydrocarbons are blown over the heated substrate surface. The result is strongly dependent on the surface material and the process parameters. Already in the early nineties monolayer graphite coatings were reported with mono crystalline TiC(111) [70] or Pt(111) [71] as substrate surface. Today CVD processes on polycrystalline substrates seem to be the most promising approaches for the cost efficient large scale production of graphene. Until now two substrate materials have come out to be best suited, nickel and copper. As precursor mostly methane and sometimes ethylene is used. Thus this section focuses on these materials.

3.3.1 Growth on Ni

Meanwhile a lot of different methods with nickel foils as substrate with slightly different parameters and varying hydrocarbon precursor gases can be found in literature. Hence just one example, the process used by Yu et al. [72], as a representative can be described in this work. They used a methane, hydrogen, argon - mixture as precursor gas where methane acts as carbon source. The Ni foils were annealed at 1000°C in a hydrogen atmosphere one hour before argon and methane were added while the pressure was kept at 1 atm. After 20 minutes they cooled the samples in Ar atmosphere. This step is critical for the thickness of the obtained graphene. Cooling to fast yields thicker coatings while to slow cooling rates prevent the carbon atoms segregating to the surface. See figure 3.3 for an illustration of this issue. Finally the substrate can be etched away (in HNO_3) so as to obtain free standing graphene or to transfer it to other substrates. The thickness varies between 1 to 4 layers (typically 3-4) at optimal conditions.
Addou et al. [73] demonstrated that at lower temperatures (550°C) growing of self limiting monolayer graphene, similar to the growth on copper substrates, also on Ni is possible.

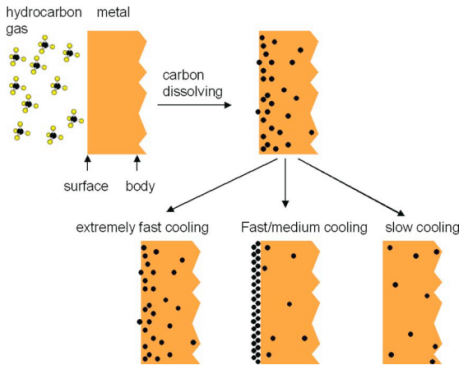

Figure 3.3: Illustration of the process of carbon segregation dependent on the cooling rate (from [72])

3.3.2 Growth on Cu

A technique similar to the one described above can be used to grow graphene on copper. Yu et al. also have developed a process with polycrystalline copper as substrate in a later work [74]. Another research group, Li et al. [75] used thin (25 µm) copper foils which were heated to 1000°C. Again at the beginning the surface was annealed with hydrogen. Then methane was blown over the surface, but in contrary to the method described above, at a very low pressure of 66 Pa and a flow rate of 35 sccm. The big advantage of this approach is the low solubility of carbon in copper at this pressures. Hence the growth of graphene is surface mediated and self limiting to one layer in thickness and thus independent of the growth time. The graphene crystals grow in domains of different orientation with gaps and defects in between, like illustrated in figure 3.4 on the left picture. Thus the carrier mobility of 4050 cm^2/Vs [75] is smaller than in mechanically exfoiled graphene. The size of the single domains can be controlled by variation of the temperature, methane partial pressure and flow rate as subsequently shown by Li et al. [76]. They also tried to fill the gaps by modifying the growth conditions. Actually they were able to rise the charge carrier mobility up to 16000 cm^2/Vs. Huang et al. [77] did STEM investigation of such grain boundaries as shown in figure 3.4 on the right picture.
Also the production of uniform bilayer graphene, with a similar method is possible as described by Lee et al. [78]. Bilayer graphene may be essential for semiconductor applications due to its band gap. Wassei et al. [79] also tried more complex hydrocarbons with more than one carbon atom per molecule, like ethane and propane as source for the selective grow of bilayer graphene on copper.

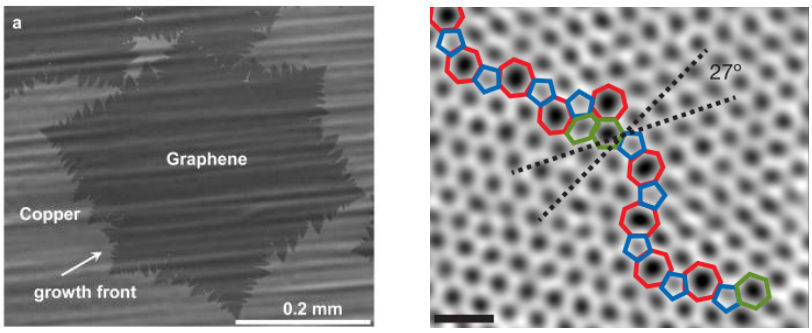

Figure 3.4: left: growth of a graphene crystal on copper (from [80]); right: structure of grain boundaries (ADF-STEM image adapted from [77], scale bar: 0.5 nm)

Bae et al. demonstrated the realizability of a large scale roll-to-roll graphene production process in [18]. They were able to fabricate a four layer graphene coated PET foil with their method with up to 30 inches in lateral size. The steps of their process are illustrated in figure 3.5 on the left. The right photograph in the figure shows the obtained graphene coated foil.

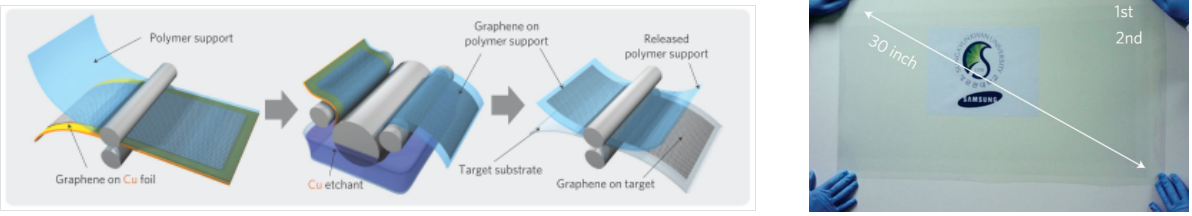

Figure 3.5: steps of a roll-on-roll process for the production of a graphene coated PET foil (from [18])

3.4 Liquid exfoliation

This section summarizes some important graphene production methods which take place in a liquid environment.

3.4.1 Reduction of graphene oxide (GO)

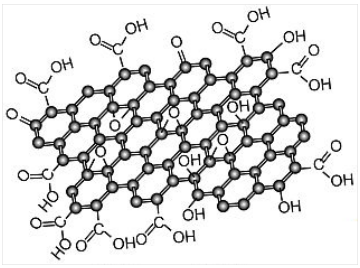

Figure 3.6: GO structure

Graphite oxide is an electrical insulating material with a similarly layered structure like graphite, but with other chemical groups, mainly epoxy bridges (>O), hydroxyl (-OH) and carboxyl (-COOH) groups, attached to some carbon atoms. Figure 3.6, adapted from [81], shows a schematic of the structure of GO. Hence the well-known planar and hexagonal lattice exhibits a lot of defects and irregularities and the interlayer distance is higher (0.71 nm), as shown in figure 3.7. In contrary to graphite, graphite oxide is hydrophilic due to the polar oxygen functional groups. This facilitates the exfoliation in a liquid ambience. Nair et al. [82] revealed that GO membranes are completely impermeable to liquids and gases except water (H_2O permeates 10^10 times faster through submicrometer-thick GO membranes than helium). GO flakes have been first synthesized in 1859 by Benjamin C. Brodie [83]. The reduction of graphene oxide was probably the first approach for the synthesis of SLG as it was already reported in 1961 by Boehm et al. [84]. For more information about the history of graphene research see [85].

3.4.1.1 Hummers method

Nearly all methods used for the synthesis of graphene oxide nowadays are derived from a method developed by Hummers and Offenman in 1957 [86]. They used an anhydrous mixture of sulfuric acid (H_2SO_4), potassium permanganate ($KMnO_4$) and sodium nitrate ($NaNO_3$) in order to oxidize graphite. After adding water, the flakes are separated due to the hydrophilic properties of GO. Figure 3.7 shows an illustration of the method.

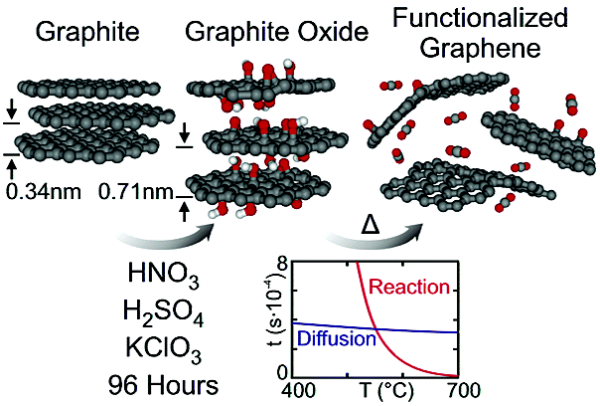

Figure 3.7: Hummers method for graphene oxide production (adapted from [87])

The process can be supported by heating and sonication (See [88] and [87] for more details). The main drawbacks of the Hummers method are the use of strong oxidizers, the small flake sizes (often referred to as graphene nanosheets) with uncontrollable thickness and the low quality of the obtained graphene flakes. In the meantime a lot of improved variations of the methods can be found in literature. Marcano et al. [89] for instance excluded $NaNO_3$ to improve the efficiency of the process.

3.4.1.2 Tang-Lau method

Another quite new approach for the production of GO is the Tang-Lau method developed by Tang et al. in 2012 [90]. It is a bottom-up assembly method using glucose, sugar or fructose dissolved in DI water as precursor. After heating at temperatures between 160 and 220°C in an autoclave lined with teflon for 70 to 660 minutes, the flakes were rinsed with water and annealed at 450 to 1300°C for 2 to 5 minutes.
Compared to the Hummers method this approach avoids some of the main drawbacks. It does not need any strong oxidizers and is thus safer and more facile to handle. Further by changing the process parameters the thickness and size (source concentration, reaction temperature, growth time) and the structural properties (annealing temperature and time) of the flakes can be controlled quite easily.

3.4.1.3 Reduction of GO

So as to obtain graphene from graphene oxide it has to be reduced. There are a lot of methods in different variations described in literature. Chemical reduction can be done for instance with reductants like hydrazine [91], dimethylhydrazine [92], ammonia [93], $NaBH_4$ [94] or ascorbic acid [95]. An electrochemical approach is described in [96]. See [97] for more details and a good overview over more chemical based reduction and exfoliation methods.
In order to reduce GO also heat or light can be used. A method using thermal annealing in an

argon atmosphere is described in [98] for instance. A light reduction method using a xenon flash lamp can be found in [99]. Eswaraiah et al. on the other hand used sun light [100]. Even microbial reduction is possible as demonstrated with bacteria in [81] and [101].
Graphene produced with the reduction of GO is always polluted with remaining functional groups and exhibits a lot of defects and imperfections. Thus generally the electron mobility is low compared with graphene prepared with other methods.

3.4.2 Direct exfoliation in a solvent

Graphite is highly hydrophobic and not soluble in common solvents like ethanol or isopropanol. Nevertheless, solvents with a proper surface tension in the range of the surface energy of graphite can be used for exfoliation in combination with low power ultrasonication (30 minutes) and centrifugation (90 minutes at 500 rmp) [102]. Hernandez et al. also tried different solvents in their work and they obtained graphene dispersions with a concentration of up to 0.01 mg/ml. Accordingly N-methylpyrrolidone (NMP), N,N-Dimethylacetamide (DMA), γ-butyrolactone (GBL) and 1,3-dimethyl-2-imidazolidinone (DMEU) seem to be suitable as solvents. High dispersion stabilities of up to 5 months were reported.
Nuvoli et al. [103] tried an ionic liquid, 1-hexyl-3-methyl-imidazolium hexafluorophosphate (HMIH). Ionic liquids are organic salts, fluid at temperatures below 100 °C. After ultrasonication over 24 hours and centrifugation (30 minutes at 4000 rpm) they obtained graphene concentrations of up to 5.33 mg/ml, which is the highest value reported so far in any solvent.
Blake et al. [104] archived a high percentage of up to 50 % monolayer graphene with DMF as solvent, 3 hours sonication and 10 min centrifugation at 13000 rpm.
The dispersions can then be used to superimpose graphene coatings on a substrate by spin casting or inkjet printing or can be dropped on a TEM grid.

3.5 Other methods

Since the graphene boom started with the publication of Novoselov and Geim in 2004, a large number of different methods for the graphene production have been published. Some mentionable methods besides those mentioned above are described in this section.

3.5.1 Metal carbon melt

By Amini et al. [105] a technique was proposed to produce large area graphene via a saturated solution of a molten transition metal (preferable copper or nickel) and carbon. To archive this, carbon atoms from a graphitic raw material were dissolved in nickel at a temperature of 1500 °C in an argon atmosphere. While cooling down the molten metal the solvability of carbon decreases and the atoms start to precipitate on the surface as FLG and SLG. The

thickness of the resulting graphene sheets can be controlled with the cooling rate. Figure 3.8 shows a SEM picture of thus produced SLG.

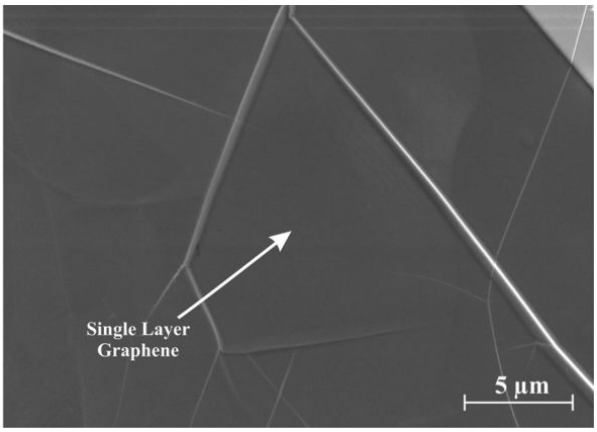

Figure 3.8: SEM picture of SLG on nickel produced with the metal carbon melting method ([105])

3.5.2 Plasma

It is possible to use a plasma in order to produce graphene. Dato et al. [106] presented a substrate-free gas-phase synthesis method in which a microwave argon plasma is used. In their patented process Argon containing small ethanol droplets is blown in the plasma reactor. During the residence time (about 0.1 s) of the droplets inside the plasma they dissociated to small graphene flakes. After rapid cooling they are collected on filters and sonicated in methanol, where they disperse easily and form a stable black suspension (see figure 3.9 for a illustration of the plasma graphene reactor). The obtained flakes are quite clean, because no chemical treatment is needed. However they are also quite small. The commercially available graphene enhanced lacey carbon TEM grids, used in this thesis as reference samples (see section 5.1 on page 43) were prepared with graphene synthesised with the substrate-free gas-phase method.

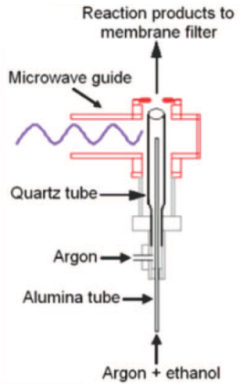

Figure 3.9: Plasma reactor (from [106])

Another way to produce graphene in a plasma is by using an arc-discharge as demonstrated by Subrahmanyam et al. [107] and Wu et al. [108] for instance.

3.5.3 Unzipping carbon nanotubes

Carbon nanotubes (CNT) can also be used as raw material for the production of small and slim graphene sheets (graphene nanoribbons) by 'unzipping'. That means that the tubular structures are opened up longitudinally. This can be done by intercalation of lithium and ammonia, as described by Cano-Márquez et al. [109], by plasma etching of CBN partly embedded in a

polymer film as reported by Jiao et al. [110] or substrate-free by unzipping multi-wall CNT in a multi-step chemical treatment process, including exfoliation, oxidation and reduction [111].

3.5.4 Bottom-up fabrication

A completely different approach is the bottom-up synthesis of graphene nanoribbons with molecular monomer precursors (PAHs - Polycyclic aromatic hydrocarbons) by surface assisted coupling. Some of the hydrogen atoms attached to the carbon atoms at the boarders of the PAHs can be substituted selectively with halogen atoms, like bromine or iodine. When they get in contact with a metal surface the carbon-halogen bondings break and the open bondings are linking to other open bondings. In this manner large polymers are formed. Figure 3.10 was adapted from [112] and shows an illustration of the process and STM pictures of the resulting zig-zag structures. This technique was reported by Cai et al. [113] and in [114]. It allows the atomically precise, defect free and tailored synthesis of complex graphene structures and therewith tuning of the electronic properties. Even the synthesis of electronic components is imaginable.

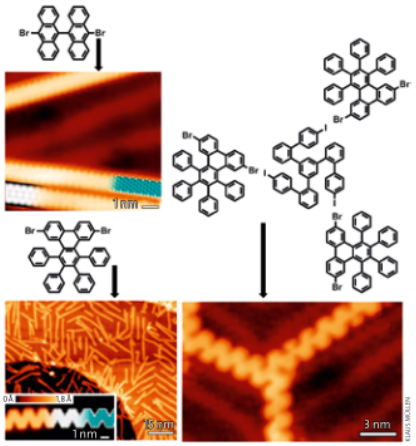

Figure 3.10: Surface-assisted coupling of halogene doped PAHs with STM pictures (from [112])

3.6 TEM grid transfer methods

Many of the presented graphene fabrication methods are substrate supported. In most cases the support material is not suitable for further applications, because it is conducting, changes the electronic properties of the supported sheets or free-standing graphene is needed for TEM investigations, for instance. Thus many different methods have been developed in order to transfer graphene to arbitrary substrates. For example Regan et al. [115] presented a method for transferring CVD graphene from a copper substrate to a TEM grid and Reina et al. [116] on the other hand reported a method for the transfer of graphene flakes prepared on a SiO_2 to potentially any type of substrate. Anyhow, this section will focus on processes used for the transfer of graphene from SiO_2 substrates to a TEM-grid, since they are important for the experimental work of this study. Three different methods, developed by Meyer and co-workers [117, 118] will be described briefly in the following listing:

1. A holey carbon Au TEM grid with mesh size 200 and a hole size of 1 µm is placed onto a chosen graphene flake and pulled into contact by the surface tension of an evaporating isopropanol drop. Then the sample is heated at 200 °C for 5 minutes on a hot plate.

Subsequently a second drop of solvent is carefully placed next to the TEM grid and squeezes in between the grid and the substrate, lifting the TEM grid gain. Only about 25 % of the graphene flakes stick on the TEM grid, but no acids, bases or polymers are needed.

2. Again a holey carbon TEM grid is pulled into contact by means of a drop of isopropanol. After heating at 200 °C for 5 minutes on a hot plate the SiO_2 substrate is dissolved in a 30 % solution of semiconductor grade potassium hydroxide. When the grid falls off it is cleaned in a water bath without drying and afterwards in isopropanol.

3. In this approach graphene is prepared on a 300 nm SiO_2 substrate coated with a 10-30 nm layer of PMMA. A holey carbon TEM grid is placed on a chosen graphene flake and pulled into contact via an evaporating solvent. After drying on a hot plate the PMMA coating is etched with acetone or methylpyrrolidone. Although SLG flakes are reported to break more frequently in this method, no acids or bases are needed.

Right before the samples were inserted in a TEM, they were heated on a hot plate for 10 to 15 minutes at 200 °C in order to reduce the amount of adsorbates. Additionally it is possible to stabilize thin regions prior to the heat treatment by electron beam activated deposition of hydrocarbons on their edges by means of a TEM or SEM, since they tend to fold up during the pre-TEM heating treatment, as recommended by [119]. This was omitted in this study, so as to keep the process as simple as possible and prevent additional contamination of adjacent regions. All of the three methods were tested and method 3 was then chosen as starting point for our experiments (see 5.4.3).
Another approach to obtain free standing graphene without using a holey carbon TEM grid, is to deposit a metal grid (3 nm Cr and100 nm Au) on top of a graphene flake via electron-beam lithography as described in [14]. Afterwards the Si is etched with 15 % tetramethylammonium hydroxide at 60 °C until a part of the grid becomes overhanging. The remaining SiO_2 is then removed in 6 % buffered hydrofluoric acid. Finally the remaining grid with the attached free standing graphene sheets is cleaned in water, isopropanol and acetone and critical point dried with liquid carbon dioxide.

4 Characterisation

4.1 Optical microscopy

Among these flakes there are only a few very thin flakes and only some of them may be few layer- (FLG) or even bi- or single-layer graphene (SLG). Almost all methods which can be used for graphene investigations on a substrate, like AFM, Raman or SEM, have a very low throughput and are thus inapplicable for finding graphene on a large area. Therefore we have to use optical identification methods. Considering the very low absorption of light for SLG of around $2,3\%$ [120] (see chapter 2.2) this seems to be very difficult. Anyhow, in order to find the thin regions among the other pieces we can use an optical trick: The SiO_2 capping on the wafer acts like an optical anti reflection coating. For a certain wavelength of the incident white light the condition for destructive interference is fulfilled for a given coating thickness value. This is actually the reason for Si wafers exhibiting different surface colors depending on their SiO_2 coatings. Figure 4.1 shows the calculated color of reflected light over the SiO_2-thickness of such a wafer. Thus we have to choose the thickness of the SiO_2 - coating so that the increase of the optical path due to a graphene flake lying on the SiO_2 yields to a change of the color of the reflected light.

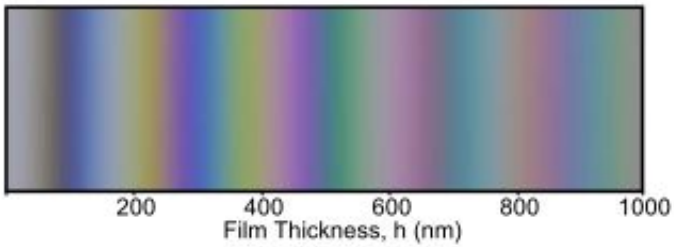

Figure 4.1: Calculated color of reflected light of a SiO_2 coated Si wafer over the coating thickness (from [121])

Calculation of the contrast of SLG on SiO_2 substrate with equation 4.1 for different wavelengths of incident light yields to the diagram shown in figure 4.2. It shows the expected contrast C over the SiO_2 thickness and wavelength. The red lines are indicating preferable thickness values. Furthermore one can see in this picture, that any substrate thickness can be used, except values below 30 nm and around 150 nm to obtain contrast for a certain wavelength.

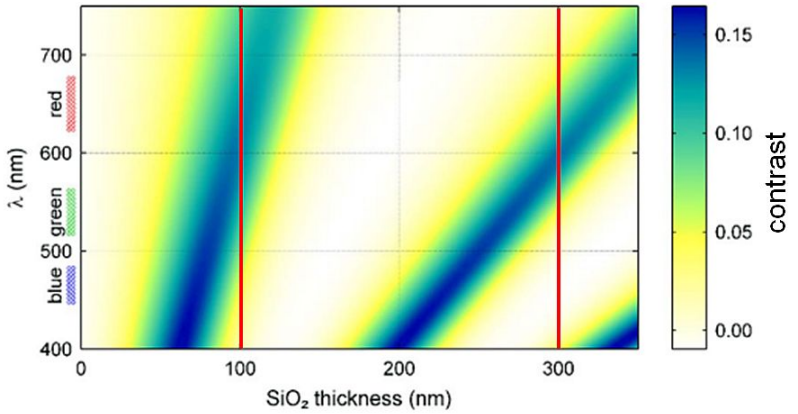

Figure 4.2: Expected contrast C over the SiO_2 thickness and wavelength (adapted from [122])

Nevertheless, if one takes in account the characteristics of the human eye and the fact that we use white light, wavelengths around 500 - 600 nm seem to be most appropriate (see equation 4.3). Accordingly this results in a color shift to blue for the reflected light. This is why in our experiments SiO_2 coatings with a thickness of 100 nm and 500 nm were used. The benchmark value in most publications, also used by Novoselov et. al. [1], is 300 nm. Blake et al. [122] recommended 90 nm for best results.

$$C = \frac{I_0 - I_{SLG}}{I_0} \tag{4.1}$$

I_0... intensity of reflected light without graphene
I_{SLG}... intensity of reflected light with attached SLG

Equation 4.2 describes a typical anti reflection (AR) coating where $n_{air} < n_{SiO_2} < n_{Si}$ (with $n_{air} \simeq 1$). Because of this, there will be an overall phase shift of $\lambda/2$ for destructive interference, $\lambda/4$ from the air/SiO_2 interface and again $\lambda/4$ from the reflection at the SiO_2/Si interface. See figure 4.3 for a schematic representation of the optical path.

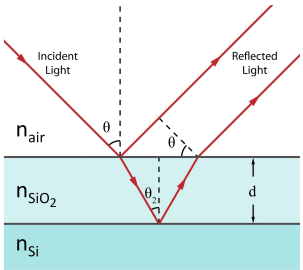

Figure 4.3: Optical path

$$2 \cdot n_{SiO_2} \cdot d \cdot cos(\theta) = (m - \frac{1}{2}) \cdot \lambda \tag{4.2}$$

In this case we assume perpendicular irradiation, $\Theta = 0$. Then the thickness for the AR - coating can be described with equation 4.3.

$$d = (m - \frac{1}{2}) \cdot \frac{\lambda}{2 \cdot n_{SiO_2}} \tag{4.3}$$

Applying n_{SiO_2}=1,47 and λ=550 nm (should be 500 nm to 600 nm, as mentioned above) to equation 4.3 delivers ideal thickness values d for the SiO_2 coating of 93,5 nm (m=1), 260,6 nm (m=2) and 467,7 nm (m=3). Thus, 100 nm, 300 nm and 500 nm seem to be good values for a suitable AR-coating for identifying graphene. The picture in figure 4.4 shows the typical color shift of graphene on 285 nm SiO_2 with rising layer counts. In this picture the images labeled with letters 'a' to 'f' show more than 10 layers with increasing thickness.

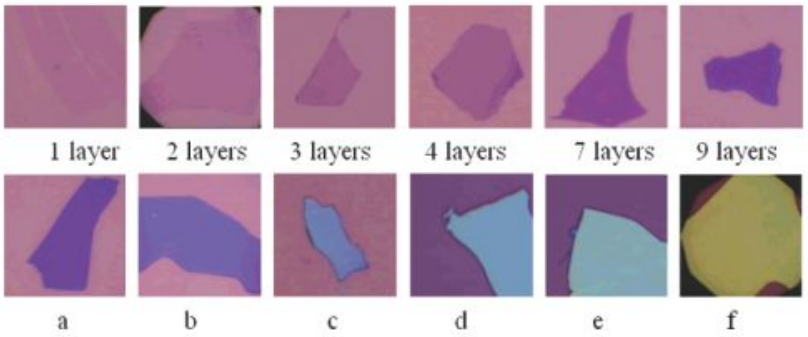

Figure 4.4: color shift of graphene and graphite on 285 nm SiO_2 (from [123])

In practice the contrast and the colour shift also strongly depend on the used light source, the numerical aperture ($\Theta \neq 0$ in equ. 4.3), the camera and other characteristics of the used optical instruments. Hence the visibility of the flakes is also dependent on the used magnification due to the properties of the objective.
It is even possible to do absolute thickness determination of graphene on SiO_2 by means of optical contrast without the need for knowing the value for SLG as reference. Ni et al. [123] showed this technique on 300 nm substrate. For further reading on this issues [122], [124] and [125] are recommended.

4.2 Raman spectroscopy

Raman spectroscopy is the most important characterization method for graphene related phonon mode investigations. The in-plane modes, which are the Raman active ones, consist of two acoustic modes (TA and LA) and two optical modes (TO and LO). Additionally there are two out of plane modes (ZA and ZO), which have a dispersion relation with a cone structure near the K-points, similar to the electronic structure. Figure 4.5 shows the calculated phonon dispersion in the left diagram.

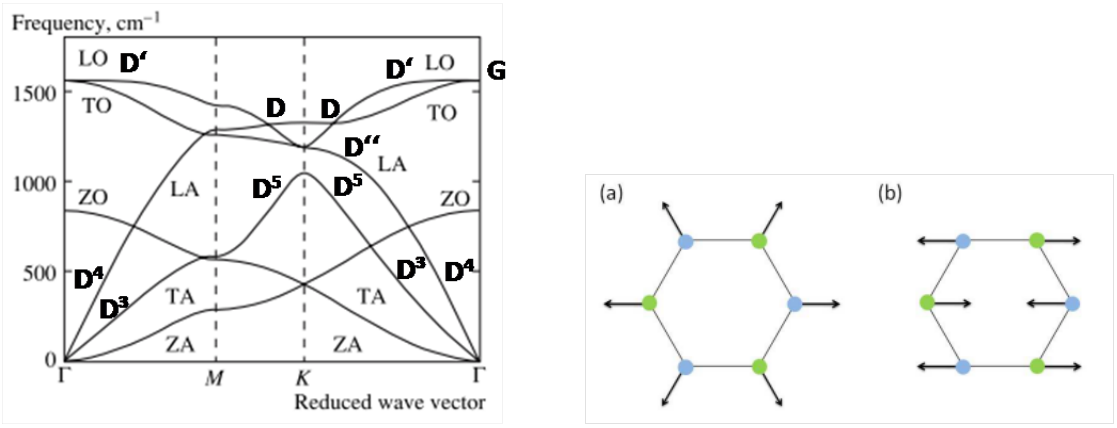

Figure 4.5: Left: Calculated phonon dispersion relations with the four Raman active in-plane modes (TA, LA, TO, LO) and the two out of plane modes (ZA, ZO) with the labels (D,G,...) corresponding to the Raman peaks (edited from [126]); right: oscillations of the carbon atoms corresponding to the graphene modes, a) D-mode, b) G-mode (from [127])

The most important characteristic Raman peaks of graphene are the G, 2D and the D peak. The G mode at the Brillouin zone centre is double degenerated (TO and LO). A representation of the oscillation mode can be seen in figure 4.5 on the right (picture b). The corresponding G peak in the Raman spectrum is located at $\sim$1580 cm^{-1}. Its intensity increases with the number of layers of the graphene sheet (see figure 4.6). It can also be used for doping investigations, since electron or hole doping is reflected in the sharpness of the peak [128]. The D mode (at $\sim$1350 cm^{-1} originates from the branches around the K-point (figure 4.5 picture a) and is forbidden in a defect free lattice. It can thus be used as indicator for defect concentration. Finally the 2D-peak (historically also referred to as G'), is sensitive to the stacking order of FLG. Its size, form and position is also strongly dependent on the thickness of a graphene sheet. For SLG it is a narrow (with a FWHM of $\sim$30 cm^{-1}), single peak at $\sim$2680 cm^{-1}, with an intensity 2-3 times the intensity of the G-peak. For bilayer graphene it is a superposition of four peaks [127], with a remarkably lower intensity and a slight shift to higher wave numbers. The origin of the 2D-peak is a bit more complicated and can be explained with a double-resonance process (see [129] or [127] for more information on Raman scattering mechanisms in graphene). The diagram in figure 4.6 on the left shows typical Raman spectra dependent on the thickness.

4.2.1 Raman thickness maps

In order to generate a thickness map of an area with graphene lying on a substrate, the region of interest is scanned pixel per pixel with a laser and for each pixel a Raman spectrum is recorded. Subsequently one can use a feature in the spectra characteristic for SLG, so as to identify monolayers in the map. Wang et al. [128] chose the intensity of the G peak, since it increases with increasing layer count (figure 4.6 on the left). Although different thickness values can be distinguished, an absolute determination is not possible with this method. Spatially

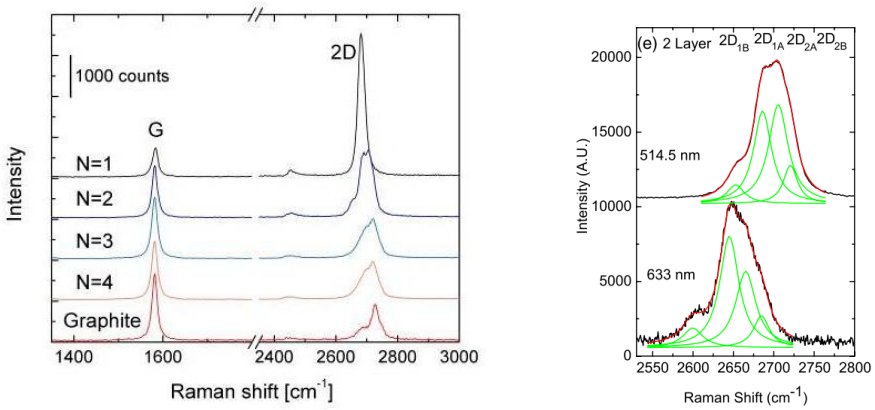

Figure 4.6: Left: Typical Raman spectra for different layer numbers N of graphene on SiO_2 (from [10]); right: close up view of the 2D-peak of bilayer graphene, consisting of 4 Lorentzian peaks (named $2D_{1B}$, $2D_{1A}$, $2D_{2A}$, $2D_{2B}$), for two different excitation wave lengths (514.5 and 633 nm)(from [130])

resolved Raman spectroscopy was also done by Graf et al. [131, 132] by using for instance the small shift of the G-peak or the FWHM of the 2D-peak. Yu et al. did investigations of grain boundaries of CVD graphene [74] via Raman thickness maps generated with different methods in comparison.
However, in the present work a different method was used. The 2D peak was fitted with 2 or 3 Lorentz peaks and the position, intensity and sharpness of the component corresponding to single layer graphene was then used as signature. By this means it was possible to distinguish SLG from FLG on a Raman thickness map quite reliably (see figure 5.16 on page 56 and figure 5.20 on page 60 per example) even though it is difficult to distinguish between two and more layers due to the complex 2D-peak composition.
A combination of both methods, by using the G-peak intensity of a single layer pre-identified via the 2D peak as reference, may be a promising improvement, but has not been tried so far.

4.3 Transmission electron microscopy (TEM)

TEM and its various modes, like STEM and analytical TEM, are the best suited methods for investigations of free-standing graphene and other two-dimensional materials at high (even atomic) resolution, in terms of structure, morphology and thickness for instance. In the scope of the present study we put the focus on the thickness determination via TEM-based techniques, so as to prove the succeeded preparation of SLG with our methods.
Furthermore graphene, deposited on a TEM grid is, due to its mono-atomic thickness, the ideal supporting material for other specimens, for example nano-particles, atomic clusters or biological samples. Even a liquid can be encapsulated betwixt graphene layers, as demonstrated by [133] (see chapter 6).

4.3.1 High resolution transmission electron microscopy (HRTEM)

Some of the most important graphene related HRTEM investigations were performed by Meyer and his co-workers in their publications [14, 119] for instance. Some of the methods presented there, were also used in the present thesis, especially concerning the transfer of samples to a TEM grid (see section 5.4.3).

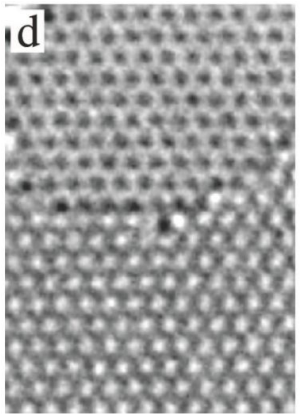

Figure 4.7: HRTEM picture of SLG (top) and BLG (bottom) [119]

For non-destructive studies an operating voltage below the knock-on damage threshold value is necessary (below 100 kV, see section 4.3.6). So as to obtain atomic resolution at low beam energies an aberration-corrected instrument is needed. Since in a TEM image at high resolution the contrast originates from the interference of the electron wave with itself (phase contrast), it is highly dependent on the thickness of the sample and the focus of the beam. In the case of SLG of course, the phase-contrast variation due to the thickness can be neglected. This is possible even for FLG, because every layer can be assumed to be in the same focus, due to the small interlayer distance. The obtained image can thus be interpreted directly. However also the tilt angle and accordingly the characteristic wrinkles of free standing graphene affect the contrast. In [119] a small positive defocus (8 nm) was used, which yielded a white atom contrast. For instance figure 4.7 shows a bright field TEM image (TEAM 0.5 TEM, monochromated, @80 kV, high-pass filtered), which was taken from the latter article, depicting SLG on the upper half and bilayer graphene on the bottom. White dots arise in the bilayer region where two carbon atoms are lying upon each other in regular AB- (or Bernal-) stacking.

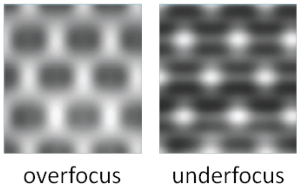

Figure 4.8: BF images of SLG with different focus [134]

However, during the interpretation it must be considered that at a different defocus a single layer area may appear as bilayer and vice versa. To back up the results, electron diffraction analysis was used in [119]. Figure 4.8 shows an example for two bright field phase contrast images of SLG, acquired with an overfocused (left) respectively underfocused (right) beam. The image was adapted from the very recommended, freely available book 'Physics and Applications of Graphene - Experiments' which was written by various authors and edited by Sergey Mikhailov [134].

4.3.2 Scanning transmission electron microscopy (STEM)

In a STEM a very focussed (ideally less than 0.1 nm) electron probe is scanned over the sample. Since the depth of focus is quite small even atomic resolution can be archived in bright field (BF) as well as in annular dark-field (ADF) and high-angle annular dark-field (HAADF)

mode. STEM imaging at atomic resolution is the best way for investigations on free-standing graphene in terms of structure, defects and chemistry, and was performed by several groups. The ADF and HAADF modes are the preferred modes because thus gained images can be interpreted quite straight forwardly compared to BF pictures based on phase contrast. It can for instance be used to distinguish single atoms of different species with an atomic number of $Z \geq 6$ (for HAADF, with ADF also single boron atoms with Z=5 were detected [135]) on or in the graphene lattice due to the Z^2 dependent scattering probability of electrons on atoms. Gass at al. [136] for instance demonstrated graphene lattice defect analysis via HAADF STEM at atomic scale complemented with thickness determination via STEM EELS using the plasmon peaks (see 4.3.4.1). Figure 4.9 shows a comparison of the same area acquired in BF-mode on the left and in HAADF-mode on the right.

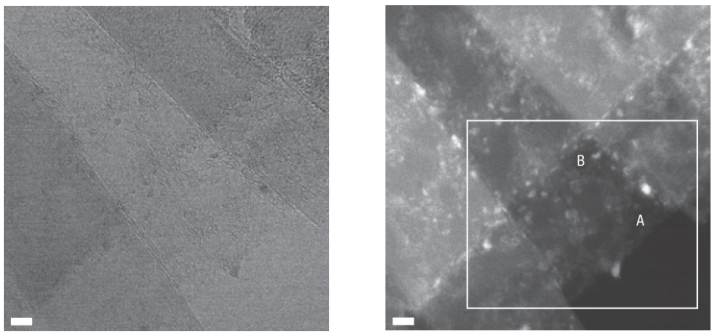

Figure 4.9: BF (left) and HAADF (right) picture of a graphene sheet containing different thicknesses in comparison, the letters A and B indicate a single- respectively a double- layer region on the right image (from [136])

4.3.2.1 Intensity profiles

The intensity relations between areas with different thickness on a (S)TEM image can also be used to gain information about the number of layers in each area. The intensity exhibits a linear dependency on the thickness for thin samples. In combination with other methods even an absolute determination is possible. Figure 4.14 for instance shows the intensity relations of areas containing one, two and five layers, which were used complementary to the thickness determination via EELS spectra in this case. Gass et al. [136] determined factors between 1,86$\pm$0.86 and 2,7$\pm$1,07 for a bilayer respectively 5$\pm$0.43 for five layers, each relative to the background subtracted intensity measured for SLG in HAADF. Figure 4.10 shows a STEM HAADF image with the intensity profile along the trace marked with the cyan box.

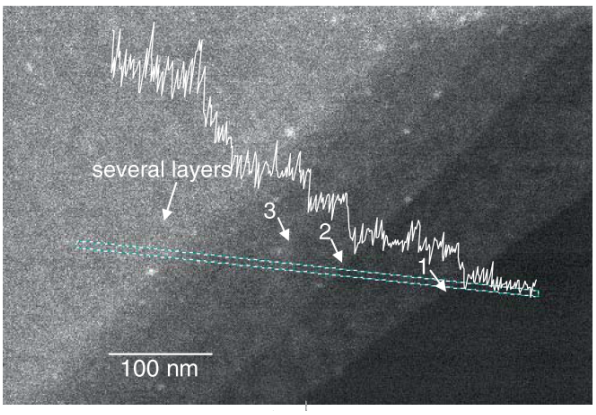

Figure 4.10: STEM HAADF image of graphene with different number of layers with an overlaid intensity profile along the cyan boxed trace (from [137])

4.3.3 Image processing

4.3.3.1 FFT filtering

In order to get rid of noise a low-pass filter with a rather smooth cut-off (∼5-10 % of the total image width) can be used. On the other hand a high-pass filter reduces the effect of an uneven illumination. Combining both filters results in a bandpass filter of which the exact parameters (cut-of position and sharpness of the cut-off edge) depend on the concrete case. This can be archived by a Fourier transformation (FFT) of the (S)TEM picture, applying a ring filter mask and transforming it back again (IFFT). Figure 4.11 illustrates these steps, performed in DigitalMicrograph via the ring masking tool.

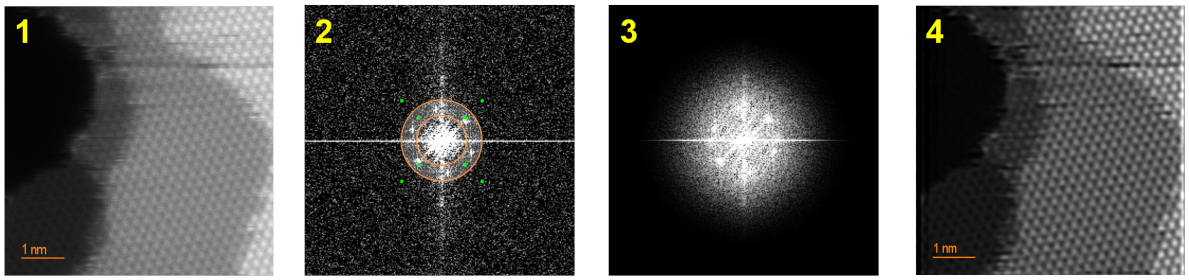

Figure 4.11: Filtering steps: 1) original STEM HAADF image (1024 x 1024 pixels, FEI Titan^3™@ 80 kV) of a graphene sheet with varying thickness, 2) FFT of the original picture with a ring filter mask (white shadowed ring marked with orange boarders), 3) Spectrum after applying the mask with a cutting-edge size of 50 pixels, 4) filtered image after IFFT adjusted in contrast

By applying adequate hexagonal filter masks in combination with bandpass filtering these results can be further improved (see the experimental results of the present thesis 5.4.3.3 on page 69).
This technique can even be used to distinguish the single layers of turbostratic graphene. This means graphene with at least two layers where the hexagonal lattices of the single sheets are

rotated at arbitrary angles with respect to each other. Such kind of graphene exhibits various MoirÃl' patterns in an HRTEM image, dependent on the number of layers and the rotation angles. Thus the sets of 6 points in the FFT picture, which correspond to each layer are also rotated by the same angles. By applying a hexagonal filter mask and performing an inverse Fourier transformation for each layer, they can be distinguished from one another. Warner et al. [138] demonstrated that up to 6 layers can be distinguished via a HRTEM picture. This has also been performed on a bilayer in the present thesis in the experimental section (5.4.3.2 on page 66).

4.3.3.2 Exit-wave reconstruction

Besides conventional FFT filtering, using band pass filters and filtering masks another approach, called electron exit-wave reconstruction, receives more and more attention. The electron beam can be treated as wavefuntion of an electron wave field. In order to examine the exact atom positions of a crystal with the highest possible resolution, one has to reconstruct the wavefunktion of the electrons leaving the specimen (called exit-wave plane). Therefore both phase and amplitude of the electron wave must be determined in the image plane. Unfortunately only the amplitude can be recorded directly. For this purpose TEM holography, which is experimentally rather complex, or focal series can be used. For the latter a series of HRTEM images, each with different focus, has to be acquired. Jinschek et al. [139] demonstrated this technique by means of graphene. For the image depicted in figure 4.12 a series consisting of 19 images was captured under the same conditions, with defocus values starting from +11 nm with a step of -1.7 nm and a acquisition time of 0.1 s for each picture. A C_s corrected TEAM instrument at NCEM, operated at 80 kV was used. For evaluation FEI's Trueimage software package was used.

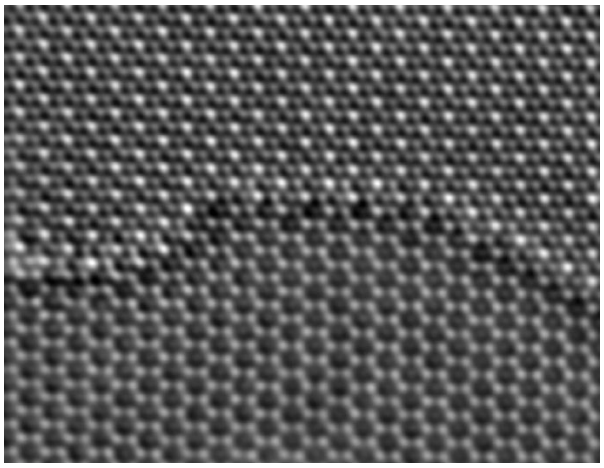

Figure 4.12: Exit-wave reconstructed HRTEM image of single- and bilayer graphene with atomic resolution (taken from [140] who cited [139])

4.3.4 Electron energy loss spectroscopy (EELS)

In EELS an electron beam with a specific and narrow energy distribution is used to characterise the elemental composition of a material in a TEM equipped with an EEL spectrometer. Some electrons will be scattered inelastically while passing the atoms of the material, whereupon they lose a characteristic amount of energy. The energy loss can be measured and interpreted in terms of its origin. One possible reason besides ionizations, phonon excitations, band transitions and Čerenkov radiation is the excitation of plasmon modes. These plasmon excitations are very useful for graphene investigations.

4.3.4.1 Plasmons

For the plasmon behaviour of graphene the local electronic bandstructure and electron density are crucial. Thus EEL spectra of the low energy loss region can be used for doping investigations, especially in terms of hydrogen and other elements with Z$\leq$6 which are not accessible via HAADF [141]. Plasmon excitations in graphene can also be used for thickness estimation since they exhibit a characteristic peak structure in electron energy loss spectra since the plasmon peaks shift to lower energies for thinner structures. In principle one can distinguish between a bulk and a surface plasmon mode, each with contributions of in-plane and out-of-plane excitations. However, the latter are rather weak due to the weak interlayer coupling. In both of them either only π-bonded electrons (π-peak) or all valence electrons (σ-π - peak) can be involved. In bulk HOPG the π-peak (corresponding to the π-π* - transition) can be found at 6.5 eV in an EEL spectrum, whereas the σ-π - peak can be found at 27 eV [142]. The diagram on the top left of figure 4.13) depicts the EEL spectrum of the plasmon region with the characteristic peaks of graphite. The peaks at 12.5 eV and 19.5 eV shown in this spectrum originate from a $\sigma - \sigma*$-transition and the out-of-plane mode respectively and are less important for our analysis.
In SLG the bulk plasmon mode vanishes and only the surface mode can exist. Accordingly the π-peak occurs at 4.7 eV and the σ-π - surface peak can be found at 14.8 eV, whereas the graphite bulk peak at 27 eV is not present [137, 143]. The diagram in figure 4.14 illustrates this behaviour dependent on the number of layers. The position and the triangular shape of the σ-π - peak is the best indicator for SLG. Bi- and few layer graphene exhibits a shift to higher energy losses and a remarkable broadening of the peak to a plateau form (compare 5.4.3.3 of the experimental section on page 69). For ten and more layers the plasmon peak structure resembles that of graphite (compare figure 4.13).

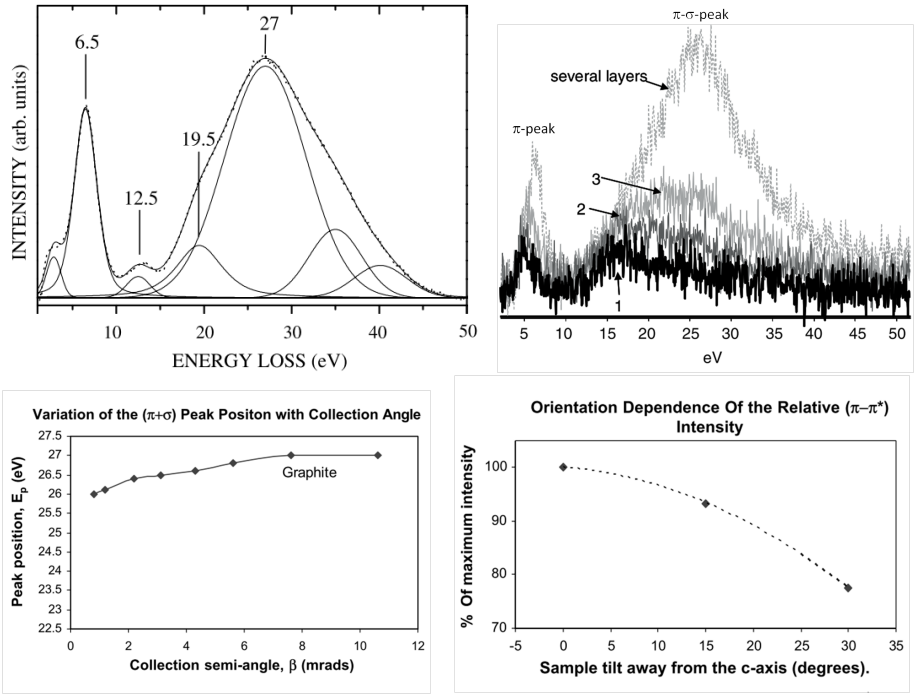

Figure 4.13: Top left: EEL spectrum of HOPG with the individual mode contributions, with experimental data points and fits (from [142]); top right: EEL spectra of graphene with different numbers of layers (adapted from [137]); bottom left: σ-π - peak position dependent on the collection semi-angle of the electron beam; bottom right: the relative π-peak intensity dependent on the sample tilt [144]

The **E** field of an moving charged particle, like an electron in an electron beam, is elongated along its travelling direction. Thus, mainly out-of-plane modes (momentum $\hbar\mathbf{q} \parallel \mathbf{E}$) should be excited when a electron passes a graphene sheet in perpendicular direction, which however are forbidden in SLG. Certainly, in a (S)TEM **q** always has a small in-plane component due to the collection angle of several mrad. Hence also modes parallel to the lattice vector **a** will be excited. This has to be considered during the interpretation of the results since the peak-positions and -intensities are dependent on the sample tilt and the collection angle as demonstrated by [144] by means of HOPG. The diagrams on the bottom line of figure 4.13 show the dependency of the σ-π - peak position on the collection angle of the electron beam (on the left) respectively the relative intensity of the π-peak as a function of the sample tilt angle. This variations due to the experimental conditions may be the reason for the different positions of the σ-π - peak in different studies (compare the spectrum for SLG in figure 4.13 on the top right diagram with a peak position above 15 eV with the spectrum depicted in figure 4.14 and exhibiting a peak maximum below 15 eV). Since typically surface contamination, which disturbs the measurements, can be found all over a graphene sample, leaving only small clean areas, this method needs to be performed localized. Hence the STEM mode is best suited for acquiring highly spatially resolved EEL spectra.

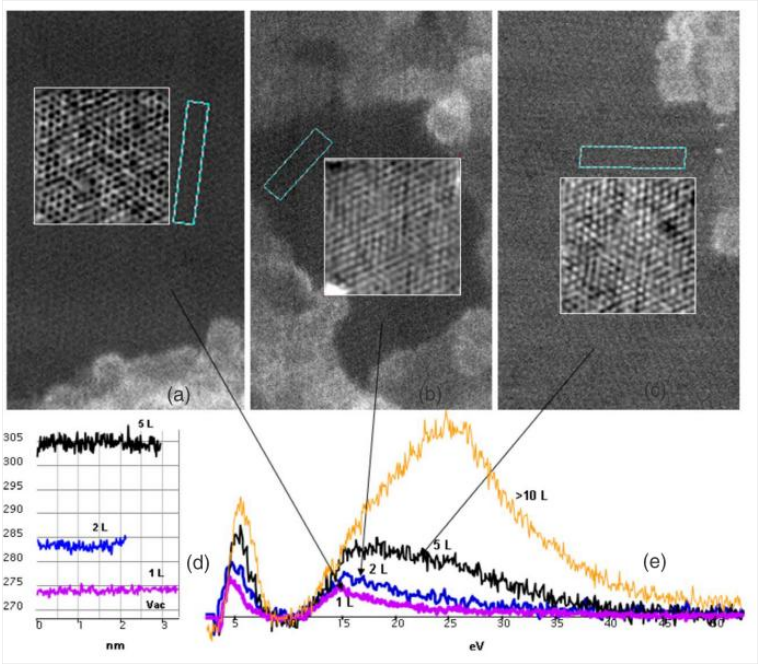

Figure 4.14: (a)-(c) HAADF STEM images of three different graphene areas revealing one, two and five layers; the white box in each picture shows a low pass filtered close up; the cyan rectangles mark the intensity traces (shown in diagram (d)) recorded along their long dimensions, diagram (e) depicts the EEL spectra for each area summed over 25 pixels (from [143])

4.3.5 Counting layers at the edge

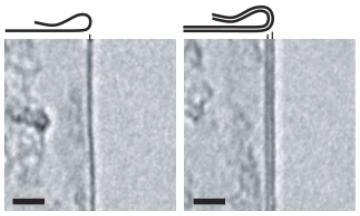

Figure 4.15: Single- (left) and bilayer graphene edge (HRTEM)

Graphene sheets tend to fold up at their edges. At such a fold the sheet is locally parallel to the electron beam and hence exhibits a strong contrast, resulting in a single line for SLG (see figure 4.15 on the left). Consequently, the thickness of FLG can also be estimated in first approximation by counting the dark lines at the boarder of a flake, separated by 0.34 nm from one another. Figure 4.15 shows two bright field HRTEM images (adapted from [14], scale bars: 2 nm) of SLG on the left, whereas the edge on the right picture may correspond to a bilayer sheet. The illustration in figure 4.16 depicts other possible formations of a double line.

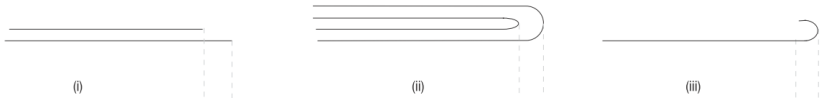

Figure 4.16: Three ways how a double line at a graphene edge can be composed of: i) staggered edges of bilayer graphene, ii) bilayer completely folded back, iii) SLG forming a nanotube on the edge (from [136])

4.3.6 Beam damage

Details of the interaction effects of accelerated electrons with graphene are still relatively unknown in detail and have received only little attention. The knock-on damage of single wall carbon nano-tubes (SWCNT) in terms of irradiation with an electron beam is believed to be at 86 keV. A similar value was assumed for graphene, due to the similar structure [145, 146]. Zobelli et al. [146] on the other hand showed that graphene exhibits greater stability than SWCNT, which was confirmed by [119]. In a 80 keV beam each electron can transfer a maximum energy of 15.73 eV to a carbon atom [147], which is below the knock-on threshold value of 23 eV, what corresponds to a beam energy of 113 keV [146]. These values are valid in the case of saturated carbon atoms. For unsaturated atoms at the edges of a layer the knock-on damage energy threshold is quite evidently lower, which was also clearly visible in our experiments. Warner et al. [147] and Girit et al. [148] performed HRTEM investigations on this edge-thinning effect. Suenaga et al. [149] on the other hand performed EELS at atomic resolution on graphene edges.
Nevertheless beam damage also occurs at lower acceleration voltages, far below the knock-on threshold. Due to radiolysis the crystalline graphene lattice turns to a nano-crystalline sheet and after further irradiation to amorphous carbon (mainly sp^2 hybridised), forming an amorphous membrane. Additionally the sample suffers a heating effect due to the excitation of phonons and plasmons. Both effects of course also depend strongly on the irradiation dose [145] and may thus become less evident at the typical low current densities in a TEM. Kotakoski et al. [150] performed aberration-corrected HRTEM investigations (@80-100 keV) of such amorphized graphene sheets in an FEI Titan 80-300. For a more detailed view on this topic also the publication of Egerton et al. [151] is recommended.

4.4 Scanning electron microscope (SEM)

SEM is frequently used to perform topographic investigation of graphene on arbitrary substrates. To this end the instruments are preferably operated below 5 keV, because of the low thickness fo graphene. The topographic contrast is mainly composed of the thickness contrast, the edge contrast and the surface roughness contrast. Figure 4.17 illustrates the contrast mechanisms in terms of corrugations and edges. Since the interaction process of the beam electrons with the specimen is very complex it can only be sketched very roughly in the scope of this section. The craggier the surface the more secondary electrons (SE) are produced and thus the intensity is higher. This is why at the edges more SE are detected because they can escape in a higher quantity. However in practice an even higher edge intensity is observed, which can be explained with an additional electron beam induced current (EBIC) [152].
Hiura et al. [153] showed that even individual layers can be distinguished in a SEM by contrast. They found a linear relationship between the contrast on insulating substrates and the number of layers. On the contrary, on conducting substrates a exponential decrease of the intensity with the number of layers can be observed [152].

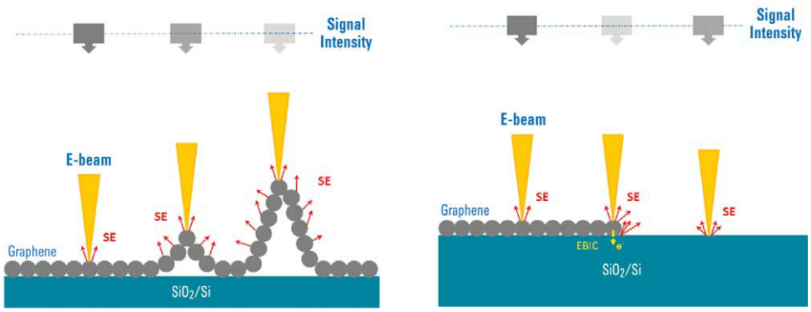

Figure 4.17: Contrast mechanisms of roughness (left) and edges (right) of graphene on SiO_2, the markers on the top of the pictures represent the intensity changings (adapted from [152])

4.5 Atomic force microscope (AFM)

AFM is also a common tool to do thickness investigations of graphene on a substrate. To this end it is mostly operated in tapping mode (TAFM) or in non-contact mode. A large variation of determined thickness values of graphene is reported in literature, ranging from 3.5 Å to 10 Å [64], relative to the substrate surface (SiO_2). Ishigami et al. [154] for instance reported values between 4.2 Å to 9 Å (non-contact mode), depending whether the measurements were performed in vacuum or in air. They reasoned this with the presence of ambient species (especially water) on or beneath the graphene sheets. Novoselov et al. also did extensive AFM studies, presented in the supplement of [1]. They determined values between 5 Å to 10 Å. In general AFM height measurements of graphene sheets are dependent on the measurement conditions (the tapping free amplitude has a strong influence [64]) and sample preparation methods.
Two different approaches for the step height evaluation were used in this work, height profiles (as used by [64]) and height histograms (used by [154]). Both were gained from the AFM topography image as described in chapter 5.
Furthermore the mechanical properties on graphene can be investigated via AFM nanoindentation [31, 155].

5 Experiments

5.1 Commercial available reference samples

5.1.1 Ni-CVD

The Ni-CVD samples were purchased from "Graphene Supermarket" [156]. They are produced by chemical vapour deposition on nickel, as described in 3.3, followed by dissolution of the Ni substrate with a subsequent transfer of the graphene film to a common copper TEM grid with, or alternatively without, a lacey carbon scaffold. This grids will be called GSM-grids in the following. A bright field TEM picture of a GSM grid without a lacey carbon scaffold can be seen on the left image of figure 5.1. The different shades of grey in this picture mark areas with varying thickness. The right image in figure 5.1 shows a picture of a lacey carbon GSM-grid taken with an optical microscope, where even here a lot of unknown blueish contamination is visible.

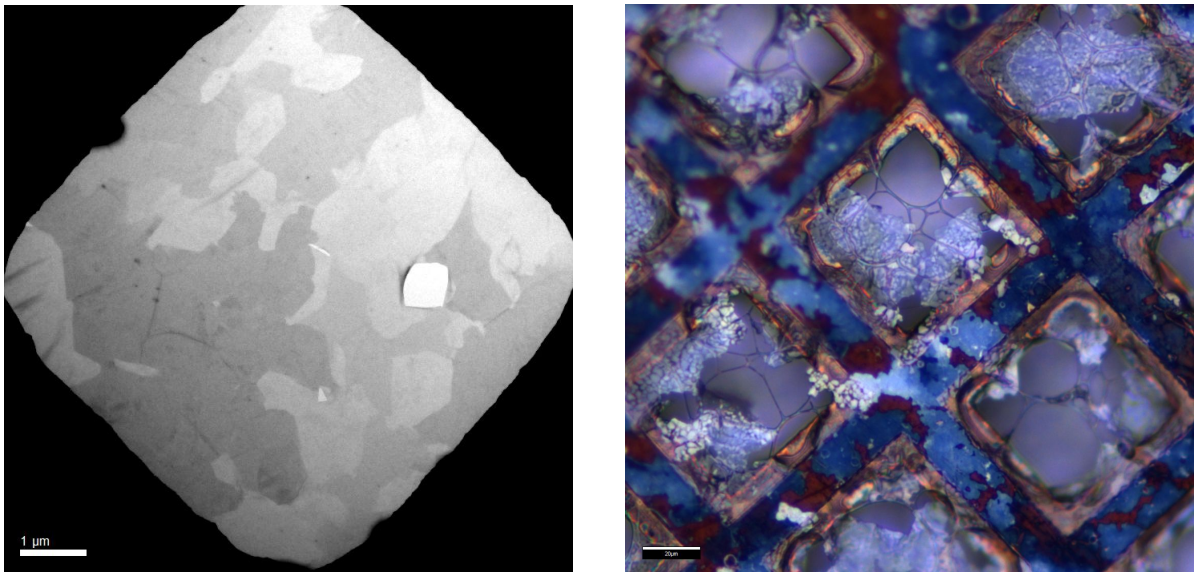

Figure 5.1: TEM - picture (FEI Tecnai™F20 at 200 kV, zero loss filtered) of Ni-CVD graphene on a TEM grid with grid size 2000 without lacey carbon scaffold (left) and a lacey carbon GSM-grid in an optical microscope (right, scale bar: 20 µm)

5.1.2 Argon-Plasma Graphene

The Argon-Plasma graphene grids are lacey carbon Ni TEM grids with a mesh size of 200, prepared with graphene gained by the substrateless plasma method according to [106] and as described in 3.5. These grids, which were used for this work, are called GF1202 and were purchased from `www.fishersci.com`. Thus gained graphene can also be bought as a graphene-ethanol solution, called GF1200, with a concentration of 0.1 mg graphene per 1 ml ethanol. With this solution one can prepare graphene enhanced TEM grids. By way of trial we prepared lacey carbon grids with this solution, which was ultrasonicated for 30 seconds prior to deposition. TEM investigations showed the same agglomerated and wrinkled structures as the GF1202 grids and exhibited more contamination. Therefore they are not discussed in the present study. In figure 5.2 TEM bright field pictures of typical graphene structures on the GF1202 grids can be seen. Thin regions down to one layer can be found in the border area of huge agglomerations of graphene sheets (marked by an arrow in the right image).

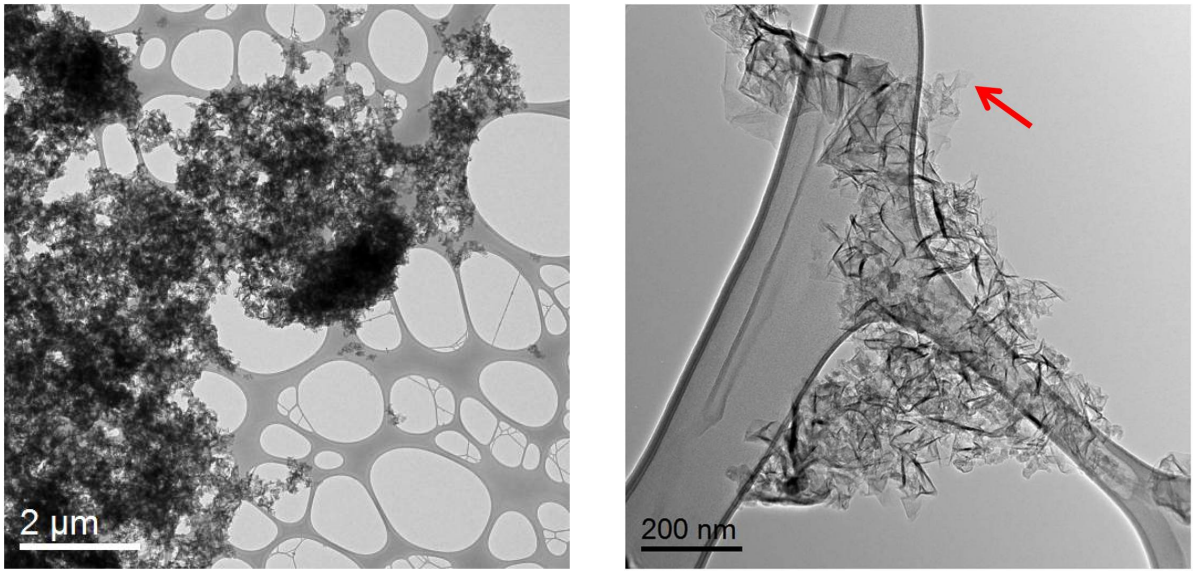

Figure 5.2: TEM BF images of a GF1202 lacey carbon grid, enhanced with argon-plasma graphene (left picture: FEI Tecnai™12 at 120 kV); right: FEI Tecnai™F20 at 200 kV (arrow marks the position of a possible monolayer region)

5.2 Analysis of the reference samples

In this section the results of the investigations of the purchased reference samples are presented. Different methods available on the FELMI-ZFE were used to characterize graphene especially with respect to its thickness in order to distinguish single layer graphene (SLG) from few layer graphene (FLG). A description of the different methods can be found in chapter 4 on page 29.

5.2.1 Ni-CVD-graphene grids

5.2.1.1 Optical microscopy

The right picture in figure 5.1 shows an image of a Ni-CVD grid, taken in an optical microscope. Already in this image a lot of blueish, presumably not graphene-related material can be seen. Figure 5.3 shows on the left side an overwiew over a large area of the grid demonstrating the spread of the contamination. The right side shows a picture of an area on the grid were no contamination can be seen. The question if there is any graphene in the region without visible contamination can not be answered with this picture, considering the low contrast of graphene in a light microscope. The blurred regions are caused by the uneven structure of the grid.

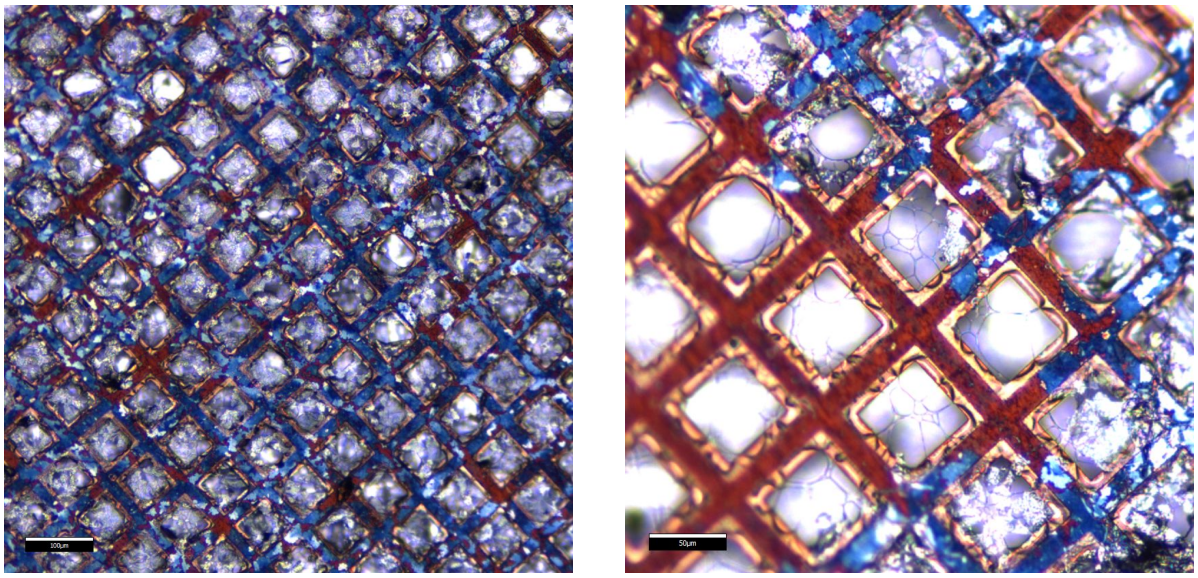

Figure 5.3: Two regions of a Ni-CVD enhanced Cu lacey carbon TEM grid in an optical microscope (scale bars: left: 100 µm; right: 50 µm)

5.2.1.2 Raman spectroscopy

Raman spectroscopy of the Ni-CVD grids turned out to be quite difficult due to the signal from the contamination dominating the spectra. Figure 5.4 shows the region we chose for the Raman spectrum image on the top left corner, and the top right picture shows four spectra from 4 different points within the area. The line colours correspond to the colours of the 3 spectrum images for 3 different signatures of the 2D peak shown at the bottom of the figure. The only deduction that can be drawn by means of the obtained spectra is that there is a huge amount indeterminable contamination and only small region of FLG could be found. There were no SLG regions findable.

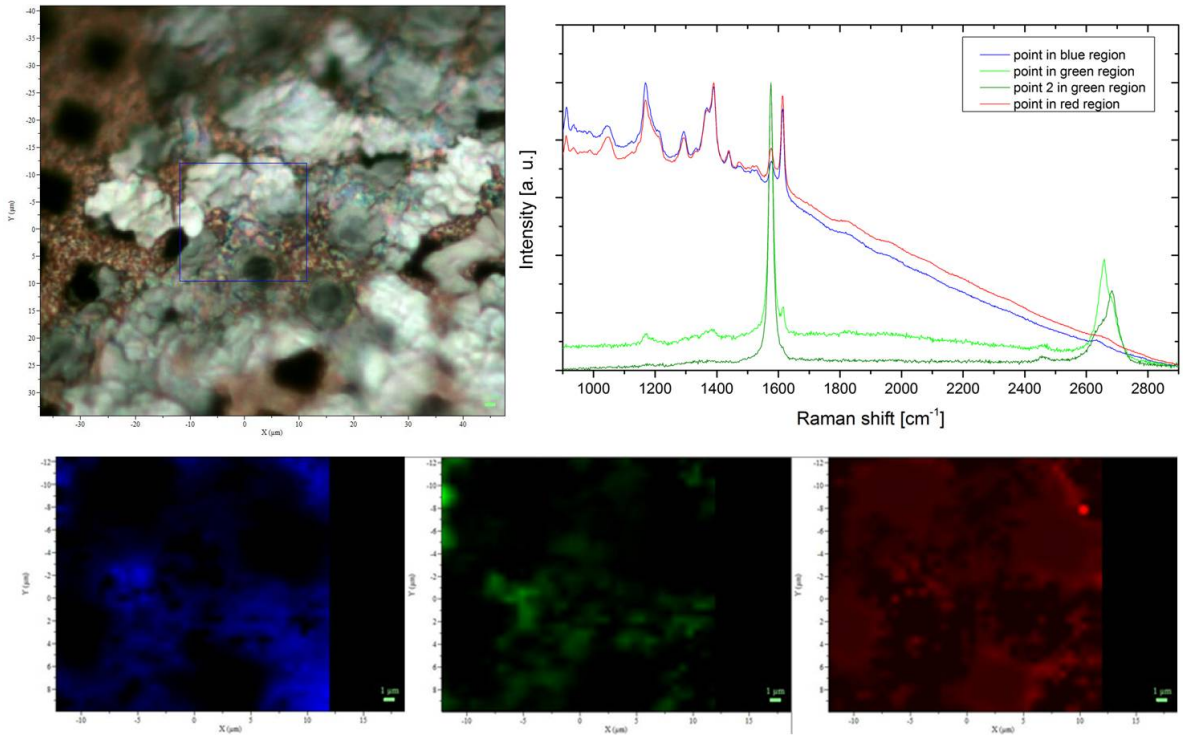

Figure 5.4: Raman spectrum images for different signatures of the 2D - peak, picture on the left top: area on the Ni-CVD grid of the Raman spectrum image (blue rectangle)

Only in the green regions graphene like spectra could be recorded. Two of them are also drawn in diagram in figure 5.4 (light green and olive) and correspond to FLG. The other 2 spectra (red and blue) are dominated by contamination with very small subjacent graphene peaks.

5.2.1.3 SEM

The two pictures in figure 5.5 were captured with a FEI ESEM Quanta 600 FEG operated at 5 kV by using the Everhart-Thornley detector. The left one shows an overview of a graphene enhanced copper 2000 mesh TEM grid without lacey carbon, whereas on the right a closer view of a particular hole in the mesh can be seen.

Thin regions expanded over large areas can be seen with different thickness values, represented by various shades of grey.

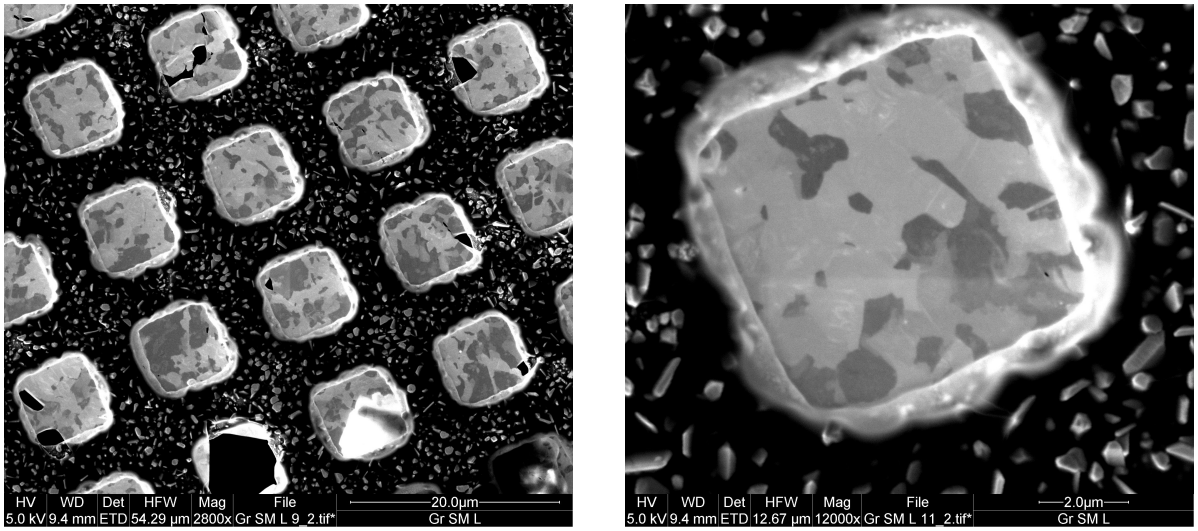

Figure 5.5: SEM pictures of a Cu 2000 mesh Ni-CVD graphene TEM grid

5.2.1.4 STEM and EELS

EELS line scans were done on this sample in order to find thin regions with less contamination, in accordance with the method described in section 4.3.4.1 on page 38. One chosen path of these scans is shown in figure 5.6 on the left, with the points chosen for evaluation marked with colours and numbers. They correspond to the line colours and numbers in the EELS diagram on the right of the figure. The measurements were done with the Philips CM 20 at 200 kV.

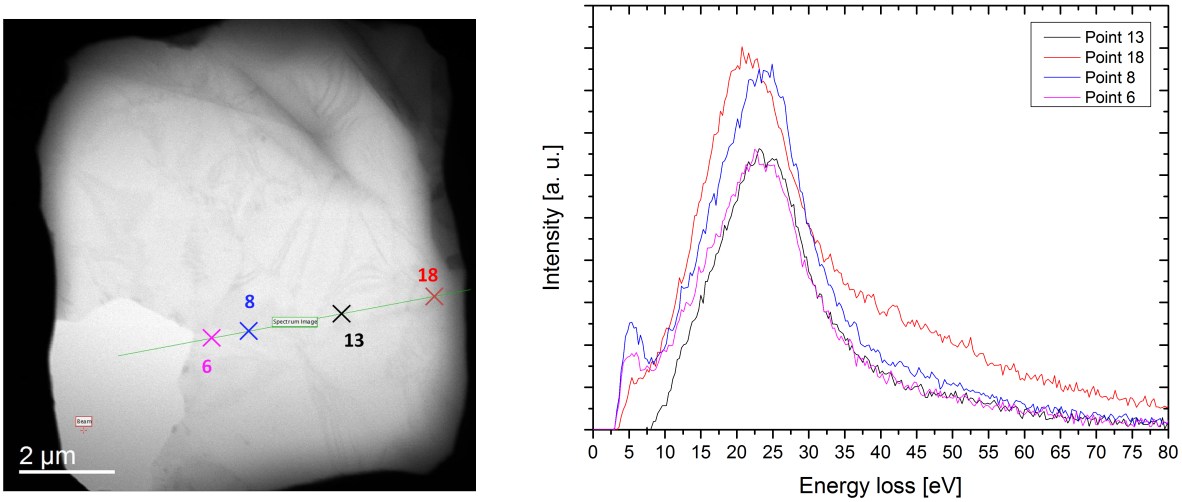

Figure 5.6: STEM-EELS line scan paths (left) and spectra of four chosen points marked on the left side pictures (right), the colours of the spectra correspond to the colours of the marks

Regions with obviously different thickness, corresponding to lower intensity values, do not

show the typical shift of the plasmon peaks in the EELS spectrum. Energy shift and peak height do not correlate as expected. Additionally the sample shows strong contamination effects like adsorption of amorphous carbon in the electron beam, even after very short illumination times of around 0,1 seconds per pixel. Supposably the spectra are dominated by the contamination signal, similar to the Raman measurements.
It was tried to get rid of the contamination by thermal annealing at 200 °C and keeping the sample in the TEM vacuum over night before the measurements. However, this procedure did not lead to better results.

5.2.1.5 Conclusion

The Ni-CVD enhanced TEM grids purchased from Graphene Supermarket, as they were analysed in this section, seem to be unfeasible in terms of support for analytical TEM investigations. Even though the graphene covered areas are large, they showed a high amount of unknown contamination and with hardly any or no SLG areas. In fact, none could be identified in our experiments.

5.2.2 Substrate-free gas-phase graphene grids

5.2.2.1 Optical microscopy

A picture of a substrate-free gas-phase graphene grid, captured with an optical microscope, can be seen in figure 5.7. The familiar extend vast graphene agglomerations can be seen as dark clusters on the lacey carbon scaffold everywhere on the grid. Some of them were marked by red arrows in figure 5.7. Thin regions can not be seen, due to their very small lateral size.

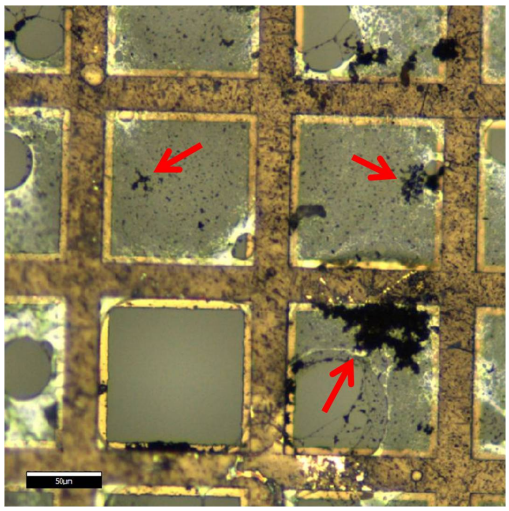

Figure 5.7: Picture of a GF1202 graphene enhanced lacey carbon copper TEM grid (IFM picture, scale bar: 50 µm)

5.2.2.2 Raman spectroscopy

Due to the very small lateral dimensions of the graphene areas below the resolution limit of the Raman spectroscope, performing Raman spectroscopy was pointless. Hence there is no Raman data available for the substrate-free gas-phase graphene grids.

5.2.2.3 SEM

Figure 5.8 shows two pictures taken with the Everhart-Thornley detector. The SEM was operated at 10 kV. The left picture shows an overview of a region on the graphene enhanced lacey carbon grid, while the left picture depicts a closer view of these agglomerations. Again the typical agglomeration structures can be seen (some of them marked with arrows on the left picture) with small thin regions at the borders (marked with an arrow on the right).

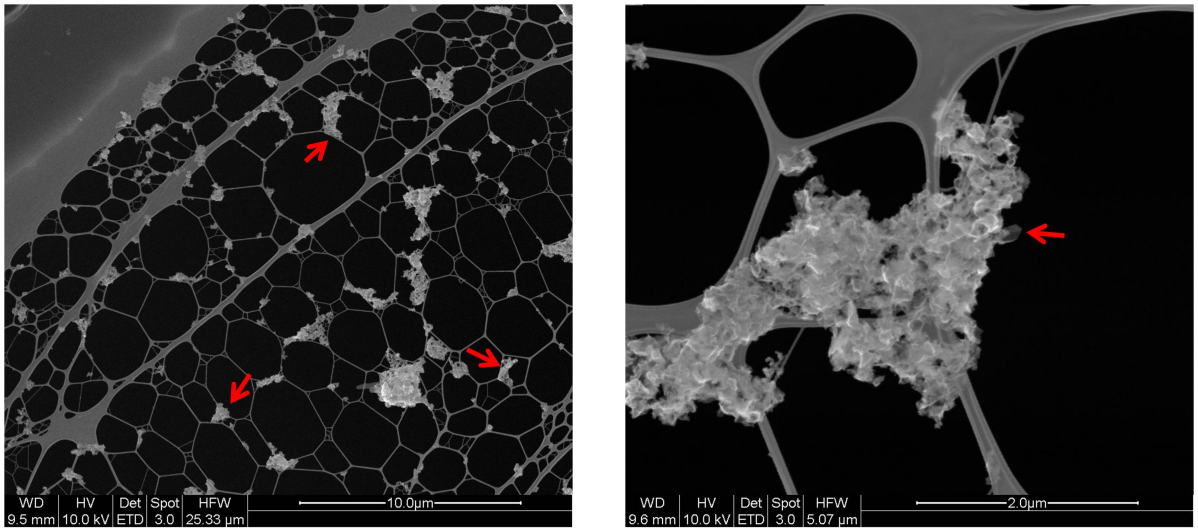

Figure 5.8: SEM pictures of a GF1202 TEM grid; left: overview picture, red arrows mark some examples for graphene agglomerations; right: close up view with a thin region marked with an arrow

5.2.2.4 TEM

In contrast to the Ni-CVD graphene enhanced TEM grids the also commercially available GF1202 grids exhibit much less contamination in an electron beam. Thus continuative analytical TEM investigations were possible with these grids. The two pictures in figure 5.9 show characteristic agglomerations (left) with only small thin areas (right) in TEM bright field. All pictures shown here were shot with a FEI Tecnai F20 operated at 200 kV.

Figure 5.10 shows a high resolution bright field picture of a small region of the agglomeration in 5.9. On the boarders the structure of a folded up multilayer can be seen. The intensity profile on the right side of figure 5.10 shows the interlayer distances of the folded up region.

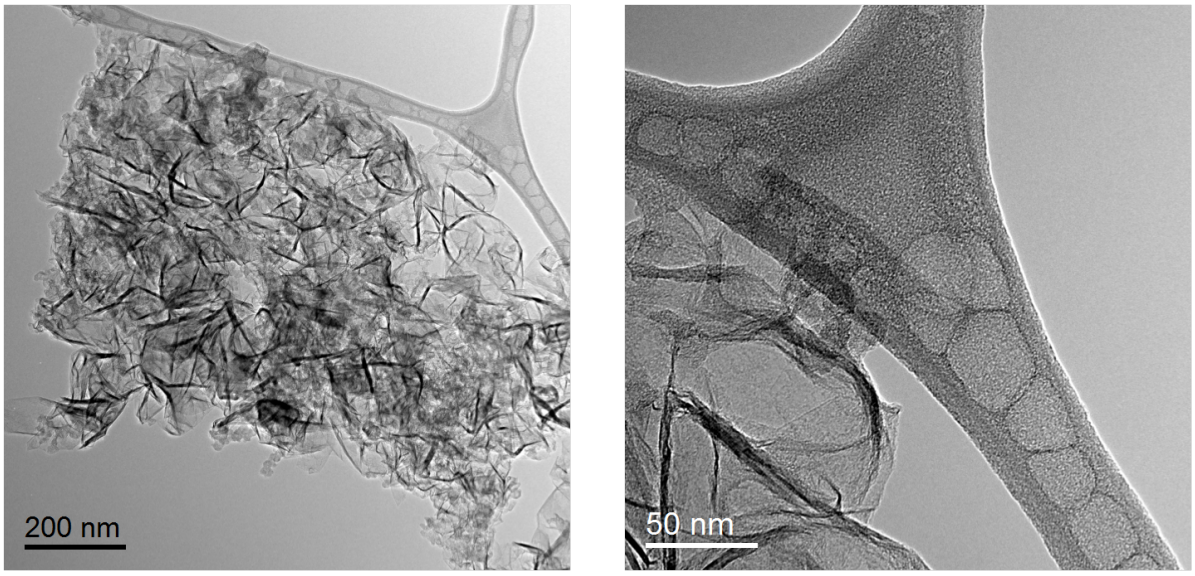

Figure 5.9: Overview of a graphene agglomeration on a GF1202 TEM grid (left) and a thin region in the upper right of the same agglomeration (right)

A distance of 357 pm was measured here, which fits very well to the theoretical interlayer distance in graphite of around 0,34 nm. In principle, the thickness of SLG and FLG up to several layers can be examined in a TEM by means of such folded structures [136].

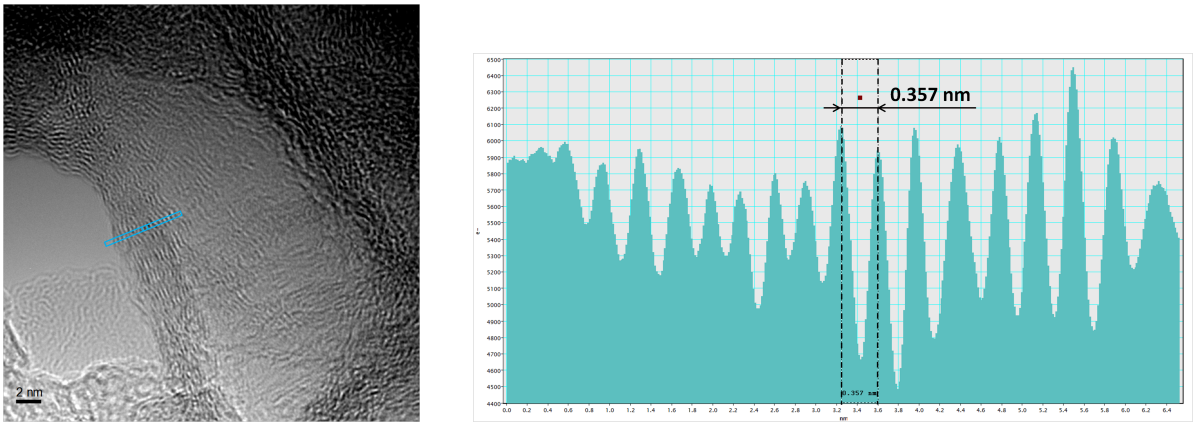

Figure 5.10: Close up view of a folded up region (left); intensity profile of the edge marked in the left picture (right)

5.2.2.5 STEM and EELS

Several STEM EELS investigations were done with GF1202 graphene enhanced lacey carbon TEM grids. Although the thin regions are very tiny on these grids, a lot of them can be found. Furthermore contamination is not such a big problem compared to the Ni-CVD graphene

enhanced TEM grids. Thereby the GF1202 grids were quite appropriate to prove and improve the thickness determination method via EELS investigations via the plasmon peaks position. In figure 5.11 an example for these measurements, done with a Philips CM 20 with a GATAN electron energy loss spectrometer, can be seen. An EELS line scan with 63 survey points over a region of interest, where we expected thin areas, was performed. The measurement time was 0,2 s for each point so as to prevent corruption of the results due to contamination. The left side picture of figure 5.11 shows the path of the scan. From this linescan six points were chosen for a closer investigation. The crosses in the survey image mark these points whereby their colours correspond to the colours of the spectra shown on the right side of the figure. The numbers beside the points in the survey image correspond to the position of these points in the line scan.

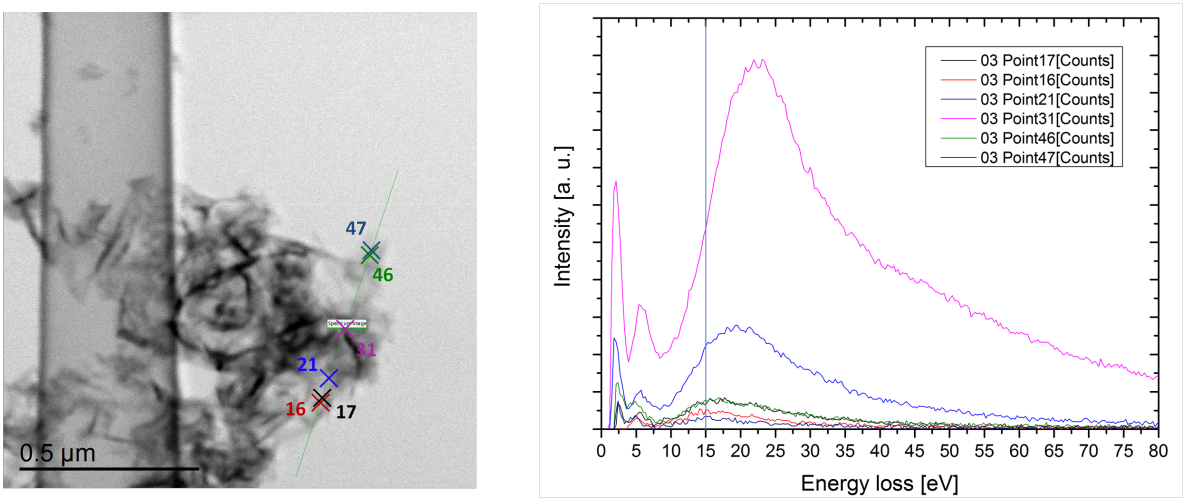

Figure 5.11: STEM EELS plasmon peak investigations of graphene on GF1202 TEM grids; Survey Image (right) and corresponding EELS spectra (right)

In the diagram on the right of figure 5.11 the typical shift of the σ-π - peak with rising thickness can be seen. Figure 5.12 shows a closer view of the spectra corresponding to thinner regions shown in figure 5.11. The line at around 15 eV in the this graph marks the expected position of this peak for SLG. After comparison with data in literature (see [137], [143] and [157] for instance) it stands to reason that at point 47 monolayer graphene can be seen, while point 16 may be a bilayer. Furthermore the points 17 and 46 could be around 4 to 6 layers thick. However it has to be confined that for reliable verification of SLG the energy resolution of the used spectrometer is not sufficient.

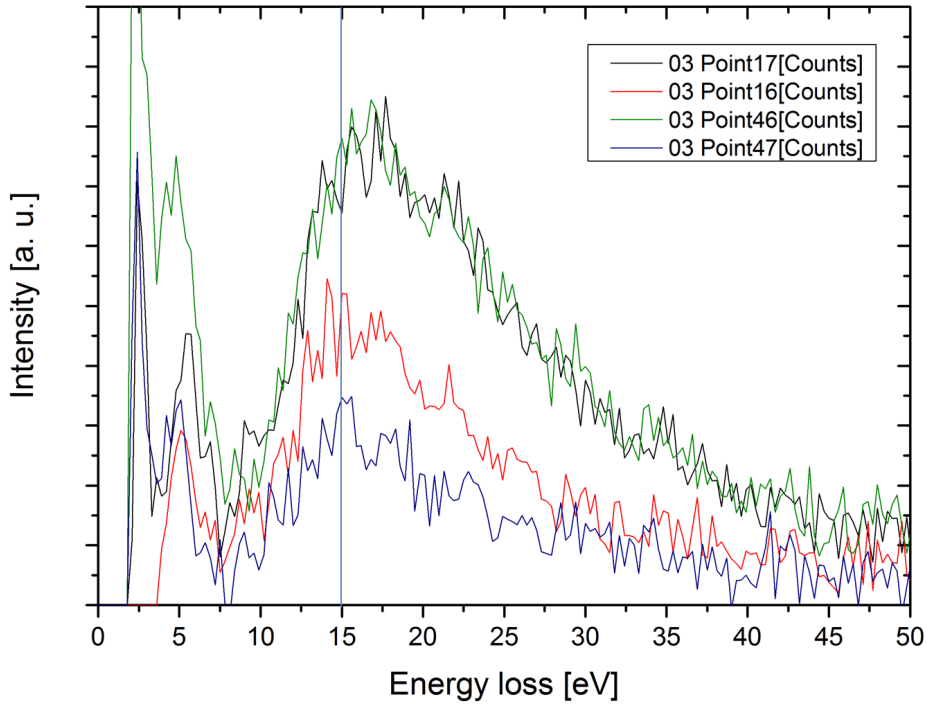

Figure 5.12: A closer view on the low intensity EELS plasmon peaks shown in figure 5.11

5.2.2.6 Conclusion

Our investigations of the lacey carbon TEM grids, enhanced with graphene produced by the substrate-free gas-phase method revealed the wrinkled and agglomerated graphene structures on the scaffold. SLG areas can presumably be found quite frequently on the boarders of such agglomerations, but their lateral dimensions are very small. However, they exhibit relatively low contamination compared to the Ni-CVD grids. Thus, for TEM investigations where only small thin areas are needed they may be an option. In this work this type of graphene enhanced grids was mainly used to evaluate the (S)TEM characterisation methods.

5.3 Self made graphene

The standard procedure for preparing a sample was a modified version of the scotch tape method [1] as described in 3.1. As a substrate a silicon wafer with a 100 nm or 500 nm layer of silicon dioxide was used. Both thickness values comply with the requirements for the search of thin layers in an optical microscope (described in 4.1) according to [158], [122] and [124].

In order to enhance the adhesive forces between the graphene flakes and the underlying substrate a thin layer of polystyrene (approx. 10 nm) was spun onto some of the wafers (see Sample 2, section 5.4.2 and Sample 3, section 5.4.4). The layer should be as thin as possible so as to preserve the optical properties of the substrate, especially because of the higher refraction index (1,62 at 435,8 nm) of polystyrene [159] compared with SiO_2 (1,47 at 400 nm) [122]. Poly(methyl methacrylate) (PMMA) with a refraction index of 1,5 (at 435,8 nm) ([159]) is better suited for this purpose (as used in [118]) but PS was easier available. This procedure enhances the achievable flake sizes significantly and moreover the transfer of the flake to a TEM grid is easier. Due to these advantages the decrease of optical contrast is acceptable. The thickness of the polystyrene film was determined via AFM measurements.

5.3.1 AFM analysis of the polystyrene film

For the preparation of the polystyrene film by means of a spin coater following parameters were used:

- Solution: 1 mg/ml polystyrene in chloroform
- Substrate: Silicon wafer with 100 nm and 500 nm SiO_2 coating
- Spin parameters: first stage: 1500 RPM for 12 s; second stage 3000 RPM for 10 s

In order to determine the thickness of the polystyrene film it was scratched with tweezers and the depth of the scratches was measured via AFM (Atomic Force Microscopy) in several places. In figure 5.13 two examples for the thickness determination via AFM can be seen. The inserts show the particular profile paths on the topography maps. The peak in the middle of both pictures marks the edge of the scratch.

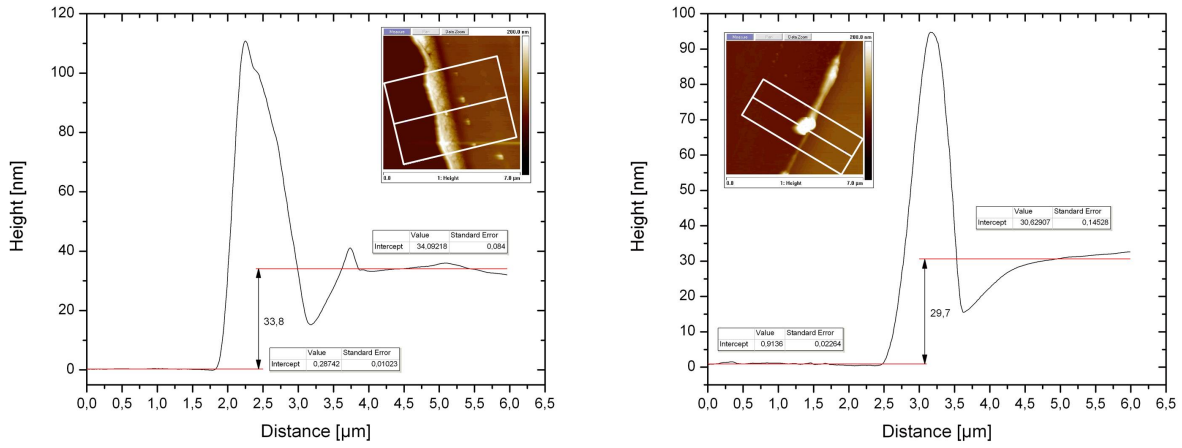

Figure 5.13: 2 examples for the height measurements of the polystyrene film in the AFM

The measured depth values vary over a range between 20 to 40 nm which should be sufficiently thin so that the optical contrast is high enough, even for few layer graphene flakes on 500 nm coated wafers. However, on a 100 nm wafer, we are already close to the low-contrast-region of around 150 nm overall, which leads to a significantly lower contrast for SLG (see chapter 3.1.1, section 'Identification'). We realized this factor after we did the preparation of Sample 3 (see 5.4.4) and observed a remarkable lowering of the colour shift caused by thin flakes.

5.4 Analysis of the self made samples

In the following 3 representative samples, each prepared with slightly different methods will be presented. Optical microscopy, Raman spectroscopy and atomic force microscopy were the methods used to make pre-TEM investigations of graphene on the substrate. In TEM mainly analytical methods like EELS and EFTEM, but also intensity profiling, STEM and FFT image data processing were used.

5.4.1 Sample 1

The first sample, that is described in this thesis, was prepared in accordance with the procedure described in 3.1 on page 16 on a wafer with a SiO_2 thickness of 100 nm without polystyrene coating. Natural graphite was the precursor material for the preparation.

5.4.1.1 Optical microscopy

Figure 5.14 shows an optical microscope picture of an interesting region of Sample 1 with some thin flakes (dark blue, marked with a red arrow) and a possible monolayer (light blue, black arrow).

5.4.1.2 Raman spectroscopy

Two regions with different shades of blue, which indicate two different thicknesses of the flakes were chosen for closer investigation. These regions are marked in figure 5.14 with arrows. The colours of the markers correspond to the colours of the Raman spectra in figure 5.15 on the left.

Comparison of the measured spectra with those from literature in figure 5.15 (right side) leads to the reasoning that the flake marked with a black arrow is a monolayer. The narrow shape and the position of the 2D-peak as well as the height proportions, the 2D-peak is 2 to 3 times higher than the G-peak, are characteristic for SLG. Further the red spectrum originates from

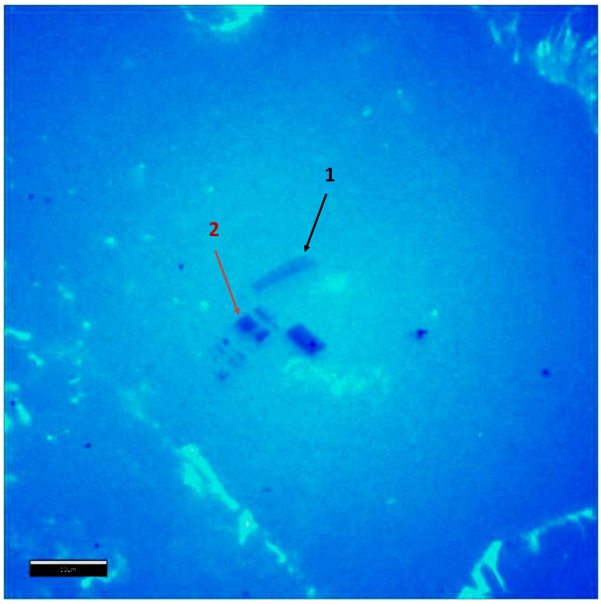

Figure 5.14: Optical IFM image of an area with some graphene flakes (possible SLG: black arrow; FLG: red marker) on Sample 1, scale bar corresponds to 10 µm (contrast-enhanced)

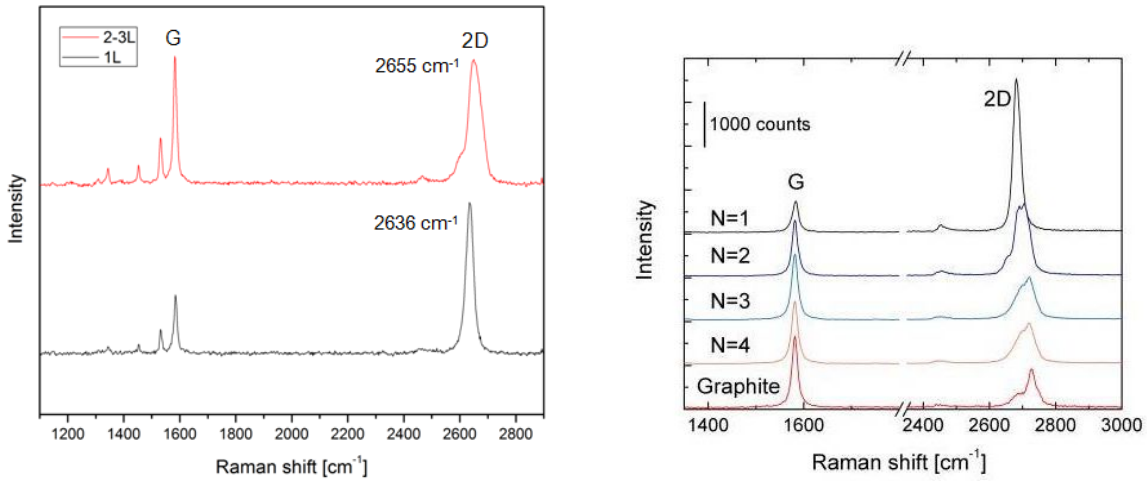

Figure 5.15: Left: Raman spectra of two points in two regions of the sample (marked in figure 5.14); right: typical Raman spectra of 1 to 4 layer graphene on SiO_2 and bulk graphite (adapted from [10])

FLG with probably two or three layers because of the broader peak shape and the height relations. For FLG the 2D peak is equal or even smaller than the G peak.
In order to generate a Raman thickness map the 2D peak was fitted with the aid of the Raman spectroscope software. The position and the shape of this peak was used to distinguish the monolayer Raman signal from the signals caused by multilayer flakes. This can be done pixel per pixel as the laser scans over the sample.
The picture on the right in figure 5.16 shows such a Raman thickness map with two components for the region marked on the left of the same figure. The red pixels correspond to the

monolayer signature of the 2D peak, whereas the green ones come from flakes with two or more layers.

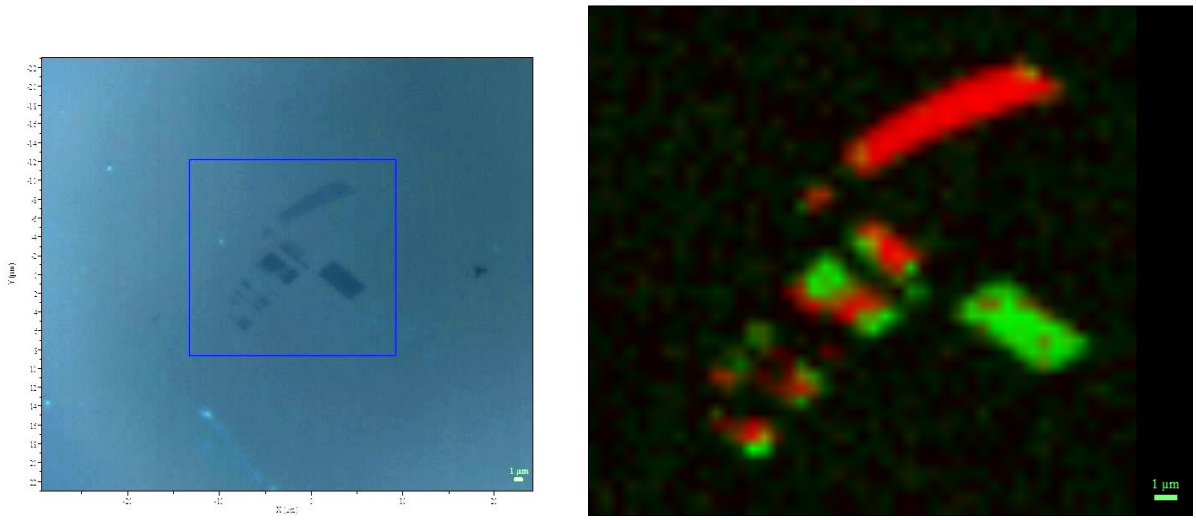

Figure 5.16: Raman scanning region marked with a blue rectangle (left) and Raman thickness map; red: monolayer signature, green: few layer signature (right)

5.4.1.3 AFM

For the AFM investigation the same region as marked in figure 5.16 was chosen. The AFM was operated in tapping mode in the repulsive regime with a relatively soft tip (cantilever length: 240 µm). The overview picture in figure 5.17 at the left shows the same region as in figure 5.16 rotated by 90° counter clockwise. Due to the very small hight differences and the amount of contamination on the flakes it is not possible to see single layer differences in this picture. That is probably the reason why the monolayer flake at the top, as it was identified in Raman, seems to be higher than other flakes in this picture. The right picture shows the area marked blue at the left. In this picture the contamination, confirmed by phase image, due to the solvent used for cleaning can clearly be seen, as it looks like small bubbles.

The area marked red in the left picture in figure 5.17 was chosen for a height profile as it contained SLG and FLG according to the Raman investigations and was less contaminated. The profiles were used so as to acquire a height-over-distance diagram, similar to the method used to determine the thickness of the polystyrene coating in section 5.3.1 on page 53. The profiles were placed on a selected region of the height map. It was oriented in a way that the graphene step edge preferably lays perpendicular to the path to get a sharp step curve. Further the path width was chosen as wide as possible to obtain an average value over many height values of the same distance on the path.
Afterwards all values representing the same step were fitted linearly with slope zero by dint

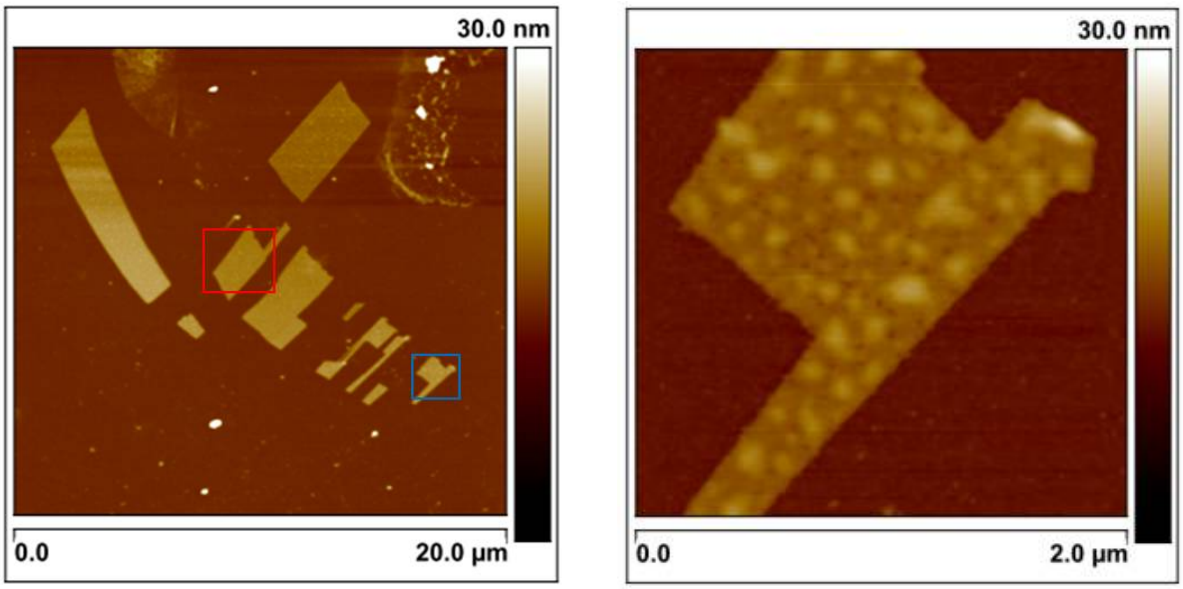

Figure 5.17: AFM picture of a region with graphene flakes on SiO_2; left: overview picture; right: close up view of the region marked blue showing remarkable contamination

of Origin 8.5. The difference between two line fits then represents the absolute height of the step. Figure 5.18 shows the result with the profile path on that area at the left bottom.

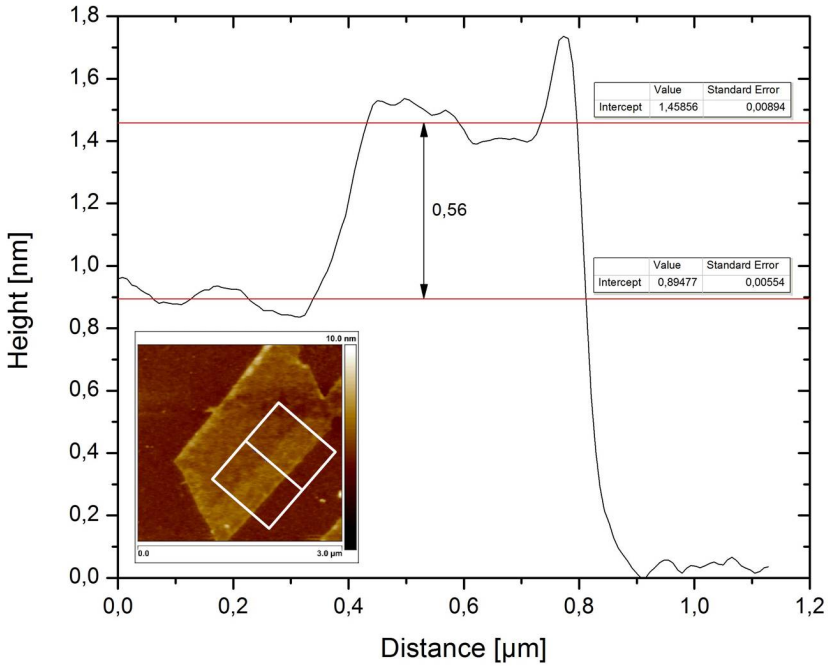

Figure 5.18: AFM height profile representing a single step; the profile path can be seen in the insert in the bottom left corner; linear fits are shown in red with the fit parameters in the two boxes on the top right

After the AFM investigation the transfer to a TEM grid was attempted. In this early try a

Ni lacey carbon grid was used. The grid was positioned over the flake with the help of the IFM. A drop of isopropanol was used to stick the grid on the substrate like described in 5.4.3 on page 64 of this work. As no plastic coating was used, the SiO_2 substrate was directly dissolved in 30% KOH. Unfortunately the graphene flakes got lost during the transfer process. It is believed that they did not stick properly on the lacey carbon grid due to its more irregular and coarse structure. It seems that the use of Quantifoil holey carbon grids, since they are much more homogeneous, is necessary, even more with the use of solvents like chloroform or toluene in the transfer process because they dissolve the lacey carbon scaffold.

5.4.1.4 Conclusion

With this sample the eligibility of the preparation and characterization methods was proven. A lot of lessons could be drawn from this try. After the detection of contaminations via AFM, cleaning of the substrate after preparation was omitted in later tries. Furthermore the failure of the transfer process showed that further improvements of the methodology is needed. All this considerations finally leaded to the succeeded preparation of Sample 2.

5.4.2 Sample 2

Sample 2 was prepared on a 500 nm Si/SIO_2 wafer with polystyrene coating. The precursor was natural graphite. The polymer coating of the substrate significantly increases the resulting flake sizes, as can be seen in figure 5.19. The preparation was done with the method described in 3.1 (on page 16) and 5.4.3 (on page 64), but the latter without steps 4 and 6. (That means that the graphene flake was not encapsulated during the KOH etching (step 5)). As a result an appreciable amount of contamination can be found on the flake.

5.4.2.1 Optical microscopy

The picture in figure 5.19 shows a FLG flake with more transparent SLG regions at its boarders (see arrows in image). The red box marks the region where the AFM measurements were performed, whereas the yellow box marks the Raman investigated area.

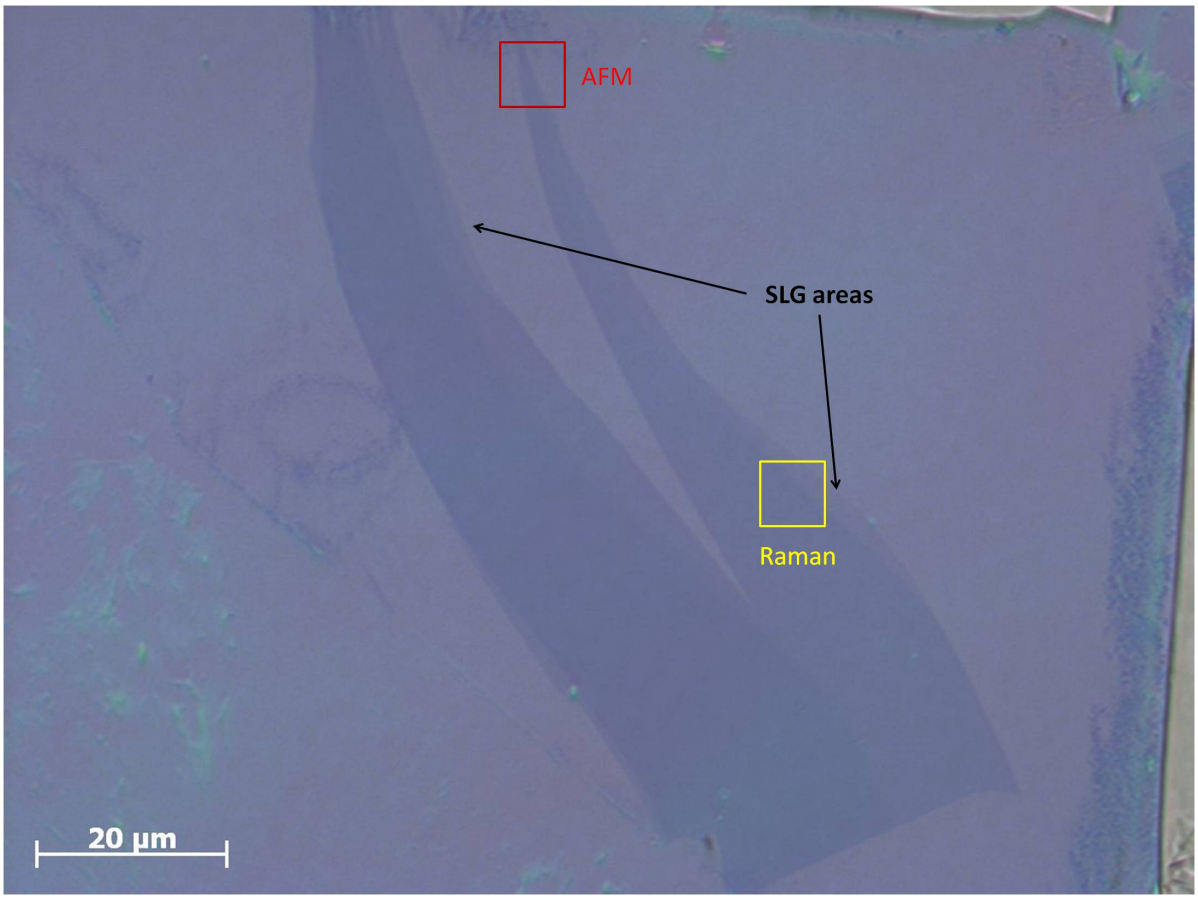

Figure 5.19: Optical image of FLG and SLG border regions on Sample 2

5.4.2.2 Raman spectroscopy

As described above for Sample 2 and in section 4.2 the Raman 2D peak was used to generate a Raman signature map to distinguish SLG regions from FLG. The result can be seen in figure 5.20.

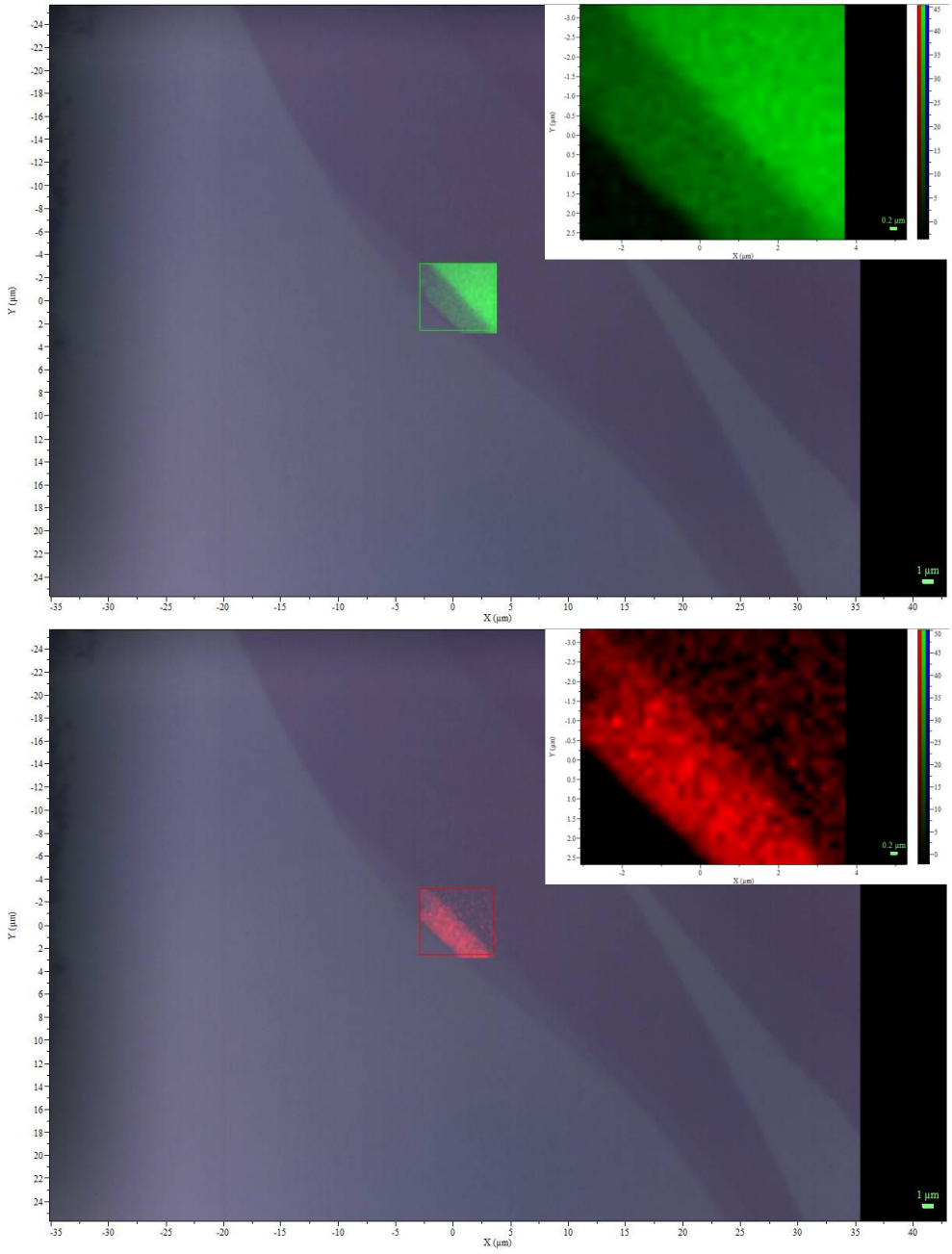

Figure 5.20: Raman signature overlaid on the corresponding region in an optical image for FLG (top) and SLG (bottom)

5.4.2.3 AFM

For the AFM investigations a small area at the top of the flake, where thin areas were expected, was chosen. The region is marked with a red rectangle in figure 5.21 in the picture at the bottom right. The other pictures show two images of the same region (overview at the top left and closer view of the border region of the flake in the picture at the top right). The picture at the bottom left shows a 3D view of the latter.

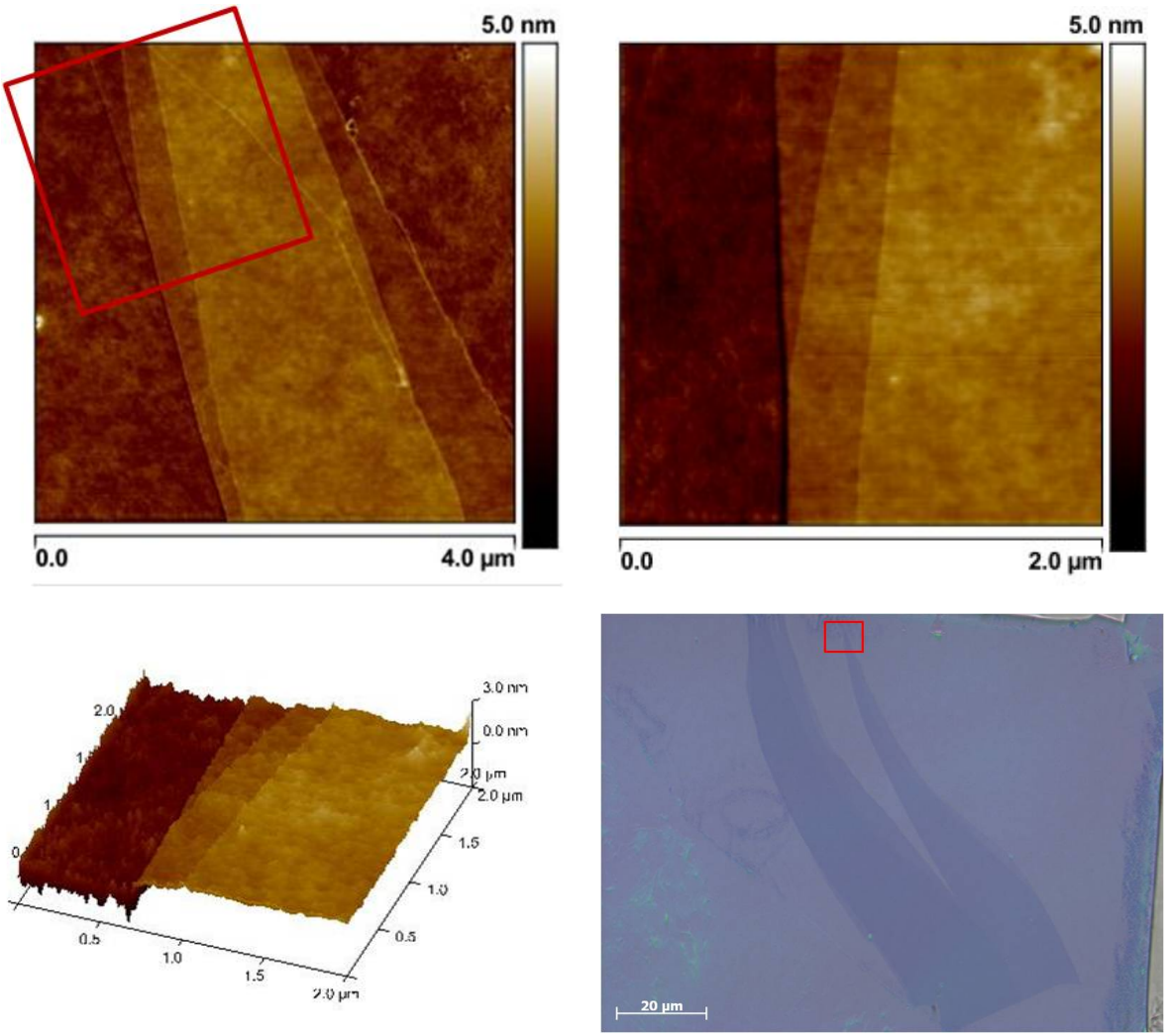

Figure 5.21: Top left: AFM height map of the region marked in the picture at the bottom right; top right: closer view to the area indicated in the first image; bottom left: 3D visualisation of the map at the top right

Instantly, the characteristic stepped structure of graphene becomes apparent. In order to determine the height of these steps two different evaluation methods were applied.
The first method uses height profiles, in accordance with the approach used for the step height determination for Sample 1 via AFM (section 5.4.1) and is described at the same place.

Six different measurements can be seen in figure 5.22. Averaging over all step height values yields a value of 415 pm.

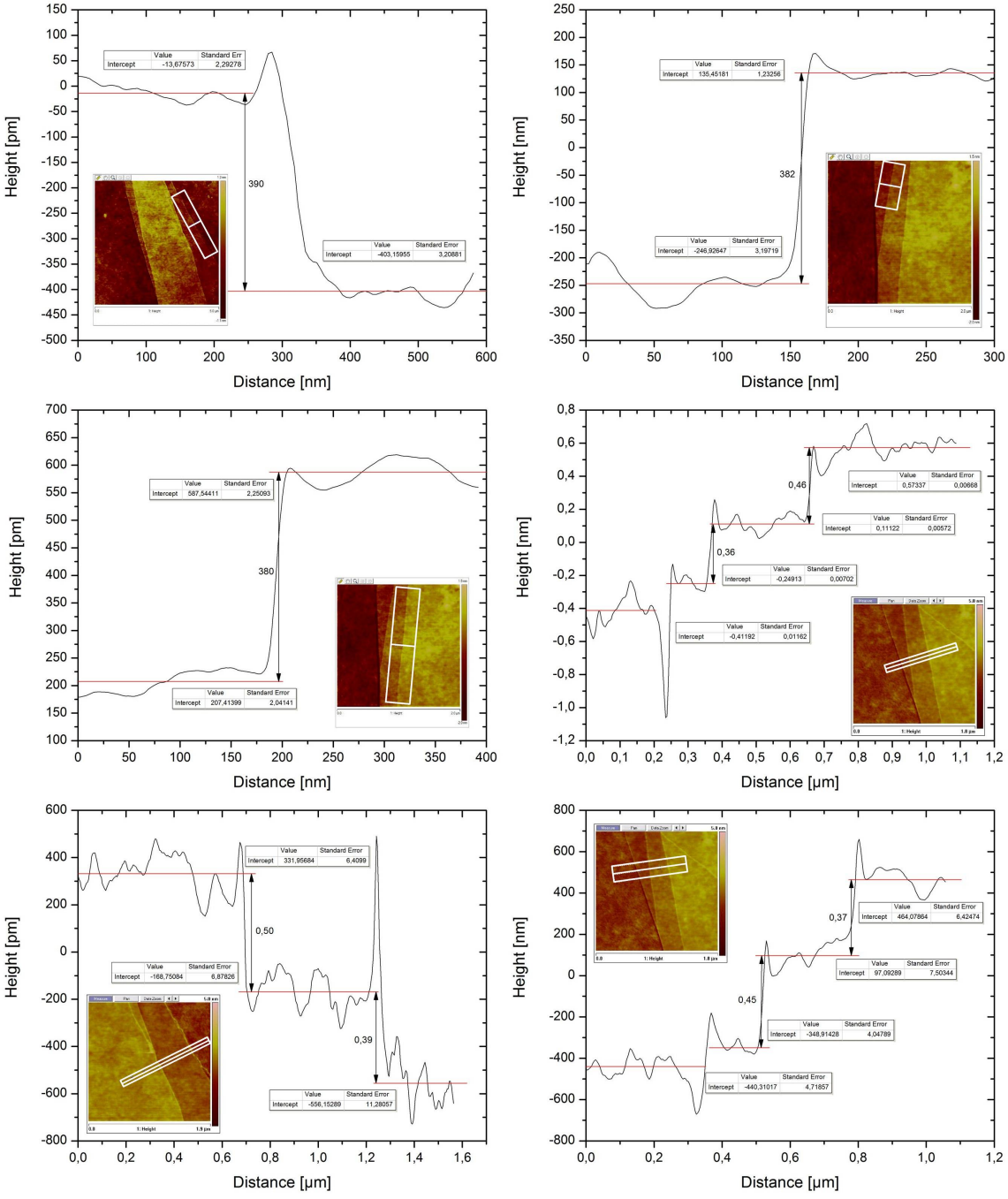

Figure 5.22: Six examples for height profiles to determine the step height (each with the corresponding path and the parameters of the linear fits shown as insert)

Another approach to determine height differences via an AFM topography image is to use a height histogram in which the frequency of a certain height value in a defined area over the

absolute height is plotted (as used for instance by [154]). The maxima in this plot represent a mean value for a certain height. As a result the difference between two maxima is the desired height difference value.
Again four regions in our AFM height map were chosen for the histogram measurements. The results are shown in figure 5.23. Gauss fits (green curves) were used to find the exact position of the peaks in the histogram. The peaks are marked with red lines and the labels display the positions of the peaks. The evaluation was done in Origin 8.5 by means of the included peak search tool.

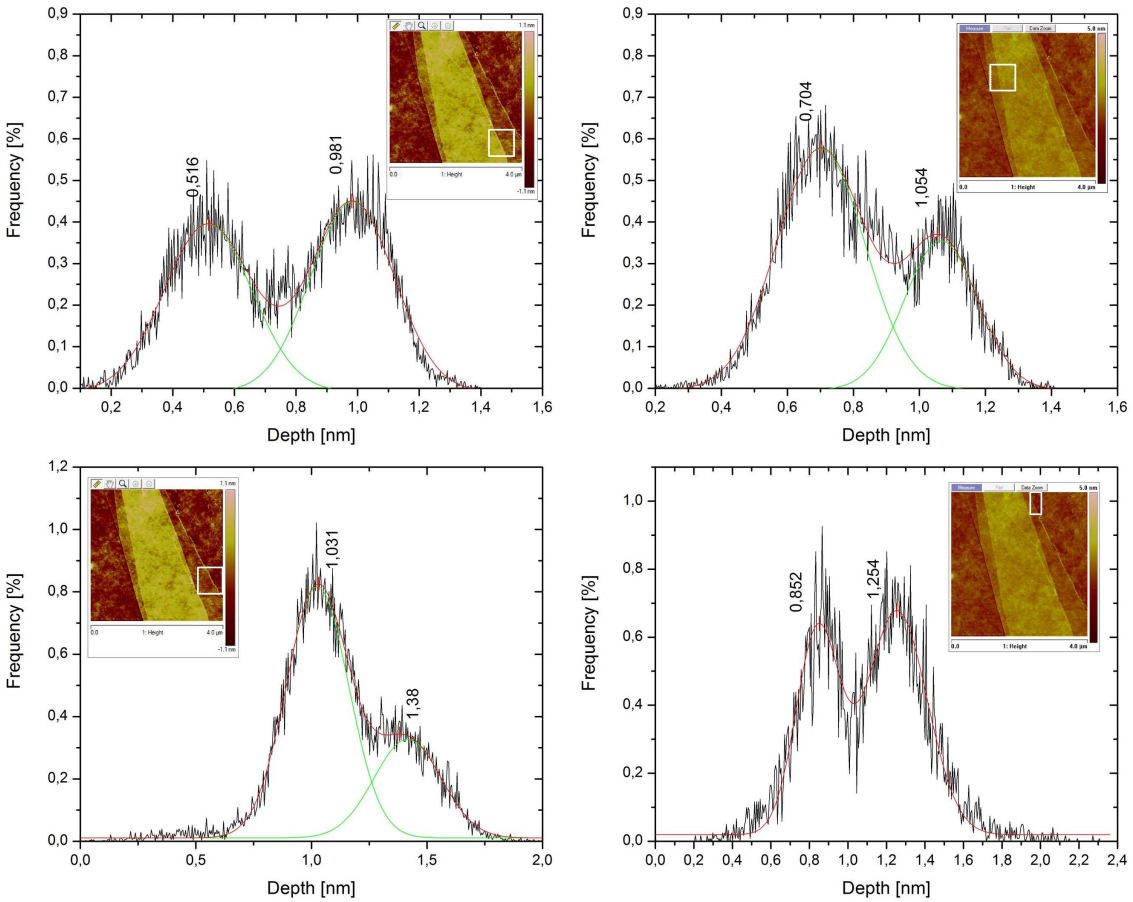

Figure 5.23: Four examples for height histograms to determine the step height, each with the corresponding region shown as insert; green curves: gauss fits, red curves: resulting curve

Averaging over the determined values gives 450 pm for the interlayer distance, which is consistent to the value measured with the first method. Considering all values of both methods yields an overall interlayer distance of 427 pm. This value agrees well with the expected value of 335 pm [106] considering the limitations of the height measurement of graphene via AFM (see [64], [124] and section 4.5 on page 42 of this work).
The step height values of the boarders of the flake are unreliable and depend strongly on the evaluation method, probably due to the very different material properties between the polystyrene substrate (insulator and soft) and graphene (conductor and very hard). Further-

more, damage of the soft substrate due to the AFM tip was observed. There were also no reference values findable for this material combination in literature.

5.4.3 TEM grid transfer

In order to make TEM investigations of the graphene samples it is necessary to transfer the flakes from the substrate to a TEM grid. We used Quantifoil 200 mesh gold grids enhanced with a holey carbon scaffold (Quantifoil R 2/1) from Quantifoil Micro Tools GmbH, Jena, Germany. The size of the holes is 2 µm as shown in a SEM picture in figure 5.24 which has been taken from the product information sheet [160].

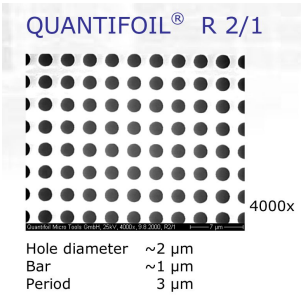

Figure 5.24: SEM image of the grid with dimensions

The following listing describes the transfer process, which is also illustrated in figure 5.25. The numbers in this illustration correspond to the step numbers in the listing.

1. locate the flake of interest in an optical microscope (IFM)
2. place the Quantifoil holey carbon grid on the flake and align it
3. apply a droplet of isopropanol (IPA) on the grid and dry it on a hot plate for 5 minutes at 200°C, the surface tension of the vaporizing IPA pulls the grid to the substrate surface
4. place a droplet of a polystyrene/chloroform solution (concentration: 10 mg/ml) on the grid, it forms an encapsulation layer after drying which protects the grid and the flake during the following step
5. etch the SiO_2-substrate in a 30% KOH-water solution
6. dissolve the remaining PS in chloroform to finally obtain free standing graphene on a TEM grid

This approach is a modified version of the transfer methods used by Jannik Meyer and his co-workers in their work, described in the supplementary information of [118] and in [117] (see chapter 3.6 in this work for more information)
It is recommended to replace polystyrene with PMMA and chloroform with toluene to obtain better results. The modified spin cast parameters for a 10 nm coating are then 60 s at 3000 rpm using a 0.3 wt% PMMA-toluene solution. This parameters are based on the data determined by Walsh et al. in [161]. It is also possible to omit polymer coatings during the preparation to simplify the process. In this case the steps 3, 4 and 6 are obsolete, but one has to be aware of contaminations due to the KOH etching step. Anyway the sample was heated right before the insertion into the TEM at ∼150°C for a few hours (or rather over night).

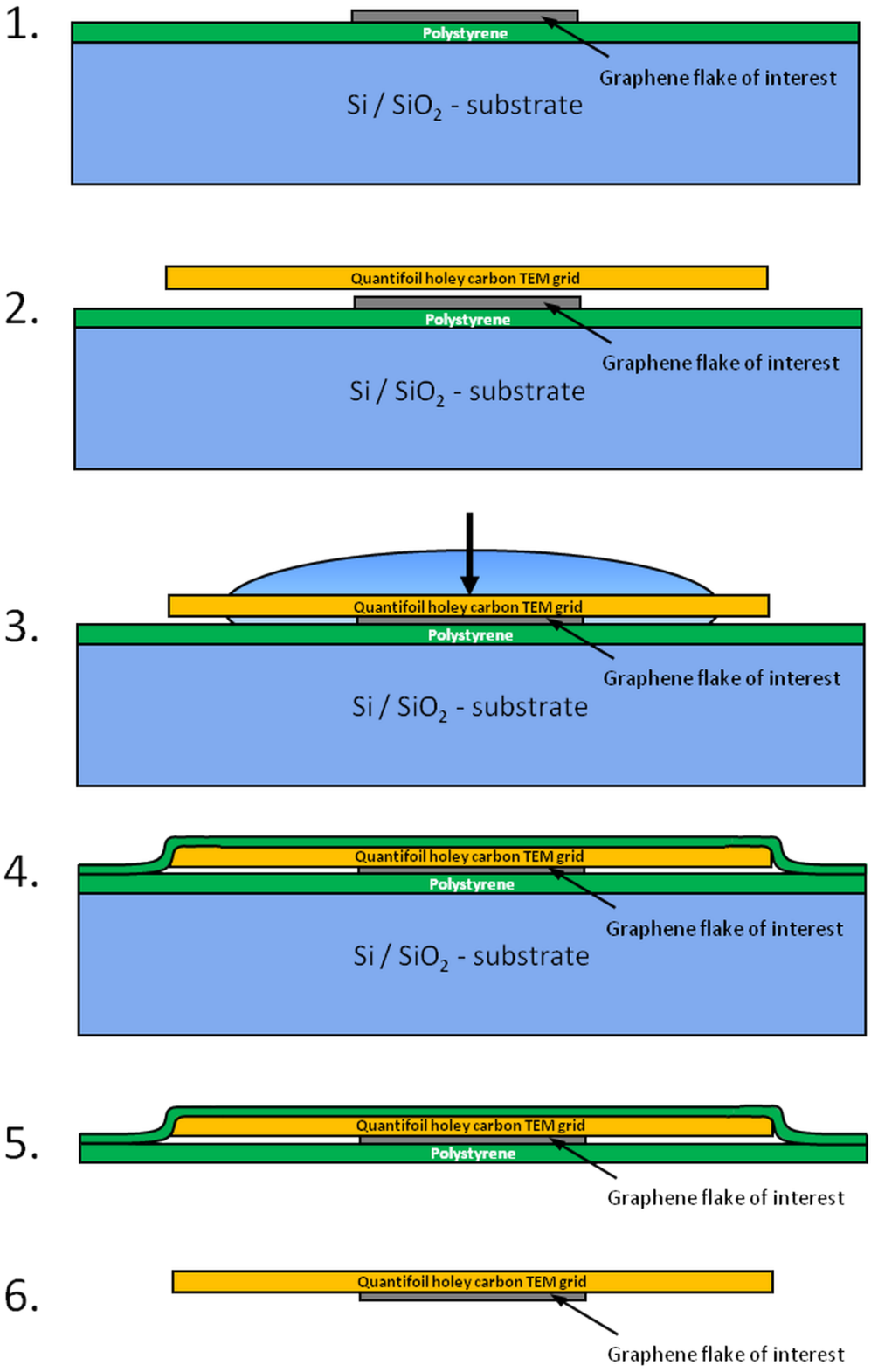

Figure 5.25: Illustration of the TEM grid transfer process; numbers correspond to the sequence on page 64

5.4.3.1 SEM

Figure 5.26 shows a comparison of the transferred graphene flake before (left) and after (right) the transfer. The right picture shows an SEM image of the flake on the Quantifoil holey carbon grid while on the left side one can see the same flake in an optical microscope on the SiO_2 substrate. (This is the same picture as shown in figure 5.38, mirrored to match the SEM image). Obviously the flake was damaged during the transfer process. Unfortunately it is broken and folded up at the thin boarders.

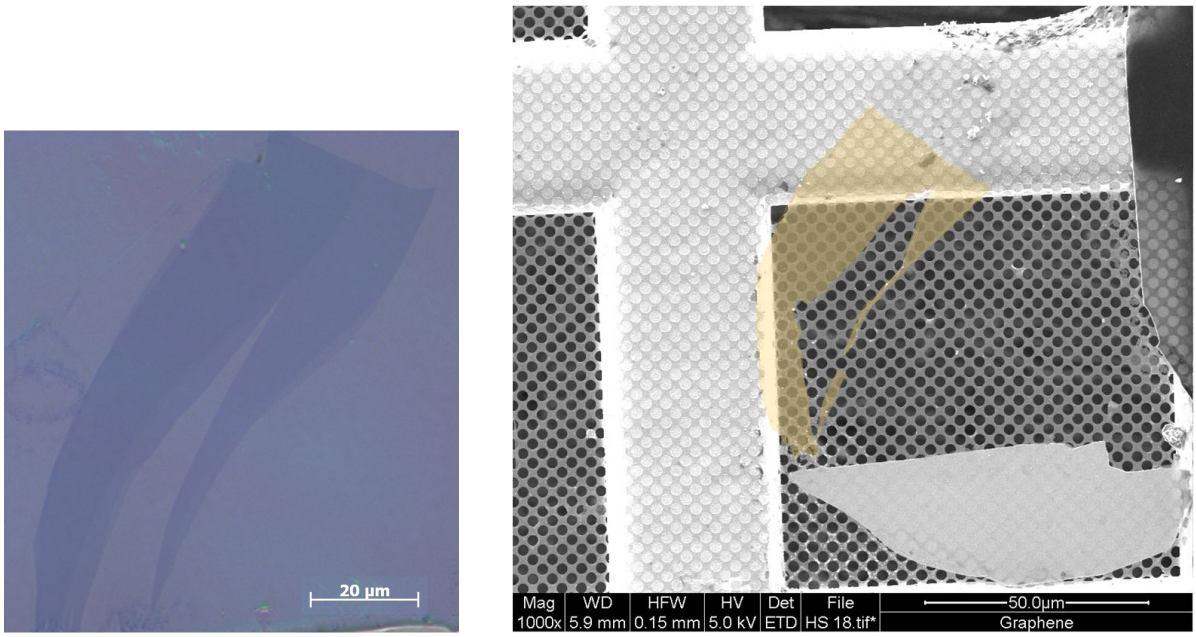

Figure 5.26: Transferred graphene flake before (left) and after transfer to the TEM grid (right); the flake was coloured orange for better visibility

5.4.3.2 TEM

After transferring the flake to a TEM grid as described before (in 5.4.3) it was investigated in an FEI Tecnai™F20 which was operated at 200 kV. Figure 5.27 shows a picture acquired during this investigations. The right image in this figure is a closer view on the area marked in red at the left. A hexagonal structure is clearly visible even without filtering, although it can be said at first glance that it is no monolayer, because of the quite irregular shapes. Obviously a Moiré pattern of two or more sheets is visible in this figure. The amorphous regions on the pictures are carbon contaminations which can be seen all over the whole sample (see red arrows).

In order to gain more information from this picture it was Fourier transformed with the Gatan Digital Micrograph software similar to the method described in [76]. Figure 5.28 illustrates

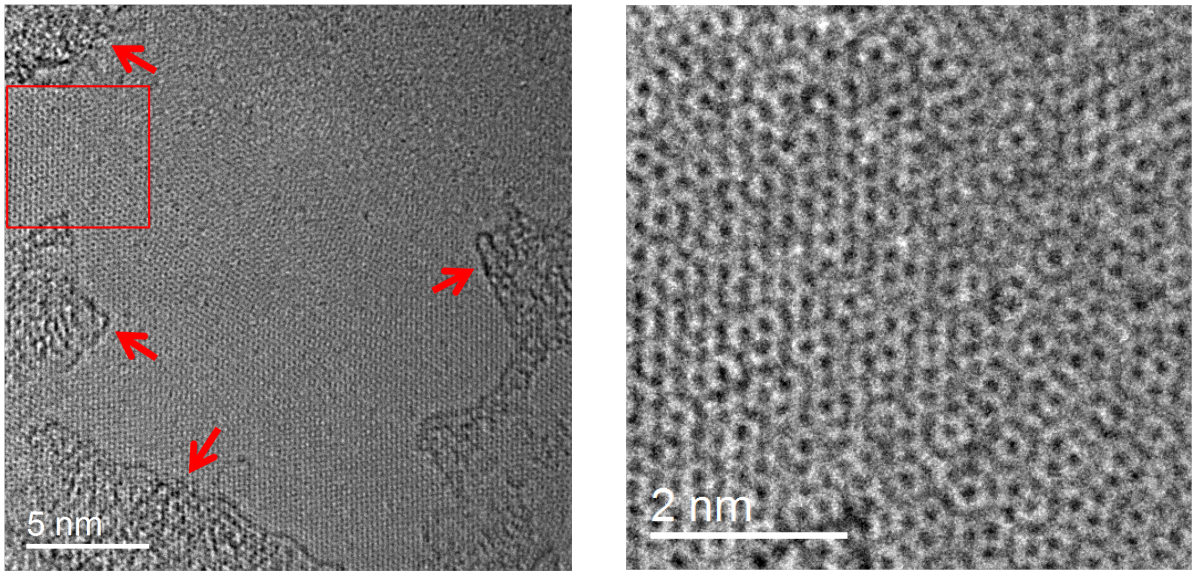

Figure 5.27: HRTEM image of graphene, marked section enlarged on the right (FEI Tecnai™F20 @ 200 kV)

the procedure and shows the centre of the resulting image spectrum on the right. Even though the resolution is quite low, a structure consisting of two overlaid hexagons can be identified. It seems that there are two layers visible in this picture, rotated with an angle of around 25° to each other.

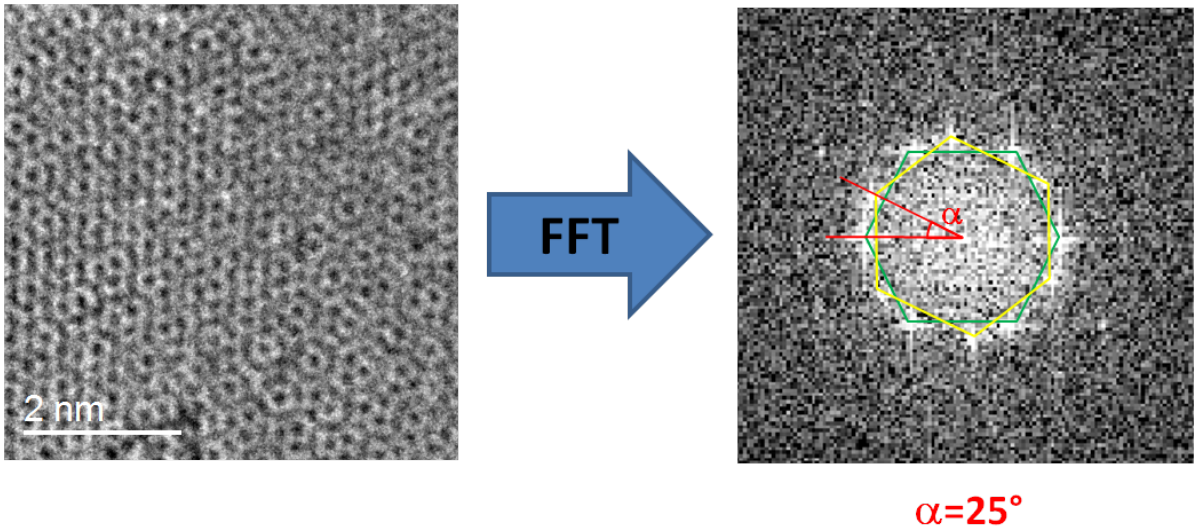

Figure 5.28: Illustration of the Fourier transformation process of the original picture (left) and the resulting FFT picture (right), with the two overlaying hexagons rotated to each other

The next step was a separation of the two layers by applying hexagonal masking filters on the image spectrum (demonstrated in [138]). This was again done in Digital Micrograph, although

other evaluation programs were tried to verify and improve the results. For example 'Image Analyser' offers a more flexible solution for image processing, can also read from DM files and can be downloaded for free. Nevertheless Digital Micrograph is more comfortable for this purpose, beacaus it offers pre-built masking patterns.
The two resulting pictures after applying the filter mask are shown in figure 5.29 on the left side. Inverse Fourier transformation then yields two images, one for each individual layer.

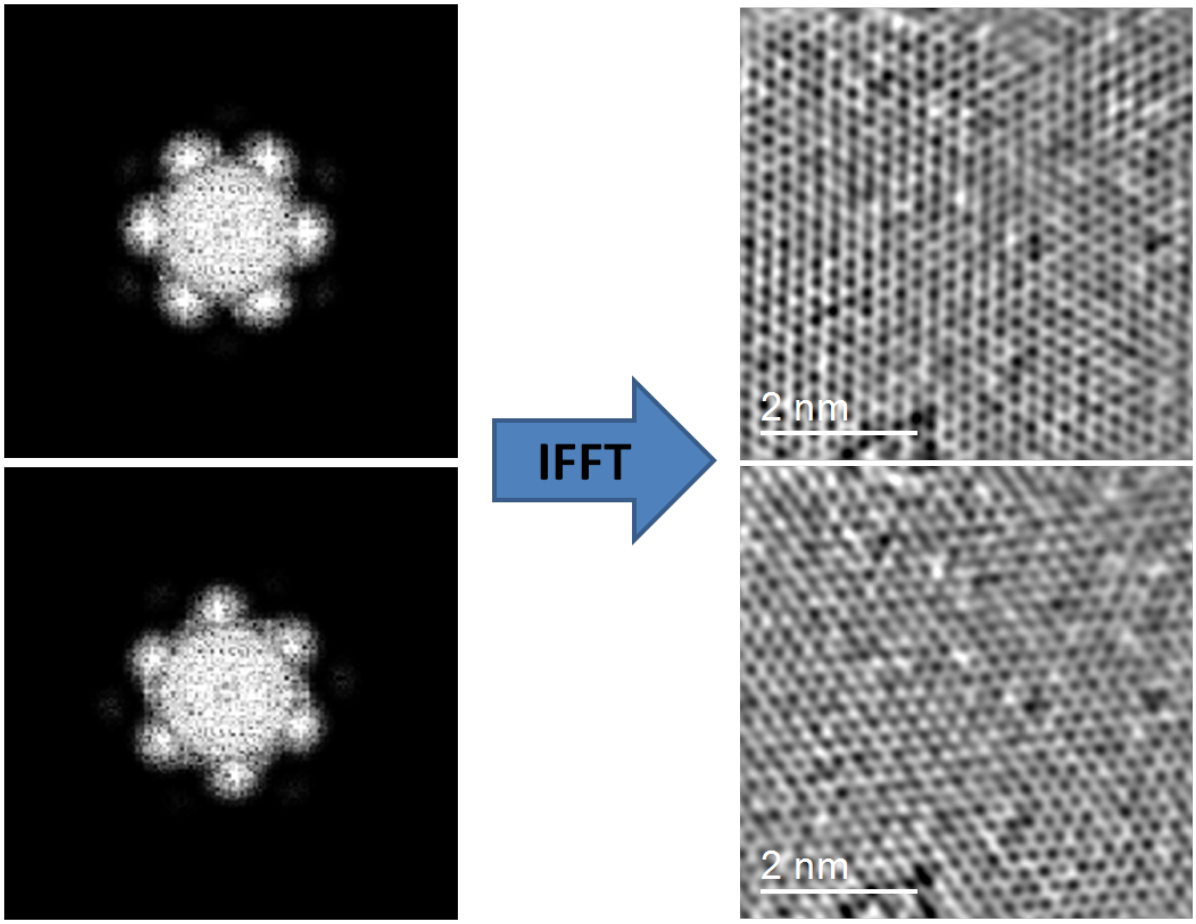

Figure 5.29: FFT images after applying the hexagonal filter mask for each layer (left) and the resulting separated two layer (right)

A intensity profile was measured in order to prove crystal geometry. In graphene the carbon atoms are placed in a distance of $a = 0.14\,\text{nm}$ to each other. With the relation $d = a \cdot \sqrt{3}$ the inner diameter d in an regular hexagon can be calculated (see figure 5.30). Substituting the bond length in the equation gives $d = 242$ pm. This is the expected distance between the hexagons in our filtered and separated HRTEM picture.

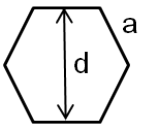

Figure 5.30

On the left of figure 5.31 the path of the intensity profile is drawn. Evaluation of the profile shown on the right of the figure gives a distance between the hexagons of 247 pm, which agrees very well with the expected value.

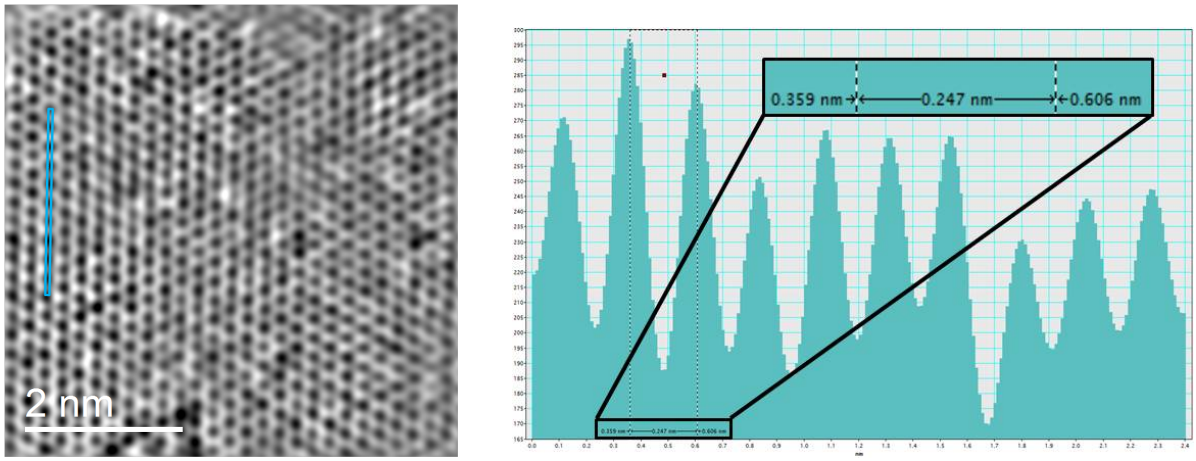

Figure 5.31: Intensity profile path (left) and the corresponding profile (right); with the determined distance

To ensure that the structures we see after filtering and separating are real and not just artefacts, the two filtered pictures were combined again by pixel per pixel addition like illustrated in 5.32. The resulting picture was then compared with the band pass filtered original image on the far right of the illustration. Both pictures show the same structures, thus it can be concluded that the two layers look like the pictures calculated with the FFT filter mask in figure 5.29.

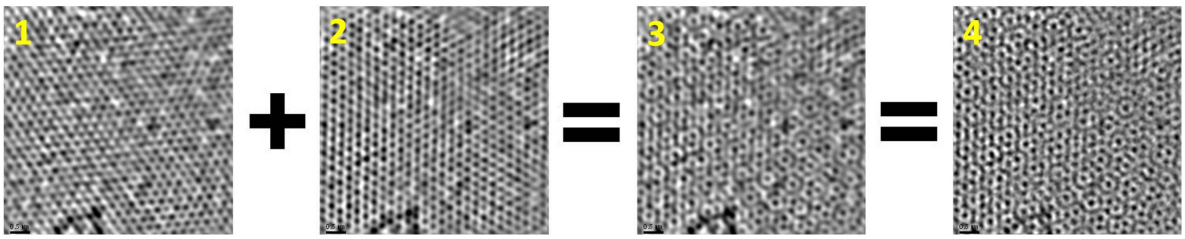

Figure 5.32: Illustration of the prove of the legitimacy of the applied filtering operations; picture 1 & 2: the two separated layers, 3: result of the pixel addition of 1 and 2, 4: bandpass filtered original picture

5.4.3.3 STEM and EELS

For further investigations the FEI Titan^3™60-300 in STEM mode, operated at 80 kV was used. Intensity profiles were made so as to characterize SLG and FLG. Figure 5.33 shows such a profile, where the background intensity was subtracted, as an example. The profile path is drawn in the insert of the graph, showing a bandpass filtered HRSTEM picture captured with the Gatan HAADF detector. The evaluation was done similar to the AFM height profiles (eg. in section 5.18) with linear fits with slope zero.

It can be seen that the second thinnest area exhibits about twice the intensity (factor 2.3) of the thinnest one. This intensity factor between mono- and bilayer graphene agrees with literature

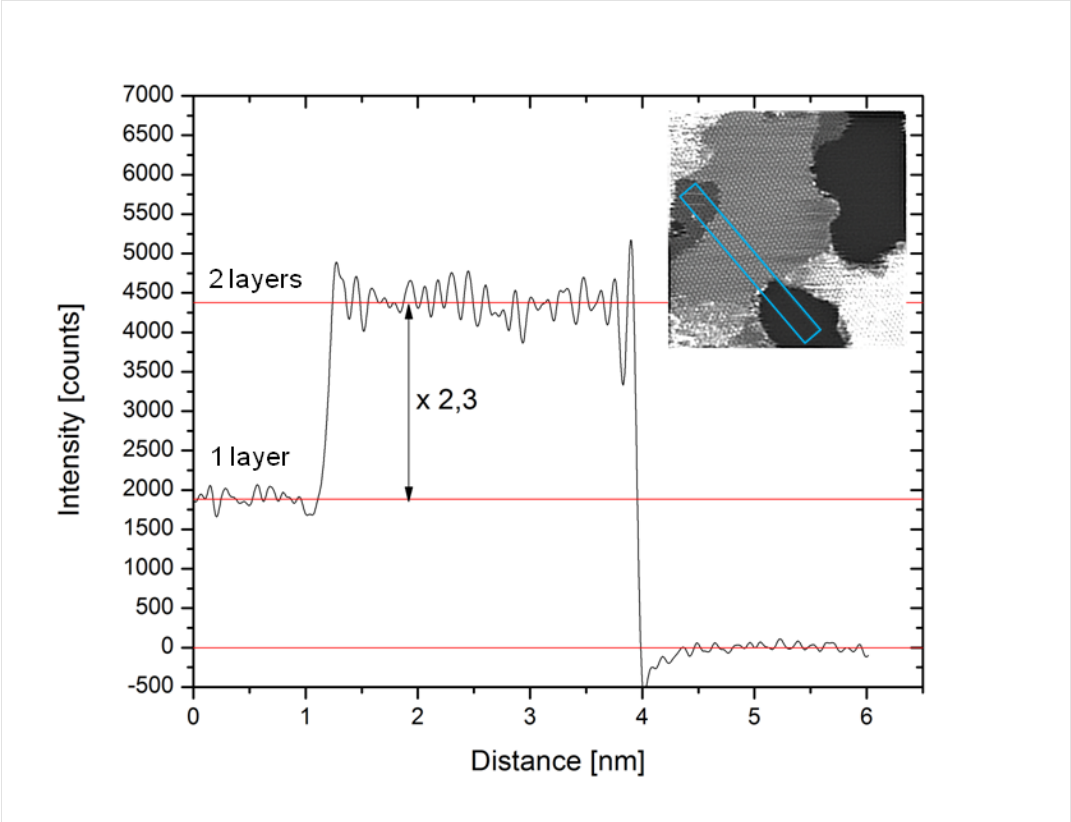

Figure 5.33: Intensity profile of the HRSTEM image shown in the insert at the top right

where Gass et al. determined a value of 2.7 [136]. Of course this method can not determine whether these are one and two or two and four layers. Nevertheless, information about the intensity ratio is very helpful for further characterization. Here it is assumed that the thinnest area is SLG, as it will be proved in the following section.
The same method was then used to characterize the image shown on the left in figure 5.34. For each area the intensity value was averaged over a region chosen as large as possible. The determined intensity values (each with subtracted background of 224399 counts) are 9238 (corresponds to 1 layer), 21194 (2 layers), 47155 (5 layers) and 69969 counts (more than 7 layers). In the right picture, where the section marked red is shown enlarged, the hexagonal structure of monolayer graphene can readily be seen.

To find and prove monolayer regions on the sample the plasmon peak method described in 4.3.4.1 on page 38 was used. Figure 5.35 shows the two areas chosen for the investigations. For the marked regions an EELS spectrum image was recorded with focus on the low energy regions were plasmon peaks occur.

Subsequently all spectra of the spectrum image (each with a size of 16 x 8 pixels) were summed up to obtain a single spectrum for each of the two regions. The π-peak at 5-7 eV has to be ignored in this case. Due to technical limitations the zero loss peak could not be recorded because of its high intensity compared to the plasmon signals. This limitation hin-

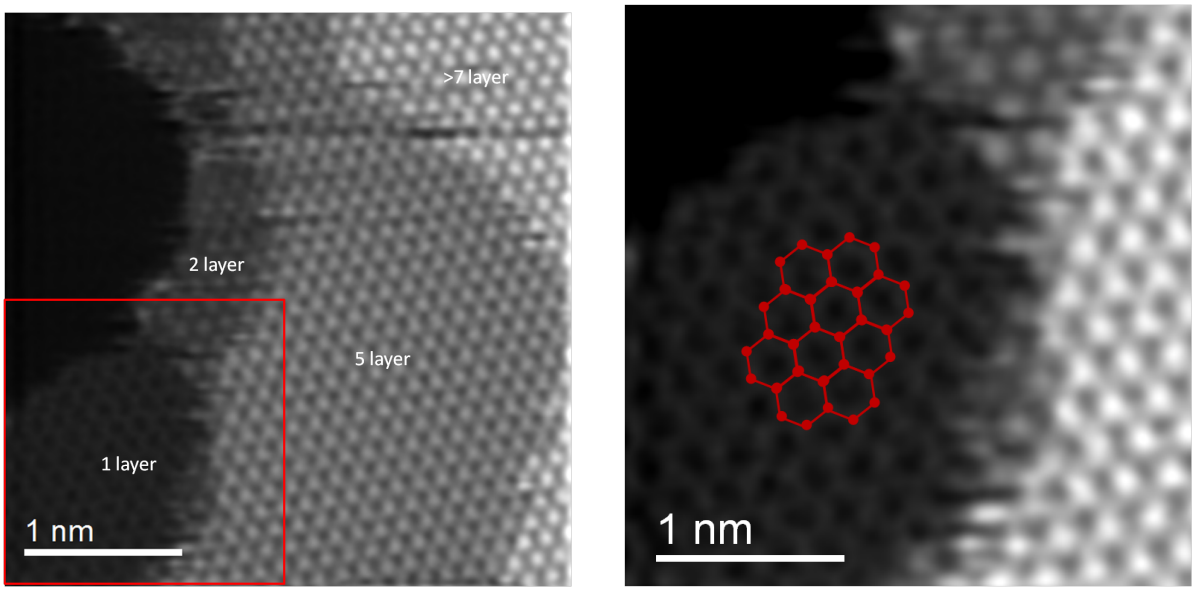

Figure 5.34: HRSTEM HAADF image bandpass filtered (left) with close up view on red marked section (red)

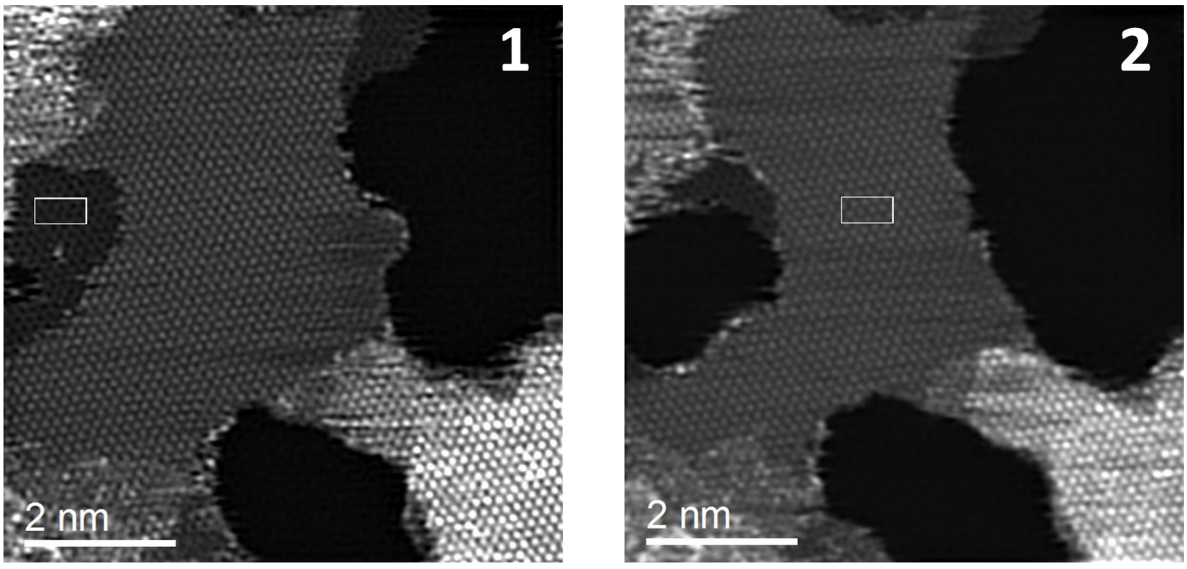

Figure 5.35: HR HAADF STEM pictures (Titan^3™@ 80 kV) of the same sample region with marked areas for the respective spectrum images

dered the exact subtraction of the zero loss signal. Since the π-peak is located very close to the zero loss peak it was not possible to reconstruct this peak properly. In this case the background subtraction was done with Origin 8.5 because it offers a more flexible fitting tool with a lot of available functions. Here the allometric power function fit was used. The numbers in the graph shown in 5.36 correspond to the numbers given in figure 5.35.
Comparison with the data from literature (see chapter 4.3.4.1) directly leads to the conclusion

that region 1 is a monolayer, due to the shape (the bulk peak is completely absent) and the position (the maximum is at 15 eV) of the σ-π-peak. The black spectrum representing region two already exhibits an bulk plasmon peak. Thus this is more than one layer. Again compared with data from the literature one can argue that there are less than 4 layers, otherwise the peak would be already shifted to a higher energy. As a result of the last section (intensity analysis, figure 5.33) we know that the thicker region has around double the intensity of the thinner one. Finally we can assume that the area containing region 2 is bilayer graphene.

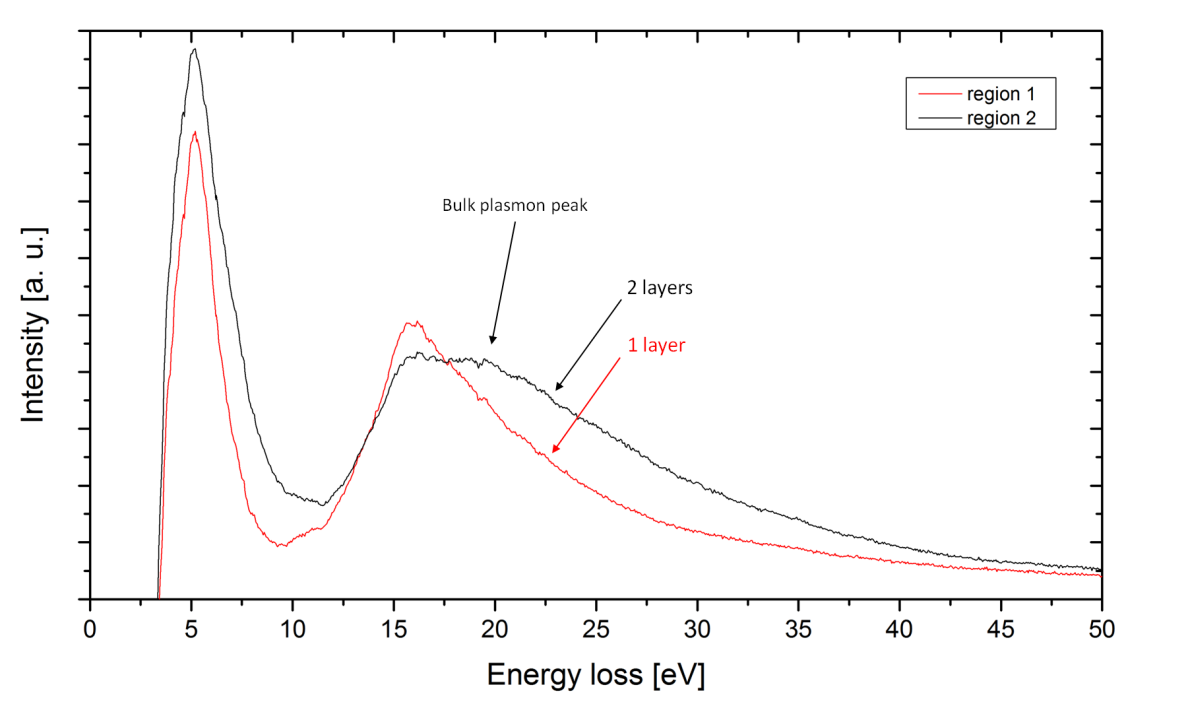

Figure 5.36: Summed up EELS spectra of the two regions

Picture (a) in figure 5.37 shows a STEM bright field image of the edge of a FLG sheet exhibiting four dark lines, each corresponding to a single layer fold. Via counting these folds the thickness of a graphene sheet can be roughly estimated at the edge of a sheet, as described in section 4.3.5 on page 40. In the present case there are four dark lines visible which leads to an estimated thickness of four to eight layers. The interlayer distance, estimated via an intensity profile (diagram (b)) amounts to 0.35 nm which agrees well with the interlayer distance of graphite of 0.335 nm. The STEM bright field image in (c) depicts an area near the edge in picture (a) showing the typical Moiré patterns of FLG.

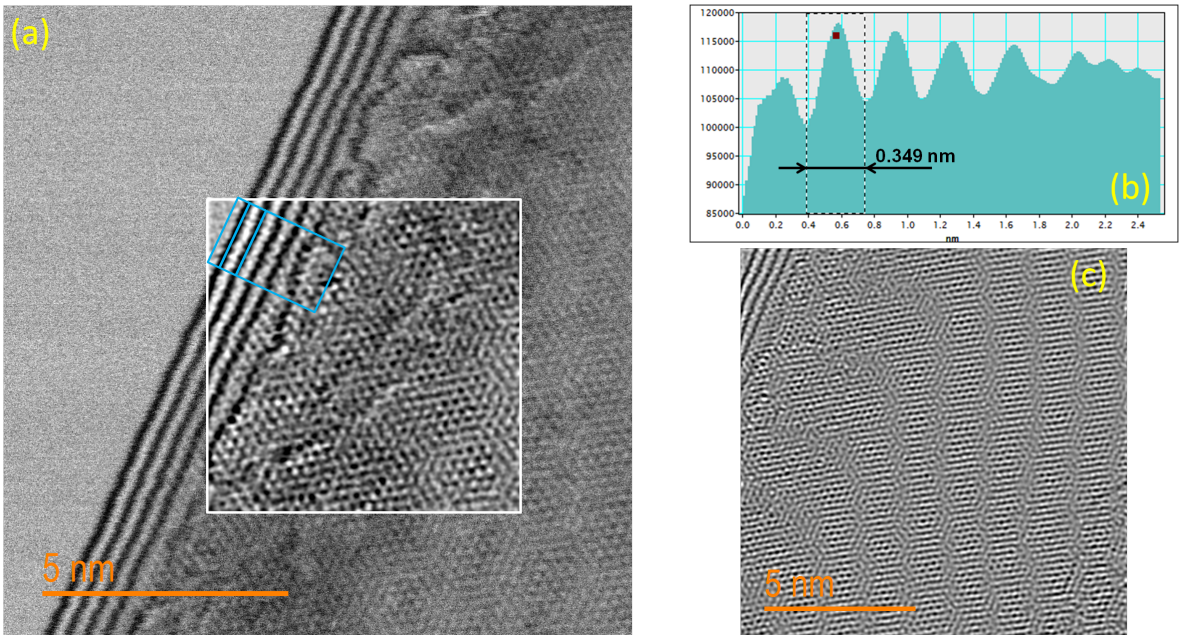

Figure 5.37: (a) STEM bright field image (Titan^3™@ 80 kV) of the fourfold edge of a graphene sheet, the section marked with an white box is bandpass filtered as against the outside area is showing the raw data; (b) intensity trace of the path marked with the cyan box in (a), showing an interlayer distance of ∼0.35 nm; (c) STEM BF image of a region farther back of the same edge exhibiting the typical Moiré patterns of FLG.

5.4.3.4 Conclusion

The methods used for preparation and characterisation were developed and improved sample by sample within the scope of our experiments. Sample 2 is reflecting one of the latest versions of our preparation methodology. Finally it is the most investigated sample. A lot of different characterisation methods were tried by means of most of the instruments available. Interestingly, Sample 2 exhibited almost no contamination in the electron beam, which facilitated our analytical TEM investigations a lot.

5.4.4 Sample 3

In contrast to the other samples HOPG was used as feedstock for the preparation of Sample 3, with polystyrene on 100 nm SiO_2 as substrate. The preparation was done with the method described in 3.1 on page 16. The transfer to the TEM grid was done with a older variant of the method described in 5.4.3 on page 64 without applying a protection layer, similar to Sample 2.

5.4.4.1 Optical microscopy

Optical characterisation showed a lot of graphite flakes sticking on the substrate with a rather shattered structure and a lot of quite small thin regions compared to the samples made from natural graphite. Figure 5.38 shows an optical image of a interesting area on Sample 1. As mentioned in section 4.1 on page 29 the colour shift of thin sheets in this case is significantly lower due to the polymer film on the 100 nm substrate, as the overall thickness is already close to the low contrast range of around 150 nm (see figure 4.2 on page 30).

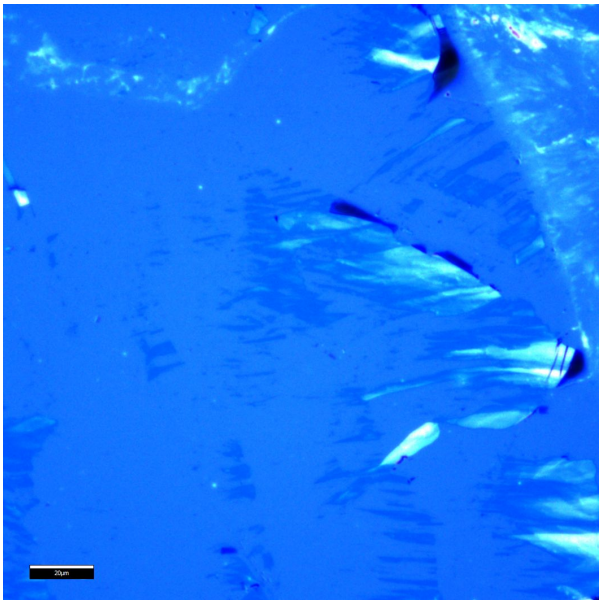

Figure 5.38: Region on Sample 3 with a lot of graphene sheets of different thicknesses (scale bar: 20 µm)

As the graphene structures on the substrate are quite shattered no particular flake, but the whole region was chosen for the transfer. No prior Raman- nor AFM-investigations were done. Thus thin regions were searched via TEM, among the flakes of the whole region.

5.4.4.2 (S)TEM and EELS

In order to specify the thickness of a chosen graphene flake, shown in figure 5.39, again EELS line scans were recorded. In this case a TEM image of the flake was aquired and is shown here instead of the STEM picture needed for the line scans, because of its better quality. Two of these scanning paths can also be seen in this figure as white lines. The white numbers are the numbers of these paths and correspond to the spectra names in figure 5.40. From each path four points were chosen, each point with number and colour correspond to a single spectrum line. All pictures and data were acquired by means of the Philips CM 20. The measuring time (0,1 s per pixel for scan 18 and 0,2 s per pixel for scan 19) was chosen as small as possible to avoid contamination on the surface.

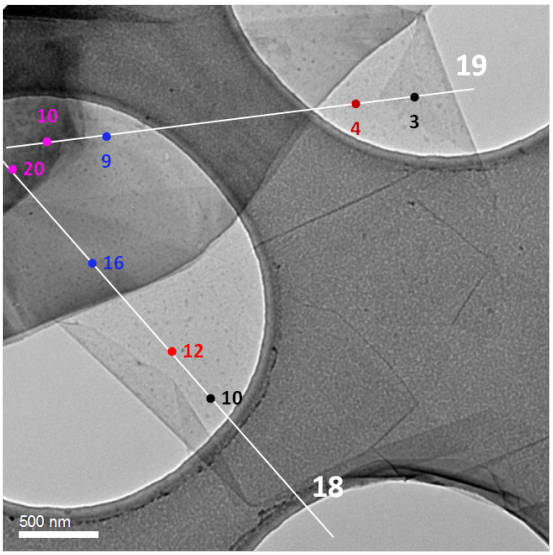

Figure 5.39: TEM image with the paths of the two STEM-EELS line scans and the evaluated points

In all spectra a remarkable bulk peak can be seen. Accordingly, there were no SLG regions on this flake. Nevertheless, in this example a lot about the interesting relations between the plasmon peaks position and the thickness could be learned. For instance, the first line scan (number 19) contains a folded up region. Hence the spectrum of point number 4 corresponds to a region double in thickness compared to the region of point 3. After comparison with data from the literature, especially concerning the position of the σ-π-peak ([157]) it can be argued that point 4 corresponds to a graphene sheet with less than 5 but more than 2 layers. If we take the peak position of point 3 in account, with which around 6 layers can be assumed, point 4 may correspond to trilayer graphene. The other 2 points in this line scan represent areas of thin graphite with more than 10 layers. After comparing the four spectra of line scan 18 with the data from [157] we can hazard a guess that the points 10 and 12 correspond to bi- or trilayer graphene, whereas the points 16 and 20 again correspond to graphite with more than 10 layers.

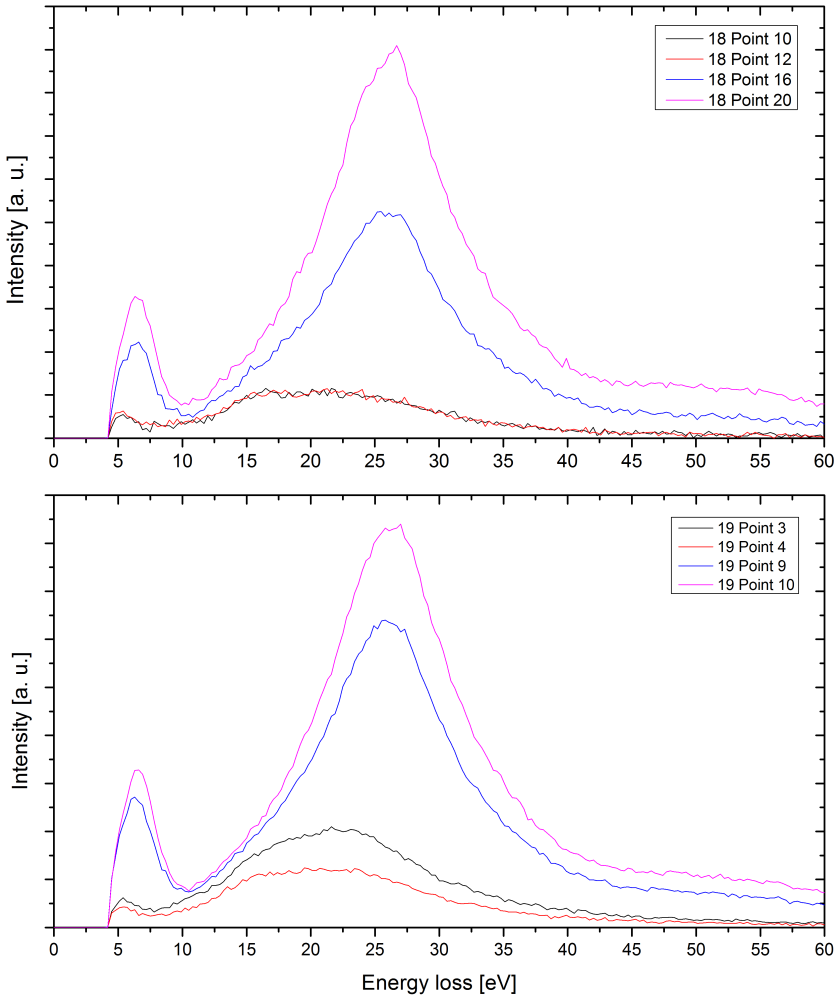

Figure 5.40: Spectra of the chosen points marked in figure 5.39, the colours and numbers correspond to the lines; top: spectra of line scan 18, bottom: spectra of line scan 19

5.4.4.3 Conclusion

With Sample 3 it could be demonstrated how the thickness of free standing graphene can be determinated by dint of the plasmon peaks in an EELS spectrum. Even though an absolute determination is not possible with this method, an approximative identification of thin regions is possible. Even with quite out-dated equipment, considering the low energy resolution of the used EELS spectra recorded with the Philips CM 20. Thus, for exact determination complementary investigations with other methods are necessary, as demonstrated with Sample 2. Nevertheless, from the measurements on this sample a lot about the methodology and the evaluation could be learned. Furthermore it can be seen that HOPG yields very shattered structures with our preparation method. Even though also a lot of thin regions can be found among the graphitic formations, they are in most cases rather small. To this end it is recommended to use natural graphite as feedstock.

6 Conclusion

6.1 Future prospects

In terms of its usability in the scope of the further research at the FELMI-ZFE especially TEM grids enhanced with graphene may be interesting. Since it has the lowest possible thickness it is the ideal substrate for TEM investigations of nanoparticles, atomic clusters, biological material and other samples exhibiting only low contrast in a TEM. Graphene enhanced TEM grids are already commercially available and two of them were analysed in the scope of this thesis (see section 5.1), both showing major drawbacks. Hence, in many cases it seems to be advantageous to produce graphene in-house via mechanical exfoliation, if only a few, very clean SLG areas are needed, as performed in this thesis, or via one of the other presented methods (Cu-CVD may be worth to be considered for large area monolayers synthesis). Thus for this purpose these methods should be improved in possible future theses. Another rather new approach using graphene as TEM substrate allows studies of specimen in a liquid environment. To this end the solution is encapsulated between two graphene sheets (see figure 6.1, forming a graphene liquid cell. Yuk et al. introduced this method for investigations of colloidal nanocrystals in their article [133].

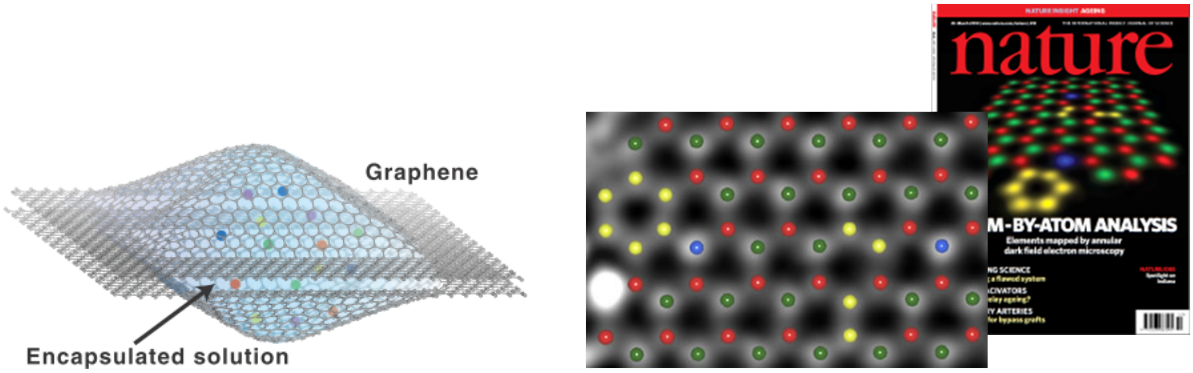

Figure 6.1: Left: illustration of a graphene liquid cell encapsulating a colloidal solution (from [133]; right: ADF STEM picture of the atomic structure of a single BN layer with impurities, overlayed coloured spheres correspond to the single atoms identified via histogram analysis (red: boron, green: nitrogen, yellow: carbon, blue oxygen; (adapted from [135])) background: cover of the nature issue containing the study

The techniques developed and applied in this thesis may also be useful for investigations of (doped) graphene or other two-dimensional materials (eg. boron nitride). Considering the comprehensive and powerful analytical facilities at FELMI-ZFE this seems to be worth to be

considered. Even though atomically resolved elemental studies of boron nitride monolayer have been performed by Krivanek et al. [135] by ADF STEM contrast or [162] by HRTEM phase contrast, an approach via analytical STEM seems to be promising. Atom-by-atom EELS spectroscopy on the other hand was performed by Suenaga et al. [149] at graphene edges, discriminating single-, double- and triple coordinated carbon atoms via analysis of the carbon edge fine structure. Furthermore for TEM at atomic resolution, exit-wave reconstruction 4.3.3.2 may also be interesting for future studies.

6.2 Summary

A lot of different instruments and various methods were used within the scope of this study in order to characterise graphene samples, purchased and self-made ones, especially in terms of their thickness. Optical microscopy, Raman spectroscopy, atomic force microscopy and scanning electron microscopy were used for pre-characterisations, in order to identify single layer graphene areas for further investigations via (scanning) transmission electron microscopy.
Two different kind of commercially available graphene enhanced TEM grids were analysed in order to evaluate them and to test different characterisation methods (see 5.1). The Ni-CVD graphene enhanced grids, purchased from `https://graphene-supermarket.com/` exhibited large thin areas, but were highly contaminated with a indeterminable substance. This has been affirmed via optical microscopy, (S)TEM EELS and Raman. Using them for analytical TEM was thus impossible. By contrast on the TEM grids enhanced with graphene, produced via the substrate-less argon-plasma method (purchased from `www.fishersci.com`), a lot of wrinkled and agglomerated graphene sheets with only a few, very small SLG patches could be found. However the contamination was found to be quite low. It was thus used as benchmark material for TEM analysis methods.
Furthermore self made graphene samples were successfully prepared and transferred to TEM grids, so as to produce free-standing graphene. For this purpose various methods based on mechanical exfoliation were tried and adapted (see section 3.1). The finally obtained sheets exhibited very clean single layer patches. Their thickness was determined by means of (S)TEM by evaluation of the intensity relations in (S)TEM images (section 4.3.2.1), the Fourier transformed (section 4.3.3.1) HRTEM pictures, electron energy loss spectra of plasmon excitations 4.3.4.1, HR(S)TEM of graphene edges (4.3.5) and STEM images at atomic resolution (4.3.2). All the mentioned characterisation methods were performed on Sample 2 and the experimental results can be found in section 5.4.2 it detail.

Bibliography

[1] K. S. Novoselov, A. K. Geim, S. V. Morozov, D. Jiang, Y. Zhang, S. V. Dubonos, I. V. Grigorieva, and A. A. Firsov. "Electric Field Effect in Atomically Thin Carbon Films". In: *Science* 306.5696 (2004), pp. 666–669.

[2] L. D. Landau. "Zur Theorie der Phasenumwandlungen II". In: *Phys. Z. Sowjetunion* 11 (1937), pp. 26–35.

[3] R. E. Peierls. "Quelques proprietes typiques des corpses solides". In: *Ann. Inst. Henri Poincare* 5 (1935), pp. 177–222.

[4] Class for Physics of the Royal Swedish Academy of Sciences. *Graphene: Scientific Background on the Nobel Prize in Physics 2010*. Ed. by Class for Physics of the Royal Swedish Academy of Sciences. 2010. URL: `http://www.nobelprize.org/nobel_prizes/physics/laureates/2010/advanced-physicsprize2010.pdf`.

[5] E. Frieden. "The Chemical Elements of Life". In: *Scientific American* 227.1 (1972), pp. 52–60. URL: `http://www.nature.com/scientificamerican/journal/v227/n1/pdf/scientificamerican0772-52.pdf`.

[6] B. Trauzettel. "Von Graphit zu Graphen". In: *Physik Journal* 7 (2007).

[7] A. K. Geim and K. S. Novoselov. "The Rise of Graphene". In: *Nature Materials* (2007), pp. 183–191.

[8] M. Han, B. Özyilmaz, Y. Zhang, and P. Kim. "Energy Band-Gap Engineering of Graphene Nanoribbons". In: *Physical Review Letters* 98.20 (2007).

[9] K. Nakada, M. Fujita, G. Dresselhaus, and M. Dresselhaus. "Edge state in graphene ribbons: Nanometer size effect and edge shape dependence". In: *Physical Review B* 54.24 (1996), pp. 17954–17961.

[10] D. R. Cooper, B. D'Anjo, N. Ghattamaneni, B. Harack, M. Hilke, A. Horth, N. Majlis, M. V. L. Massicotte, E. Whiteway, and V. Yu. "Experimental review of graphene". In: *ISRN Condensed Matter Physics* 2012.501686 (2012).

[11] M. J. Carlsson. "Graphene: Buckle or break". In: *Nature Materials* 6 (2007), pp. 801–802.

[12] N. D. Mermin. "Crystalline Order in Two Dimensions". In: *Physical Review* 176.1 (1968), pp. 250–254. URL: `http://dx.doi.org/10.1103/PhysRev.176.250`.

[13] J. A. Venables, G. D. T. Spiller, and M. Hanbucken. "Nucleation and growth of thin films". In: *Reports on Progress in Physics* 47.4 (1984), pp. 399–459.

[14] J. C. Meyer, A. K. Geim, M. I. Katsnelson, K. S. Novoselov, T. J. Booth, and S. Roth. "The structure of suspended graphene sheets". In: *Nature* 446.7131 (2007), pp. 60–63.

[15] U. Bangert, M. H. Gass, A. L. Bleloch, R. R. Nair, and A. K. Geim. "Manifestation of ripples in free-standing graphene in lattice images obtained in an aberration-corrected scanning transmission electron microscope". In: *physica status solidi (a)* 206.6 (2009), pp. 1117–1122.

[16] J. Brivio, D. T. L. Alexander, and A. Kis. "Ripples and Layers in Ultrathin MoS 2 Membranes". In: *Nano Letters* 11.12 (2011), pp. 5148–5153.

[17] R. R. Nair, P. Blake, A. N. Grigorenko, K. S. Novoselov, T. J. Booth, T. Stauber, N. M. R. Peres, and A. K. Geim. "Fine Structure Constant Defines Visual Transparency of Graphene". In: *Science* 320.5881 (2008), p. 1308.

[18] S. Bae, H. Kim, Y. Lee, X. Xu, J.-S. Park, Y. Zheng, J. Balakrishnan, T. Lei, H. Ri Kim, Y. I. Song, Y.-J. Kim, K. S. Kim, B. Özyilmaz, J.-H. Ahn, B. H. Hong, and S. Iijima. "Roll-to-roll production of 30-inch graphene films for transparent electrodes". In: *Nature Nanotechnology* 5.8 (2010), pp. 574–578.

[19] P. R. Wallace. "The Band Theory of Graphite". In: *Physical Review* 71.9 (1947), pp. 622–634. URL: http://dx.doi.org/10.1103/PhysRev.71.622.

[20] S. Das Sarma, S. Adam, E. Hwang, and E. Rossi. "Electronic transport in two-dimensional graphene". In: *Reviews of Modern Physics* 83.2 (2011), pp. 407–470.

[21] B. Partoens and F. Peeters. "From graphene to graphite: Electronic structure around the K point". In: *Physical Review B* 74.7 (2006).

[22] J. Hass, W. A. d. Heer, and E. H. Conrad. "The growth and morphology of epitaxial multilayer graphene". In: *Journal of Physics: Condensed Matter* 20.32 (2008), p. 323202.

[23] C. N. R. Rao, K. Biswas, K. S. Subrahmanyam, and A. Govindaraj. "Graphene, the new nanocarbon". In: *Journal of Materials Chemistry* 19.17 (2009), p. 2457.

[24] K. Bolotin, K. Sikes, Z. Jiang, M. Klima, G. Fudenberg, J. Hone, P. Kim, and H. Stormer. "Ultrahigh electron mobility in suspended graphene". In: *Solid State Communications* 146.9-10 (2008), pp. 351–355.

[25] J.-H. Chen, C. Jang, S. Xiao, M. Ishigami, and M. S. Fuhrer. "Intrinsic and extrinsic performance limits of graphene devices on SiO2". In: *Nature Nanotechnology* 3.4 (2008), pp. 206–209.

[26] K. S. Novoselov, A. K. Geim, S. V. Morozov, D. Jiang, M. I. Katsnelson, I. V. Grigorieva, S. V. Dubonos, and A. A. Firsov. "Two-dimensional gas of massless Dirac fermions in graphene". In: *Nature* 438.7065 (2005), pp. 197–200.

[27] K. S. Novoselov, D. Jiang, F. Schedin, T. J. Booth, V. V. Khotkevich, S. V. Morozov, and A. K. Geim. "Two-dimensional atomic crystals". In: *Proceedings of the National Academy of Sciences* 102.30 (2005), pp. 10451–10453.

[28] A. K. Geim. “Graphene: Status and Prospects”. In: *Science* 324.5934 (2009), pp. 1530–1534.

[29] A. K. Geim and A. H. MacDonald. “Graphene: Exploring Carbon Flatland”. In: *Physics Today* 60.8 (2007), p. 35.

[30] A. H. Castro Neto, N. M. R. Peres, K. S. Novoselov, and A. K. Geim. “The electronic properties of graphene”. In: *Reviews of Modern Physics* 81.1 (2009), pp. 109–162.

[31] C. Lee, X. Wei, J. W. Kysar, and J. Hone. “Measurement of the Elastic Properties and Intrinsic Strength of Monolayer Graphene”. In: *Science* 321.5887 (2008), pp. 385–388.

[32] M. A. Rafiee, J. Rafiee, Z. Wang, H. Song, Z.-Z. Yu, and N. Koratkar. “Enhanced Mechanical Properties of Nanocomposites at Low Graphene Content”. In: *ACS Nano* 3.12 (2009), pp. 3884–3890.

[33] V. Adamyan and V. Zavalniuk. “Phonons in graphene with point defects”. In: *Journal of Physics: Condensed Matter* 23.1 (2011), p. 015402.

[34] A. A. Balandin, S. Ghosh, W. Bao, I. Calizo, D. Teweldebrhan, F. Miao, and C. N. Lau. “Superior Thermal Conductivity of Single-Layer Graphene”. In: *Nano Letters* 8.3 (2008), pp. 902–907.

[35] S. Ghosh, I. Calizo, D. Teweldebrhan, E. P. Pokatilov, D. L. Nika, A. A. Balandin, W. Bao, F. Miao, and C. N. Lau. “Extremely high thermal conductivity of graphene: Prospects for thermal management applications in nanoelectronic circuits”. In: *Applied Physics Letters* 92.15 (2008), p. 151911.

[36] K. H. Lee, H.-J. Shin, J. Lee, I.-y. Lee, G.-H. Kim, J.-Y. Choi, and S.-W. Kim. “Large-Scale Synthesis of High-Quality Hexagonal Boron Nitride Nanosheets for Large-Area Graphene Electronics”. In: *Nano Letters* 12.2 (2012), pp. 714–718.

[37] D. Kopeliovich. *Boron nitride as solid lubricant*. 2012. URL: `http://www.substech.com/dokuwiki/doku.php?id=boron_nitride_as_solid_lubricant`.

[38] J. N. Coleman, M. Lotya, A. O’Neill, S. D. Bergin, P. J. King, U. Khan, K. Young, A. Gaucher, S. De, R. J. Smith, I. V. Shvets, S. K. Arora, G. Stanton, H.-Y Kim, K. Lee, G. T. Kim, G. S. Duesberg, T. Hallam, J. J. Boland, J. J. Wang, J. F. Donegan, J. C. Grunlan, G. Moriarty, A. Shmeliov, R. J. Nicholls, J. M. Perkins, E. M. Grieveson, K. Theuwissen, D. W. McComb, P. D. Nellist, and V. Nicolosi. “Two-Dimensional Nanosheets Produced by Liquid Exfoliation of Layered Materials”. In: *Science* 331.6017 (2011), pp. 568–571.

[39] L. Song, L. Ci, H. Lu, P. B. Sorokin, C. Jin, J. Ni, A. G. Kvashnin, D. G. Kvashnin, J. Lou, B. I. Yakobson, and P. M. Ajayan. “Large Scale Growth and Characterization of Atomic Hexagonal Boron Nitride Layers”. In: *Nano Letters* 10.8 (2010), pp. 3209–3215.

[40] G. Giovannetti, P. Khomyakov, G. Brocks, P. Kelly, and J. van den Brink. “Substrate-induced band gap in graphene on hexagonal boron nitride: Ab initio density functional calculations”. In: *Physical Review B* 76.7 (2007).

[41] H. S. S. Ramakrishna Matte, A. Gomathi, A. K. Manna, D. J. Late, R. Datta, S. K. Pati, and C. N. R. Rao. "MoS2 and WS2 Analogues of Graphene". In: *Angewandte Chemie International Edition* (2010), n/a.

[42] B. Radisavljevic, A. Radenovic, J. Brivio, V. Giacometti, and A. Kis. "Single-layer MoS2 transistors". In: *Nature Nanotechnology* 6.3 (2011), pp. 147–150.

[43] R. Mas-Ballesté, C. Gómez-Navarro, J. Gómez-Herrero, and F. Zamora. "2D materials: to graphene and beyond". In: *Nanoscale* 3.1 (2011), p. 20.

[44] K. S. Novoselov and A. H. Castro Neto. "Two-dimensional crystals-based heterostructures: materials with tailored properties". In: *Physica Scripta* 146 (2012), p. 014006.

[45] K. Takeda and K. Shiraishi. "Theoretical possibility of stage corrugation in Si and Ge analogs of graphite". In: *Physical Review B* 50.20 (1994), pp. 14916–14922.

[46] P. Vogt, P. d. Padova, C. Quaresima, J. Avila, E. Frantzeskakis, M. Asensio, A. Resta, B. Ealet, and G. Le Lay. "Silicene: Compelling Experimental Evidence for Graphene-like Two-Dimensional Silicon". In: *Physical Review Letters* 108.15 (2012).

[47] B. Lalmi, H. Oughaddou, H. Enriquez, A. Kara, S. Vizzini, B. Ealet, and B. Aufray. "Epitaxial growth of a silicene sheet". In: *Applied Physics Letters* 97.22 (2010), p. 223109.

[48] B. Feng, Z. Ding, S. Meng, Y. Yao, X. He, P. Cheng, L. Chen, and K. Wu. "Evidence of Silicene in Honeycomb Structures of Silicon on Ag(111)". In: *Nano Letters* 12.7 (2012), pp. 3507–3511.

[49] L. Chen, C.-C. Liu, B. Feng, X. He, P. Cheng, Z. Ding, S. Meng, Y. Yao, and K. Wu. "Evidence for Dirac Fermions in a Honeycomb Lattice Based on Silicon". In: *Physical Review Letters* 109.5 (2012).

[50] A. Kara, H. Enriquez, A. P. Seitsonen, L. Lew Yan Voon, S. Vizzini, B. Aufray, and H. Oughaddou. "A review on silicene — New candidate for electronics". In: *Surface Science Reports* 67.1 (2012), pp. 1–18.

[51] F. Schedin, A. K. Geim, S. V. Morozov, E. W. Hill, P. Blake, M. I. Katsnelson, and K. S. Novoselov. "Detection of individual gas molecules adsorbed on graphene". In: *Nature Materials* 6.9 (2007), pp. 652–655.

[52] A. A. Kaverzin, S. M. Strawbridge, A. S. Price, F. Withers, A. K. Savchenko, and D. W. Horsell. "Electrochemical doping of graphene". PhD thesis. Exeter and UK: University of Exeter, 2010.

[53] B. Guo, L. Fang, B. Zhang, and J. R. Gong. "Graphene Doping: A Review". In: *Insciences Journal* (2011), pp. 80–89.

[54] L. S. Panchakarla, K. S. Subrahmanyam, S. K. Saha, A. Govindaraj, H. R. Krishnamurthy, U. V. Waghmare, and C. N. R. Rao. "Synthesis, Structure, and Properties of Boron- and Nitrogen-Doped Graphene". In: *Advanced Materials* (2009), NA.

[55] L. Zhao, R. He, K. T. Rim, T. Schiros, K. S. Kim, H. Zhou, C. Gutierrez, S. P. Chockalingam, C. J. Arguello, L. Palova, D. Nordlund, M. S. Hybertsen, D. R. Reichman, T. F. Heinz, P. Kim, A. Pinczuk, G. W. Flynn, and A. N. Pasupathy. "Visualizing Individual Nitrogen Dopants in Monolayer Graphene". In: *Science* 333.6045 (2011), pp. 999–1003.

[56] J. C. Meyer, S. Kurasch, H. J. Park, V. Skakalova, D. Künzel, A. Groß, A. Chuvilin, G. Algara-Siller, S. Roth, T. Iwasaki, U. Starke, J. H. Smet, and U. Kaiser. "Experimental analysis of charge redistribution due to chemical bonding by high-resolution transmission electron microscopy". In: *Nature Materials* 10.3 (2011), pp. 209–215.

[57] D. C. Elias, R. R. Nair, T. M. G. Mohiuddin, S. V. Morozov, P. Blake, M. P. Halsall, A. C. Ferrari, D. W. Boukhvalov, M. I. Katsnelson, A. K. Geim, and K. S. Novoselov. "Control of Graphene's Properties by Reversible Hydrogenation: Evidence for Graphane". In: *Science* 323.5914 (2009), pp. 610–613.

[58] L. Yan, Y. B. Zheng, F. Zhao, S. Li, X. Gao, B. Xu, P. S. Weiss, and Y. Zhao. "Chemistry and physics of a single atomic layer: strategies and challenges for functionalization of graphene and graphene-based materials". In: *Chemical Society Reviews* 41.1 (2011), p. 97.

[59] A. K. Geim and P. Kim. "Carbon Wonderland". In: *Scientific American* 298.4 (2008), pp. 90–97.

[60] J. Rafiee, X. Mi, H. Gullapalli, A. V. Thomas, F. Yavari, Y. Shi, P. M. Ajayan, and N. A. Koratkar. "Wetting transparency of graphene". In: *Nature Materials* 11.3 (2012), pp. 217–222.

[61] D. Sen, K. S. Novoselov, P. M. Reis, and M. J. Buehler. "Tearing Graphene Sheets From Adhesive Substrates Produces Tapered Nanoribbons". In: *Small* 6.10 (2010), pp. 1108–1116.

[62] S. P. Koenig, N. G. Boddeti, M. L. Dunn, and J. S. Bunch. "Ultrastrong adhesion of graphene membranes". In: *Nature Nanotechnology* 6.9 (2011), pp. 543–546.

[63] Z. Liu, J. Z. Liu, Y. Cheng, Z. Li, L. Wang, and Q. Zheng. "Interlayer binding energy of graphite: A mesoscopic determination from deformation". In: *Physical Review B* 85.20 (2012).

[64] P. Nemes-Incze, Z. Osváth, K. Kamarás, and L. Biró. "Anomalies in thickness measurements of graphene and few layer graphite crystals by tapping mode atomic force microscopy". In: *Carbon* 46.11 (2008), pp. 1435–1442.

[65] A. Chuvilin, U. Kaiser, E. Bichoutskaia, N. A. Besley, and A. N. Khlobystov. "Direct transformation of graphene to fullerene". In: *Nature Chemistry* 2.6 (2010), pp. 450–453.

[66] C. Berger, Z. Song, T. Li, X. Li, A. Y. Ogbazghi, R. Feng, Z. Dai, A. N. Marchenkov, E. H. Conrad, P. N. First, and W. A. d. Heer. "Ultrathin Epitaxial Graphite: 2D Electron Gas Properties and a Route toward Graphene-based Nanoelectronics". In: *The Journal of Physical Chemistry B* 108.52 (2004), pp. 19912–19916.

[67] K. V. Emtsev, A. Bostwick, K. Horn, J. Jobst, G. L. Kellogg, L. Ley, J. L. McChesney, T. Ohta, S. A. Reshanov, J. Röhrl, E. Rotenberg, A. K. Schmid, D. Waldmann, H. B. Weber, and T. Seyller. "Towards wafer-size graphene layers by atmospheric pressure graphitization of silicon carbide". In: *Nature Materials* 8.3 (2009), pp. 203–207.

[68] W. Choi, I. Lahiri, R. Seelaboyina, and Y. S. Kang. "Synthesis of Graphene and Its Applications: A Review". In: *Critical Reviews in Solid State and Materials Sciences* 35.1 (2010), pp. 52–71.

[69] Z. Sun, Z. Yan, J. Yao, E. Beitler, Y. Zhu, and J. M. Tour. "Growth of graphene from solid carbon sources". In: *Nature* 468.7323 (2010), pp. 549–552.

[70] H. Itoh, T. Ichnose, C. Oshima, T. Ichinokowa, and T. Aizawa. "Scanning tunneling microscopy of monolayer graphite epitaxially grown on a TiC(111) surface". In: *Surface Science Letters* 254.1-3 (1991), pp. L437–L442.

[71] T. Land, T. Michely, R. Behm, J. Hemminger, and G. Comsa. "STM investigation of single layer graphite structures produced on Pt(111) by hydrocarbon decomposition". In: *Surface Science* 264.3 (1992), pp. 261–270.

[72] Q. Yu, J. Lian, S. Siriponglert, H. Li, Y. P. Chen, and S.-S. Pei. "Graphene segregated on Ni surfaces and transferred to insulators". In: *Applied Physics Letters* 93.11 (2008), p. 113103.

[73] R. Addou, A. Dahal, P. Sutter, and M. Batzill. "Monolayer graphene growth on Ni(111) by low temperature chemical vapor deposition". In: *Applied Physics Letters* 100.2 (2012), p. 021601.

[74] Q. Yu, L. A. Jauregui, W. Wu, R. Colby, J. Tian, Z. Su, H. Cao, Z. Liu, D. Pandey, D. Wei, T. F. Chung, P. Peng, N. P. Guisinger, E. A. Stach, J. Bao, S.-S. Pei, and Y. P. Chen. "Control and characterization of individual grains and grain boundaries in graphene grown by chemical vapour deposition". In: *Nature Materials* 10.6 (2011), pp. 443–449.

[75] X. Li, W. Cai, J. An, S. Kim, J. Nah, D. Yang, R. Piner, A. Velamakanni, I. Jung, E. Tutuc, S. K. Banerjee, L. Colombo, and R. S. Ruoff. "Large-Area Synthesis of High-Quality and Uniform Graphene Films on Copper Foils". In: *Science* 324.5932 (2009), pp. 1312–1314.

[76] X. Li, C. W. Magnuson, A. Venugopal, J. An, J. W. Suk, B. Han, M. Borysiak, W. Cai, A. Velamakanni, Y. Zhu, L. Fu, E. M. Vogel, E. Voelkl, L. Colombo, and R. S. Ruoff. "Graphene Films with Large Domain Size by a Two-Step Chemical Vapor Deposition Process". In: *Nano Letters* 10.11 (2010), pp. 4328–4334.

[77] P. Y. Huang, C. S. Ruiz-Vargas, A. M. van der Zande, W. S. Whitney, M. P. Levendorf, J. W. Kevek, S. Garg, J. S. Alden, C. J. Hustedt, Y. Zhu, J. Park, P. L. McEuen, and D. A. Muller. "Grains and grain boundaries in single-layer graphene atomic patchwork quilts". In: *Nature* 469.7330 (2011), pp. 389–392.

[78] S. Lee, K. Lee, and Z. Zhong. "Wafer Scale Homogeneous Bilayer Graphene Films by Chemical Vapor Deposition". In: *Nano Letters* 10.11 (2010), pp. 4702–4707.

[79] J. K. Wassei, M. Mecklenburg, J. A. Torres, J. D. Fowler, B. C. Regan, R. B. Kaner, and B. H. Weiller. “Chemical Vapor Deposition of Graphene on Copper from Methane, Ethane and Propane: Evidence for Bilayer Selectivity”. In: *Small* 8.9 (2012), pp. 1415–1422.

[80] X. Li, C. W. Magnuson, A. Venugopal, R. M. Tromp, J. B. Hannon, E. M. Vogel, L. Colombo, and R. S. Ruoff. “Large-Area Graphene Single Crystals Grown by Low-Pressure Chemical Vapor Deposition of Methane on Copper”. In: *Journal of the American Chemical Society* 133.9 (2011), pp. 2816–2819.

[81] G. Wang, F. Qian, C. W. Saltikov, Y. Jiao, and Y. Li. “Microbial reduction of graphene oxide by Shewanella”. In: *Nano Research* 4.6 (2011), pp. 563–570.

[82] R. R. Nair, H. A. Wu, P. N. Jayaram, I. V. Grigorieva, and A. K. Geim. “Unimpeded Permeation of Water Through Helium-Leak-Tight Graphene-Based Membranes”. In: *Science* 335.6067 (2012), pp. 442–444.

[83] B. C. Brodie. “On the Atomic Weight of Graphite”. In: *Philosophical Transactions of the Royal Society of London* 149.0 (1859), pp. 249–259.

[84] H. P. Boehm, A. Claus, G. O. Fischer, and U. Hofmann. “Dunnste Kohlenstoff-Folien”. In: *Zeitschrift für Naturforschung* 17.b (1962), pp. 150–153.

[85] A. K. Geim. “Graphene prehistory”. In: *Physica Scripta* 146 (2012), p. 014003.

[86] W. S. Hummers and R. E. Offeman. “Preparation of Graphitic Oxide”. In: *Journal of the American Chemical Society* 80.6 (1958), p. 1339.

[87] M. J. McAllister, J.-L. Li, D. H. Adamson, H. C. Schniepp, A. A. Abdala, J. Liu, M. Herrera-Alonso, D. L. Milius, R. Car, R. K. Prud’homme, and I. A. Aksay. “Single Sheet Functionalized Graphene by Oxidation and Thermal Expansion of Graphite”. In: *Chemistry of Materials* 19.18 (2007), pp. 4396–4404.

[88] W. Zhang, W. He, and X. Jing. “Preparation of a Stable Graphene Dispersion with High Concentration by Ultrasound”. In: *The Journal of Physical Chemistry B* 114.32 (2010), pp. 10368–10373.

[89] D. C. Marcano, D. V. Kosynkin, J. M. Berlin, A. Sinitskii, Z. Sun, A. Slesarev, L. B. Alemany, W. Lu, and J. M. Tour. “Improved Synthesis of Graphene Oxide”. In: *ACS Nano* 4.8 (2010), pp. 4806–4814.

[90] L. Tang, X. Li, R. Ji, K. S. Teng, G. Tai, J. Ye, C. Wei, and S. P. Lau. “Bottom-up synthesis of large-scale graphene oxide nanosheets”. In: *Journal of Materials Chemistry* 22.12 (2012), p. 5676.

[91] S. Stankovich, D. A. Dikin, R. D. Piner, K. A. Kohlhaas, A. Kleinhammes, Y. Jia, Y. Wu, S. T. Nguyen, and R. S. Ruoff. “Synthesis of graphene-based nanosheets via chemical reduction of exfoliated graphite oxide”. In: *Carbon* 45.7 (2007), pp. 1558–1565.

[92] S. Stankovich, D. A. Dikin, G. H. B. Dommett, K. M. Kohlhaas, E. J. Zimney, E. A. Stach, R. D. Piner, S. T. Nguyen, and R. S. Ruoff. "Graphene-based composite materials". In: *Nature* 442.7100 (2006), pp. 282–286.

[93] X. Li, H. Wang, J. T. Robinson, H. Sanchez, G. Diankov, and H. Dai. "Simultaneous Nitrogen Doping and Reduction of Graphene Oxide". In: *Journal of the American Chemical Society* 131.43 (2009), pp. 15939–15944.

[94] H.-J. Shin, K. K. Kim, A. Benayad, S.-M. Yoon, H. K. Park, I.-S. Jung, M. H. Jin, H.-K. Jeong, J. M. Kim, J.-Y. Choi, and Y. H. Lee. "Efficient Reduction of Graphite Oxide by Sodium Borohydride and Its Effect on Electrical Conductance". In: *Advanced Functional Materials* 19.12 (2009), pp. 1987–1992.

[95] J. Zhang, H. Yang, G. Shen, P. Cheng, J. Zhang, and S. Guo. "Reduction of graphene oxide vial-ascorbic acid". In: *Chemical Communications* 46.7 (2010), p. 1112.

[96] Z. Wang, X. Zhou, J. Zhang, F. Boey, and H. Zhang. "Direct Electrochemical Reduction of Single-Layer Graphene Oxide and Subsequent Functionalization with Glucose Oxidase". In: *The Journal of Physical Chemistry C* 113.32 (2009), pp. 14071–14075.

[97] S. Park and R. S. Ruoff. "Chemical methods for the production of graphenes". In: *Nature Nanotechnology* 4.4 (2009), pp. 217–224.

[98] W. Gao, L. B. Alemany, L. Ci, and P. M. Ajayan. "New insights into the structure and reduction of graphite oxide". In: *Nature Chemistry* 1.5 (2009), pp. 403–408.

[99] L. J. Cote, R. Cruz-Silva, and J. Huang. "Flash Reduction and Patterning of Graphite Oxide and Its Polymer Composite". In: *Journal of the American Chemical Society* 131.31 (2009), pp. 11027–11032.

[100] V. Eswaraiah, S. S. Jyothirmayee Aravind, and S. Ramaprabhu. "Top down method for synthesis of highly conducting graphene by exfoliation of graphite oxide using focused solar radiation". In: *Journal of Materials Chemistry* 21.19 (2011), p. 6800.

[101] Y. Tanizawa, Y. Okamoto, K. Tsuzuki, Y. Nagao, N. Yoshida, R. Tero, S. Iwasa, A. Hiraishi, Y. Suda, H. Takikawa, R. Numano, H. Okada, R. Ishikawa, and A. Sandhu. "Microorganism mediated synthesis of reduced graphene oxide films". In: *Journal of Physics: Conference Series* 352 (2012), p. 012011.

[102] Y. Hernandez, V. Nicolosi, M. Lotya, F. M. Blighe, Z. Sun, S. De, I. T. McGovern, B. Holland, M. Byrne, Y. K. Gun'Ko, J. J. Boland, P. Niraj, G. Duesberg, S. Krishnamurthy, R. Goodhue, J. Hutchison, V. Scardaci, A. C. Ferrari, and J. N. Coleman. "High-yield production of graphene by liquid-phase exfoliation of graphite". In: *Nature Nanotechnology* 3.9 (2008), pp. 563–568.

[103] D. Nuvoli, L. Valentini, V. Alzari, S. Scognamillo, S. B. Bon, M. Piccinini, J. Illescas, and A. Mariani. "High concentration few-layer graphene sheets obtained by liquid phase exfoliation of graphite in ionic liquid". In: *Journal of Materials Chemistry* 21.10 (2011), p. 3428.

[104] P. Blake, P. D. Brimicombe, R. R. Nair, T. J. Booth, D. Jiang, F. Schedin, L. A. Ponomarenko, S. V. Morozov, H. F. Gleeson, E. W. Hill, A. K. Geim, and K. S. Novoselov. "Graphene-Based Liquid Crystal Device". In: *Nano Letters* 8.6 (2008), pp. 1704–1708.

[105] S. Amini, J. Garay, G. Liu, A. A. Balandin, and R. Abbaschian. "Growth of large-area graphene films from metal-carbon melts". In: *Journal of Applied Physics* 108.9 (2010), p. 094321.

[106] A. Dato, V. Radmilovic, Z. Lee, J. Phillips, and M. Frenklach. "Substrate-Free Gas-Phase Synthesis of Graphene Sheets". In: *Nano Letters* 8.7 (2008), pp. 2012–2016.

[107] K. S. Subrahmanyam, L. S. Panchakarla, A. Govindaraj, and C. N. R. Rao. "Simple Method of Preparing Graphene Flakes by an Arc-Discharge Method". In: *The Journal of Physical Chemistry C* 113.11 (2009), pp. 4257–4259.

[108] C. Wu, G. Dong, and L. Guan. "Production of graphene sheets by a simple helium arc-discharge". In: *Physica E: Low-dimensional Systems and Nanostructures* 42.5 (2010), pp. 1267–1271.

[109] A. G. Cano-Márquez, F. J. Rodríguez-Macías, J. Campos-Delgado, C. G. Espinosa-González, F. Tristán-López, D. Ramírez-González, D. A. Cullen, D. J. Smith, M. Terrones, and Y. I. Vega-Cantú. "Ex-MWNTs: Graphene Sheets and Ribbons Produced by Lithium Intercalation and Exfoliation of Carbon Nanotubes". In: *Nano Letters* 9.4 (2009), pp. 1527–1533.

[110] L. Jiao, L. Zhang, X. Wang, G. Diankov, and H. Dai. "Narrow graphene nanoribbons from carbon nanotubes". In: *Nature* 458.7240 (2009), pp. 877–880.

[111] D. V. Kosynkin, A. L. Higginbotham, A. Sinitskii, J. R. Lomeda, A. Dimiev, B. K. Price, and J. M. Tour. "Longitudinal unzipping of carbon nanotubes to form graphene nanoribbons". In: *Nature* 458.7240 (2009), pp. 872–876.

[112] K. Müllen. "Graphen aus dem Chemielabor". In: *Spektrum der Wissenschaft* 8 (2012), pp. 82–89.

[113] J. Cai, P. Ruffieux, R. Jaafar, M. Bieri, T. Braun, S. Blankenburg, M. Muoth, A. P. Seitsonen, M. Saleh, X. Feng, K. Müllen, and R. Fasel. "Atomically precise bottom-up fabrication of graphene nanoribbons". In: *Nature* 466.7305 (2010), pp. 470–473.

[114] L. Dössel, L. Gherghel, X. Feng, and K. Müllen. "Graphene Nanoribbons by Chemists: Nanometer-Sized, Soluble, and Defect-Free". In: *Angewandte Chemie International Edition* 50.11 (2011), pp. 2540–2543.

[115] W. Regan, N. Alem, B. Alemán, B. Geng, C. Girit, L. Maserati, F. Wang, M. Crommie, and A. Zettl. "A direct transfer of layer-area graphene". In: *Applied Physics Letters* 96 (2010).

[116] A. Reina, H. Son, L. Jiao, B. Fan, M. S. Dresselhaus, Z. Liu, and J. Kong. "Transferring and Identification of Single- and Few-Layer Graphene on Arbitrary Substrates". In: *Journal of Physical Chemistry C* 112.46 (2008), pp. 17741–17744.

[117] J. C. Meyer, C. O. Girit, M. F. Crommie, and A. Zettl. "Hydrocarbon lithography on graphene membranes". In: *Applied Physics Letters* 92.12 (2008), p. 123110.

[118] J. C. Meyer, C. O. Girit, M. F. Crommie, and A. Zettl. "Imaging and dynamics of light atoms and molecules on graphene". In: *Nature* 454.7202 (2008), pp. 319–322.

[119] J. C. Meyer, C. Kisielowski, R. Erni, M. D. Rossell, M. F. Crommie, and A. Zettl. "Direct Imaging of Lattice Atoms and Topological Defects in Graphene Membranes". In: *Nano Letters* 8.11 (2008), pp. 3582–3586.

[120] A. Kuzmenko, E. van Heumen, F. Carbone, and D. van der Marel. "Universal Optical Conductance of Graphite". In: *Physical Review Letters* 100.11 (2008).

[121] J. Henrie, S. Kellis, S. M. Schultz, and A. Hawkins. *Electronic color charts for dielectric films on silicon*. 2004.

[122] P. Blake, E. W. Hill, A. H. Castro Neto, K. S. Novoselov, D. Jiang, R. Yang, T. J. Booth, and A. K. Geim. "Making graphene visible". In: *Applied Physics Letters* 91.6 (2007), p. 063124.

[123] Z. H. Ni, H. M. Wang, J. Kasim, H. M. Fan, T. Yu, Y. H. Wu, Y. P. Feng, and Z. X. Shen. "Graphene Thickness Determination Using Reflection and Contrast Spectroscopy". In: *Nano Letters* 7.9 (2007), pp. 2758–2763.

[124] C. Casiraghi, A. Hartschuh, E. Lidorikis, H. Qian, H. Harutyunyan, T. Gokus, K. S. Novoselov, and A. C. Ferrari. "Rayleigh Imaging of Graphene and Graphene Layers". In: *Nano Letters* 7.9 (2007), pp. 2711–2717.

[125] I. Jung, M. Pelton, R. Piner, D. A. Dikin, S. Stankovich, S. Watcharotone, M. Hausner, and R. S. Ruoff. "Simple Approach for High-Contrast Optical Imaging and Characterization of Graphene-Based Sheets". In: *Nano Letters* 7.12 (2007), pp. 3569–3575.

[126] L. A. Falkovsky. "Phonon dispersion in graphene". In: *Journal of Experimental and Theoretical Physics* 105.2 (2007), pp. 397–403.

[127] V. Yu. "Optics and Chemical Vapour Deposition of Graphene Monolayers on Various Substrates". PhD thesis. Montréal and Canada: McGill University, 2010. URL: `http://digitool.library.mcgill.ca/R/?func=dbin-jump-full\&object_id=97052\&local_base=GEN01-MCG02`.

[128] Y. y. Wang, Z. h. Ni, T. Yu, Z. X. Shen, H. m. Wang, Y. h. Wu, W. Chen, and A. T. Shen Wee. "Raman Studies of Monolayer Graphene: The Substrate Effect". In: *Journal of Physical Chemistry C* 112.29 (2008), pp. 10637–10640.

[129] L. Malard, M. Pimenta, G. Dresselhaus, and M. Dresselhaus. "Raman spectroscopy in graphene". In: *Physics Reports* 473.5-6 (2009), pp. 51–87.

[130] A. C. Ferrari, J. C. Meyer, V. Scardaci, C. Casiraghi, M. Lazzeri, F. Mauri, S. Piscanec, D. Jiang, K. S. Novoselov, S. Roth, and A. K. Geim. "Raman Spectrum of Graphene and Graphene Layers". In: *Physical Review Letters* 97.18 (2006).

[131] D. Graf, F. Molitor, K. Ensslin, C. Stampfer, A. Jungen, C. Hierold, and L. Wirtz. “Spatially Resolved Raman Spectroscopy of Single- and Few-Layer Graphene”. In: *Nano Letters* 7.2 (2007), pp. 238–242.

[132] D. Graf, F. Molitor, K. Ensslin, C. Stampfer, A. Jungen, C. Hierold, and L. Wirtz. “Raman imaging of graphene”. In: *Solid State Communications* 143.1-2 (2007), pp. 44–46.

[133] J. M. Yuk, J. Park, P. Ercius, K. Kim, D. J. Hellebusch, M. F. Crommie, J. Y. Lee, A. Zettl, and A. P. Alivisatos. “High-Resolution EM of Colloidal Nanocrystal Growth Using Graphene Liquid Cells”. In: *Science* 336.6077 (2012), pp. 61–64.

[134] S. Mikhailov, ed. *Physics and Applications of Graphene - Experiments*. 2011.

[135] O. L. Krivanek, M. F. Chisholm, V. Nicolosi, T. J. Pennycook, G. J. Corbin, N. Dellby, M. F. Murfitt, C. S. Own, Z. S. Szilagyi, M. P. Oxley, S. T. Pantelides, and S. J. Pennycook. “Atom-by-atom structural and chemical analysis by annular dark-field electron microscopy”. In: *Nature* 464.7288 (2010), pp. 571–574.

[136] M. H. Gass, U. Bangert, A. L. Bleloch, P. Wang, R. R. Nair, and A. K. Geim. “Free-standing graphene at atomic resolution”. In: *Nature Nanotechnology* 3.11 (2008), pp. 676–681.

[137] U. Bangert, T. Eberlein, R. R. Nair, R. Jones, M. Gass, A. L. Bleloch, K. S. Novoselov, A. K. Geim, and P. R. Briddon. “STEM plasmon spectroscopy of free standing graphene”. In: *physica status solidi (a)* 205.9 (2008), pp. 2265–2269.

[138] J. H. Warner, M. H. Rümmeli, T. Gemming, B. BuÌĹchner, and G. A. D. Briggs. “Direct Imaging of Rotational Stacking Faults in Few Layer Graphene”. In: *Nano Letters* 9.1 (2009), pp. 102–106.

[139] J. R. Jinschek, E. Yucelen, H. A. Calderon, and B. Freitag. “Quantitative atomic 3-D imaging of single/double sheet graphene structure”. In: *Carbon* 49.2 (2011), pp. 556–562.

[140] K. W. Urban. “Electron microscopy: The challenges of graphene”. In: *Nature Materials* 10.3 (2011), pp. 165–166.

[141] U. Bangert, C. T. Pan, R. R. Nair, and M. H. Gass. “Structure of hydrogen-dosed graphene deduced from low electron energy loss characteristics and density functional calculations”. In: *Applied Physics Letters* 97.25 (2010), p. 253118.

[142] L. Calliari, S. Fanchenko, and M. Filippi. “Plasmon features in electron energy loss spectra from carbon materials”. In: *Carbon* 45.7 (2007), pp. 1410–1418.

[143] T. Eberlein, U. Bangert, R. Nair, R. Jones, M. Gass, A. Bleloch, K. Novoselov, A. Geim, and P. Briddon. “Plasmon spectroscopy of free-standing graphene films”. In: *Physical Review B* 77.23 (2008).

[144] H. Daniels, R. Brydson, A. Brown, and B. Rand. “Quantitative valence plasmon mapping in the TEM: viewing physical properties at the nanoscale”. In: *Ultramicroscopy* 96.3-4 (2003), pp. 547–558.

[145] D. Teweldebrhan and A. A. Balandin. “Modification of graphene properties due to electron-beam irradiation”. In: *Applied Physics Letters* 94.1 (2009), p. 013101.

[146] A. Zobelli, A. Gloter, C. Ewels, G. Seifert, and C. Colliex. “Electron knock-on cross section of carbon and boron nitride nanotubes”. In: *Physical Review B* 75.24 (2007).

[147] J. H. Warner, M. H. Rümmeli, L. Ge, T. Gemming, B. Montanari, N. M. Harrison, B. Büchner, and G. A. D. Briggs. “Structural transformations in graphene studied with high spatial and temporal resolution”. In: *Nature Nanotechnology* 4.8 (2009), pp. 500–504.

[148] C. O. Girit, J. C. Meyer, R. Erni, M. D. Rossell, C. Kisielowski, L. Yang, C.-H Park, M. F. Crommie, M. L. Cohen, S. G. Louie, and A. Zettl. “Graphene at the Edge: Stability and Dynamics”. In: *Science* 323.5922 (2009), pp. 1705–1708.

[149] K. Suenaga and M. Koshino. “Atom-by-atom spectroscopy at graphene edge”. In: *Nature* 468.7327 (2010), pp. 1088–1090.

[150] J. Kotakoski, A. Krasheninnikov, U. Kaiser, and J. Meyer. “From Point Defects in Graphene to Two-Dimensional Amorphous Carbon”. In: *Physical Review Letters* 106.10 (2011).

[151] R. F. Egerton, P. Li, and M. Malac. “Radiation damage in the TEM and SEM”. In: *Micron (Oxford, England : 1993)* 35.6 (2004), pp. 399–409.

[152] J. Xie and J. P. Spallas. *Different Contrast Mechanisms in SEM Imaging of Graphene*. 2012. URL: http://cp.literature.agilent.com/litweb/pdf/5991-0782EN.pdf.

[153] H. Hiura, H. Miyazaki, and K. Tsukagoshi. “Determination of the Number of Graphene Layers: Discrete Distribution of the Secondary Electron Intensity Stemming from Individual Graphene Layers”. In: *Applied Physics Express* 3.9 (2010), p. 095101.

[154] M. Ishigami, J. H. Chen, W. G. Cullen, M. S. Fuhrer, and E. D. Williams. “Atomic Structure of Graphene on SiO 2”. In: *Nano Letters* 7.6 (2007), pp. 1643–1648.

[155] C. Lee, X. Wei, Q. Li, R. Carpick, J. W. Kysar, and J. Hone. “Elastic and frictional properties of graphene”. In: *physica status solidi (b)* 246.11-12 (2009), pp. 2562–2567.

[156] Graphene Laboratories Inc. *Graphene Supermarket*. 2012. URL: https://graphene-supermarket.com/.

[157] L. Persichetti, F. Tombolini, S. Casciardi, M. Diociaiuti, M. Fanfoni, G. Palleschi, A. Sgarlata, F. Valentini, and A. Balzarotti. “Folding and stacking defects of graphene flakes probed by electron nanobeam”. In: *Applied Physics Letters* 99.4 (2011), p. 041904.

[158] D. S. L. Abergel, A. Russell, and V. I. Fal’ko. “Visibility of graphene flakes on a dielectric substrate”. In: *Applied Physics Letters* 91.6 (2007), p. 063125.

[159] S. N. Kasarova, N. G. Sultanova, C. D. Ivanov, and I. D. Nikolov. “Analysis of the dispersion of optical plastic materials”. In: *Optical Materials* 29.11 (2007), pp. 1481–1490.

[160] Quantifoil Micro Tools GmbH. *Support Films for Electron Microscopy: EM-Products 2003*. 2003. URL: http://www.quantifoil.com/download/EM_Products_2003.pdf.

[161] C. B. Walsh and E. I. Franses. "Ultrathin PMMA films spin-coated from toluene solutions". In: *Thin Solid Films* 429.1-2 (2003), pp. 71–76.

[162] C. Jin, F. Lin, K. Suenaga, and S. Iijima. "Fabrication of a Freestanding Boron Nitride Single Layer and Its Defect Assignments". In: *Physical Review Letters* 102.19 (2009).